ANALYSIS OF AEROSOLS IN THE ATMOSPHERE OF DIFFERENT OPTICAL DOMAINS

A Thesis submitted to Goa University for the award of

The Degree of Doctor of Philosophy

In

Marine Science

By

Mr Shrivardhan Hulswar (M.Sc.)

Research Guide

Prof. Harilal B. Menon

GOA UNIVERSITY

Taleigao Plateau, Goa

2017

STATEMENT

As required by the university ordinance OA 19.8(vi), I state that the present thesis entitled "*Analysis of Aerosols in the Atmosphere of Different Optical Domains"* is my original contribution and the same has not been submitted on any pervious occasion. To the best of my knowledge the present study is the first comprehensive work of its kind from area mentioned. The literature related to the problem investigated has been cited. Due acknowledgments have been made wherever facilities and suggestions have been availed of.

Shrivardhan Hulswar

CERTIFICATE

This is to certify that the thesis entitled "*Analysis of Aerosols in the Atmosphere of Different Optical Domains*", submitted by Mr. Shrivardhan Hulswar for the award of Doctor of philosophy in Marine Sciences is based on his original studies carried out by him under my supervision. The thesis or any part thereof has not been previously submitted for any degree or diploma in any universities or Institutions.

Prof. H. B. Menon

Department of Marine sciences

Goa University

Taleigao Plateau, Goa- 403206, India

RESUME

SHRIVARDHAN HULSWAR

Department of Marine Sciences Tel: +918407970111

Goa University, Taleigao Plateau, Goa – 403206

Email: hulswar@gmail.com

Education

2003 – 2005 B.Sc, in Physics, St. Xavier's College, Mumbai, India

2008 – 2010 M.Sc, in Marine sciences, Goa University, Goa, India.

Thesis title: *Analysis of Aerosols in the Atmosphere of Different Optical Domains*

Advisor: Prof. H.B. Menon.

Oceanography Cruise Experience:

1) ORV Akademik Boris Petrov
    - June 9 2009 – July 10 2009
    - Central Indian Ocean.
2) ORV Sagar Kanya
    - 14 September 2011 – 24 October 2011
    - Equator – Time Series at 0^{o}, 80^{o}E and 0^{o}, 80.5^{o}E
3) ORV Sagar Nidhi
    - 25 December 2011 – 2 February 2012
    - Southern Ocean Expedition – 6
4) MV Ivan Papanin
    - 23 January 2013 – 27th March 2013
    - 32^{nd} Indian Scientific Expedition to Antarctica at Indian Antarctica stations Bharati (67.3^{o}S, 71.3^{o}E) and Maitri (70.7^{o}S, 11.7^{o}E)
5) ORV Sagar Nidhi
    - 29 May 2014 – 26 June 2014
    - South-West Tropical Indian Ocean (SWTIO), Time Series at 8^{o}S, 68^{o}E

6) ORV Sagar Nidhi
    - 9 January 2015 – 26 February 2015
    - Southern Ocean Expedition – 8
7) ORV Sagar Nidhi
    - 4 December 2015 – 23 December 2015
    - International Indian Ocean Expedition (IIOE) – 2

Master's Thesis

Dissertation - Spectral and Temporal Variations of Aerosol Optical Depth (AOD) over a Coastal Station (2010)

Advisor: Prof. H.B. Menon

Presentation

"Physical Characterization of aerosol in different sectors of the Indian sector of Southern Ocean, estimation of aerosol radiative forcing and heating rate", Oral presentation at Meeting of the review of SOE projects at NCAOR, June 2015

Publications

- Menon H. B., Shrivardhan Hulswar, N. Anilkumar, Achuthankutty Chittur Thelakkat, K.Krishna Moorthy, Suresh Babu; 2015; "Spatial heterogeneity in spectral variability of aerosol optical depth and its implications to aerosol radiative forcing in the Tropical Indian Ocean and in the Indian Ocean Sector of Southern Ocean"; Deep-Sea Res. II (2015), http://dx.doi.org/10.1016/j.dsr2.2015.03.012i
- Shrivardhan Hulswar, H.B. Menon; "Microphysical characteristics of aerosols and associated radiative forcing over Tropical Indian Ocean – results of International Indian Ocean Expedition – II". – under review

Conferences

- National Conference of Young Researchers (NCYR-2017)
    - Position Held: Joint Secretary (Organising Committee)
    - Date: March 16-17, 2017
    - Venue: Goa University, Goa

- National Conference on Polar Sciences (NCPS-2017)
    - Topic: Implications of intra-annual transformation processes of aerosols on radiative forcing over the Indian Sector Of Southern Ocean; Shrivardhan Hulswar, Prof. H.B. Menon
    - Organised by: National Centre for Antarctic and Ocean Research
    - Date: May 16-17, 2017
    - Venue: NCAOR, Goa
- 14th Annual Meeting, Asia Oceania Geosciences Society (AOGS-2017)
    - Topic 1: Microphysical Characteristics Of Aerosols And Associated Radiative Forcing Over Tropical Indian Ocean – Results Of International Indian Ocean Expedition – II; Shrivardhan Hulswar, Prof H.B. Menon
    - Topic 2: Spatial And Temporal Variability Of Aerosol Optical Depth (AOD), BC Mass Concentration And Associated Radiative Forcing Over Oceanic Domain Of Tropics, Sub-tropics And Polar Waters Of Indian Ocean.; Shrivardhan Hulswar, Prof H.B. Menon
    - Organised by: Asia Oceania Geosciences Society
    - Date: August 6-11, 2017
    - Venue: Suntec Singapore Convention & Exhibition Centre, Singapore

ACKNOWLEDGEMENT

There is a never ending list of people I would like to wholeheartedly thank or appreciate their presence and help rendered during the making of this thesis. In the time span beginning from 2010, after my post-graduation till today, many people became a part of my life, some continue to stay while some parted ways. Nevertheless, each one of them contributed to the person I am today.

I would begin with thanking my friend who also happens to be my guide for this work, Prof. H.B. Menon. I was first introduced to the topic of 'Aerosols' by him as a student in M.Sc. Marine Sciences and convinced me about its importance in day-to-day life. I feel grateful to him for believing in me, letting me discover things myself as they come, under his esteemed guidance, improving me wherever, whenever needed.

I thank Space Physics Laboratory, Indian Space Research Organisation **(SPL-ISRO)** for the funding and support provided for completion of this work. I feel indebted to the Director, National Institute of Oceanography **(NIO)** for permitting me to join the cruise to Equator 2011 which truly marked the beginning of the data generation for this thesis. I'm grateful to Director, National Centre for Antarctic and Ocean Research **(NCAOR)** for allowing me to participate in the Southern Ocean Expedition Program, Indian Antarctic Expedition and the South-Western Tropical Indian Ocean Expedition which contributes to most of the data used in this thesis. I also extend by gratitude to Director, Earth System Science Organization – Indian National Centre for Ocean Information Services **(ESSO-INCOIS)** for their permission to participate in the second International Indian Ocean Expedition which concluded the data generation for this thesis work.

Most of all, I thank my parents for supporting me in all that I experienced in course of this work for the thesis, their patience and confidence in me.

Shrivardhan Hulswar

"We have defined ourselves by the ability to overcome the impossible.
We count these moments when we dare to aim higher, to break barriers, to make the unknown known, we count these moments as our proudest achievements.
We are the pioneers, and we have barely begun.
Our greatest achievements cannot be behind us because our destiny lies above us"

-- Christopher Nolan

INDEX

INTRODUCTION

1.1 Introduction

Aerosols are suspended particulate matter in the atmosphere. They could be in solid, liquid or in mixed phase state. The aerosols in the atmosphere are seen to have an effect on human health, weather and also the Earth's climate (IPCC, 2013).

Aerosols are the end products of the various physical and chemical processes because of which they exhibit a great deal of variability with respect to space and time. Their interaction with the incoming solar radiation may also depend on their physical and chemical properties. Hence, in order to study the aerosols, their classification based on the physical and chemical properties was undertaken. Seinfeld and Pandis, (1998) have elaborately classified the aerosols by size ranging from a few nanometres to micrometres (fig 1.1).

Based on the process of formation, they are classified into primary and secondary aerosols. Primary aerosols are formed directly or emitted from sources, such as sea spray and dust, also known as bulk to particle conversion (BPC). Secondary particles are formed due to gas to particle conversion (GPC). These aerosols can also act as a site for other aerosols or gases to coagulate or condense to form coarser particles, e.g. cloud or fog formation, where the water-vapour condenses on aerosols forming small water droplets.

Aerosols can be in-situ generated or transported from a distance. The transportation depends on the wind speed, direction which govern the residence time of the aerosols. The residence time of aerosols in turn depend on the aerosol size, and the weather that may have existed all along the path from source locations to the location of study. Hence, the study of aerosols includes the role of weather.

1.2 Classification

In order to facilitate a systematic study, the aerosols are classified as follows.

1.2.1 **Genesis**: The aerosols are mainly classified as primary and secondary aerosols. A major component of the global aerosol system is contributed by Bulk to Particle conversion (BPC) or mechanical fragmentation processes (Prospero et al., 1983), which include processes such as weathering, rising dust, sea-spray, biological dirt and volcanic dust. Secondary aerosols are usually the product of Gas to Particle Conversion (GPC). Example when dimethyl sulphite (DMS) is generated as a by-product of the primary productivity, it is liberated in the atmosphere and forms sulphate aerosols when optimum atmospheric temperature and relative humidity prevails.

1.2.2 **Size**: In the global atmosphere, the aerosol size distribution is highly variable. However, they can be classified into four major modes. Whitby (1978) and Hoppel (1988) have classified aerosols based on aerodynamic diameter of particle (Dp) into Nucleation mode (Dp < 0.01 µm), Aitken mode (0.01 < Dp < 0.1 µm), Accumulation mode (0.1 < Dp < 1 µm) and Coarse mode (Dp > 1 µm).

1.2.3 **Source**: Based on the study undertaken, the aerosols may also be referred to as man-made or anthropogenic and natural aerosols. Anthropogenic aerosols account for the sulphates and nitrates which are the direct result of industrialization and/or different anthropogenic processes. Natural aerosols mostly are sea-spray, dust, sulphate aerosols which are a result of gas to particle conversion (GPC) of dimethyl sulphide (DMS).

1.2.4 Geographical origin: Normally, the aerosols that are observed in a study area may or may not be produced in the same area. There is always a local component and a remote component in the total aerosol content. In order to understand the effect of local and remote component, the aerosols are classified as either marine, continental, volcanic, urban, rural, desert or Antarctic origin.

Based on the objectives of the study, the aerosols are categorised in more than one way to facilitate better understanding of the issues being addressed.

1.3 Residence Time

The most important aspect of the aerosol interaction with the atmosphere and radiation is the time during which they are in suspension. Residence time is the ratio between rates of production of aerosol to which they are removed from the system. The processes like production, transformation and removal impact the residence time (Jaenicke 1993). It can vary from a few weeks to as long as years as in case of stratospheric aerosols.

1.4 Removal processes

Wet and dry depositions are the major removal processes for a variety of aerosols. They are important factors determining the residence time and concentrations of tropospheric aerosols. (Sportisse, 2007; Petroff et al., 2008). About 80–90% of aerosols are removed annually from the atmosphere by either wet deposition or dry deposition.

Wet deposition processes are when parts of cloud droplets come down as precipitation reaching Earth's surface which removes the aerosols from cloud as well as the column of air below the cloud and deposition form of aerosols in high elevation ecosystems due to interception of cloud droplets by vegetation. Dry deposition processes include turbulent diffusion in case of large particles (diameter larger than 1 μm), eddy diffusivity becomes

significant, gravitational settling (sedimentation) where larger particles fall back to the surface under the influence of gravity. Impaction occurs when a particle is unable to follow the streamline flow around an obstacle (e.g. a larger particle). Randomly moving smaller particles bump each other or to a larger particle. This process dominates all particle sizes below 0.2 µm. Brownian diffusion coefficient increases as particle diameter decreases. Furthermore, in a very thin (about 1 mm) layer over the surface, the Brownian diffusion of larger particles becomes more important too.

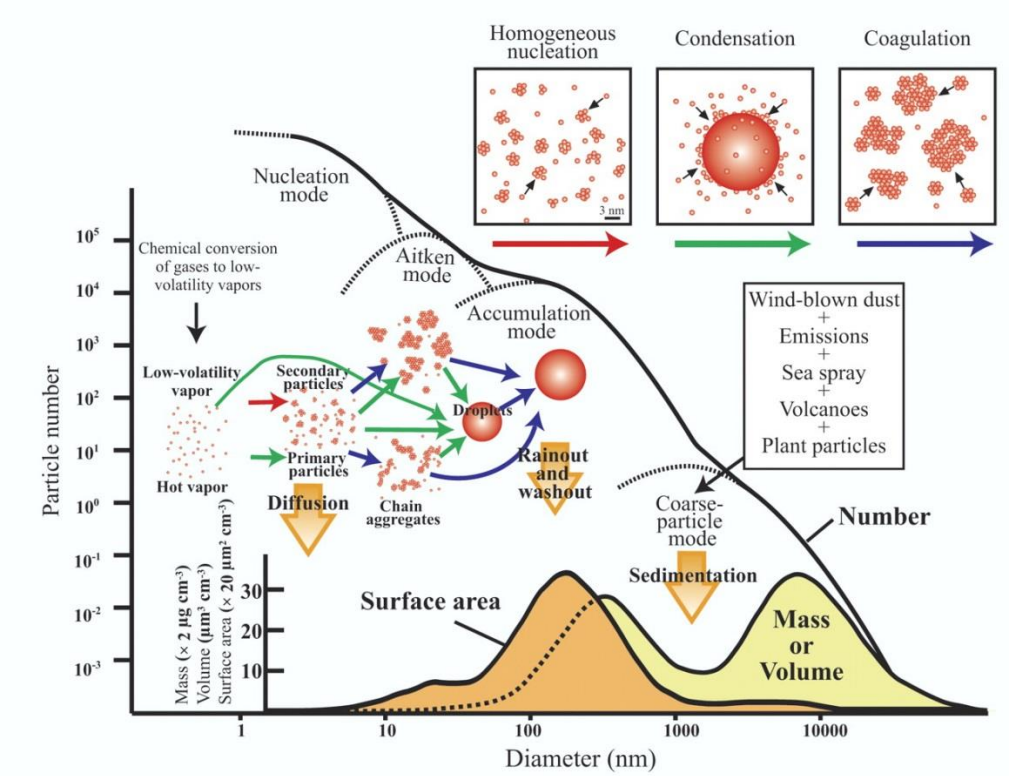

Fig 1.1 Aerosol size distribution, growth and removal processes

Source: SCANTECH ENVIRONMENTAL AND BIOMEDICAL TESTING – CONSULTING SERVICES

1.5 Aerosols and Climate

Aerosols scatter and absorb sunlight, modifying the Earth's radiative balance (Fig 1.2). Generally scattering aerosols make the planet more reflective, and tends to cool the atmosphere, while absorption by aerosol results in warming of the atmosphere and hence the

climate system. The balance between cooling and warming depends on aerosol properties and environmental conditions.

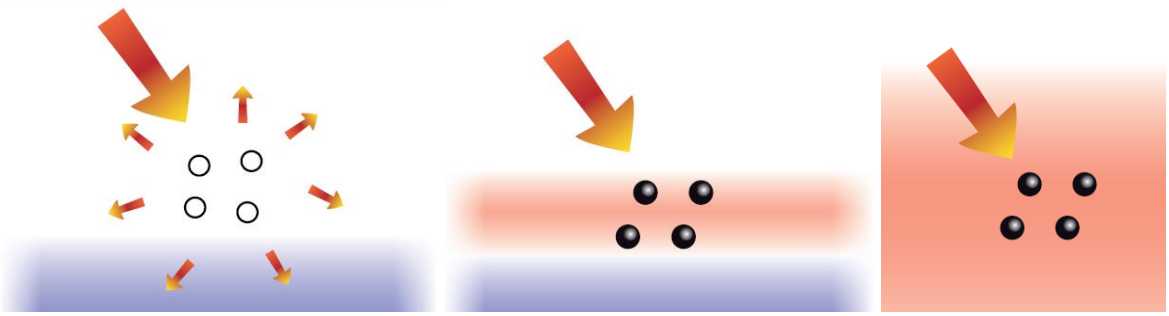

Fig 1.2 (a) Scattering of incoming radiation leading to surface cooling

(b) Absorption of incoming radiation at an altitude may lead to heating of aerosol layer and surface cooling

(c) Absorption of incoming radiation at surface may lead to surface heating

Source: IPCC – 2013

One of the uncertainties comes from black carbon, an absorbing aerosol that not only is difficult to estimate as compared to scattering aerosols, but also induces a complicated cloud response. Aerosols also serve as condensation and ice nucleation sites, on which cloud droplets and ice particles can form (fig 1.3). When influenced by more aerosol particles, clouds of liquid water droplets tend to have more, but smaller, droplets causing them to reflect more insolation.

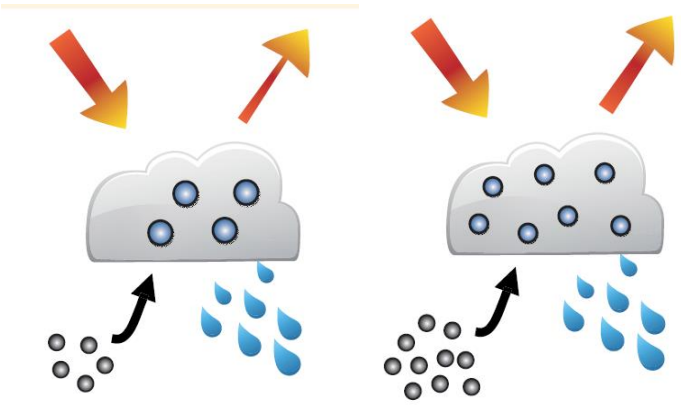

Fig 3. (a) Aerosols act as cloud condensation nuclei upon which liquid droplets form.

(b) More aerosols result in a larger concentration of smaller droplets, leading to a brighter cloud.

Source: IPCC – 2013

Based on climate models and satellite observations, it has been seen that the net effect of aerosols such as sulphates on clouds is cooling the climate system. However, since aerosols are dispersed unevenly in the atmosphere, they can heat and cool the atmosphere in patterns changing the weather and eventually the climate. Efforts to simulate these effects by a model can be futile as their interaction with the atmosphere is non-linear and complex. Anthropogenic aerosol emissions have increased significantly over the industrial period, which has offset some of the warming that would otherwise have occurred from higher concentrations of well mixed greenhouse gases (IPCC, 2013).

The impact of aerosols on the global mean surface temperature over a period of time is assumed to be small. It is projected, however, that emissions of anthropogenic aerosols will ultimately decrease in response to air quality policies, which would suppress their cooling influence on the Earth's surface, thus leading to increased warming.

1.6 Rationale for the Study

The literature shows the effect of presence of greenhouse gases (GHGs) in the atmosphere on climate is well understood. However, it is different in the case of aerosols. Though the scientific community has a general idea of aerosols and the process of their formation, their effect on local environment, many aspects of their interaction with the incoming solar radiation are still unknown. One of the important progresses in aerosol research in the last decade has been the awareness that it will be impossible to fully understand the state of atmosphere without accounting for aerosol species.

Anthropogenic aerosols like black carbon are responsible for a radiative forcing as a result of their interaction with radiation and clouds. Quantification of this forcing involves many uncertainties (Haywood and Boucher, 2000; Lohmann and Feichter, 2005) and uncertainty due to aerosols dominate total radiative forcing (Forster et al., 2007; Haywood and Schulz,

2007; IPCC 2013). Our inability to quantify non-greenhouse gas RFs, primarily due to aerosol–cloud interactions, is due to the difficulties in constraining climate sensitivity from observations even if we had a perfect knowledge of the temperature record (Andreae et al., 2005). Thus a complete understanding of past and future climate change requires a thorough evaluation of aerosol–cloud–radiation interactions.

An increasing understanding of aerosols and the associated research during the past decade can be ascribed to the change in the way aerosol measurements in general are carried out. Investigators are recognizing that meaningful progress in understanding aerosol properties and processes requires a variety of measurement techniques at the same time. This approach adds new vigour to aerosol field measurements and is becoming increasingly important as the understanding of aerosols is increasing.

The approach has been used effectively in Aerosol Characterization Experiment (ACE) -1 (Covert, et al., 1998; Huebert, et al., 1998; Quinn and Coffman, 1998), Troposphere Aerosol Radiative Forcing Observational Experiment (TARFOX) (Russell, et al., 1999) and ACE-2 (Collins, et al., 2000; Durkee, et al., 2000a; Livingston, et al., 2000; Neusüß, et al., 2000; Putaud, et al., 2000; Russell and Heintzenberg, 2000; Schmid, et al., 2000) and has been a key strategy of Indian Ocean Experiment (INDOEX) and ACE-Asia (McFarquhar et al., 1994; Ramanathan et al, 1995(a); Ramanathan et al, 1996(b); Rhoads et al., 1997; Krishnamurti et al., 1997; Satheesh et al., 1997; Krishna Moorthy et al., 1997; Jayaraman et al., 1998).

Indian scientists carried out campaigns in connection with aerosol, gas and radiation over land, ocean and atmosphere (Integrated Campaign for Aerosols, gases and Radiation Budget – ICARB , and Winter – Integrated Campaign on Aerosols, Gases and Radiation Budget – W-ICARB), with an objective to understand the aerosols of continental origin and their effect

over ocean basins adjacent to Indian continent due to seasonally reversing winds (Kalapureddy et al., 2008, Aloysius et al., 2008, Krishna Moorthy et al., 2008, Kumar et al., 2011, Sinha et al., 2011, Sreekanth et al., 2011). This culminated in the establishment network stations generating data on aerosol optical depth across India under the aegis of Aerosol Radiative Forcing over India (ARFI), by Geosphere Biosphere Programme (GBP) of Indian Space Research Organisation (ISRO). The important results of ARFI studies are well documented (Menon et al., 2011, Moorthy et al., 2013a, 2013b, Narasimhan and Satheesh., 2013, Mukunda et al., 2014 , Menon et al, 2014).

ICARB and WICARB were dedicated primarily to studies on air-sea coupling and the associated effects on aerosols and radiation primarily limited to the north Indian Ocean. As a result, there is limited knowledge on the effect of aerosols advection from continent over the Indian Ocean, south of 10^{o}N (D'Adamo, 2015, Babu et al; 2010 and Chaubey et al., 2013). The last two studies highlighted the latitudinal gradient of aerosol and their possible effect on climate.

1.6.1 CLAW Hypothesis

The CLAW is an acronym formed using the first letter of the surnames of Robert Jay Charlson, James Lovelock, Meinrat Andreae and Stephen G. Warren. The CLAW hypothesis put forward a negative feedback loop that exists between ocean ecosystems and the Earth's climate. The hypothesis specifically suggests that phytoplankton that produce dimethyl sulphide (DMS) respond to variations in climate forcing, and that these responses act to stabilise the temperature of the Earth's atmosphere (Charlson et al., 1987). This hypothesis is important because it attempts to provide a relation between phytoplankton and the climate. While, the role of DMS to produce sulphate aerosols which may form cloud condensation

nuclei (CCN) is known, no direct study explains the hypothetical loop explaining the role of phytoplankton in altering the radiative forcing that affects the regional climate.

Hence with an objective to advance our understanding of aerosols over the Indian Ocean and their role in the Earth's System, present study has been carried out with the following objectives.

1.6.1 To analyse spectral variation of Aerosol Optical Depth (AOD), to estimate aerosol size spectrum (α) and atmospheric turbidity (β) parameter in the Atmosphere of different optical domains with the help of in-situ and satellite observations.

1.6.2 To estimate black carbon (BC) mass concentration (aerosol absorbing solar radiation)

1.6.3 To differentiate size fraction of aerosols using Quartz Crystal Microbalance (QCM) impactor.

1.6.4 To estimate Direct Aerosol Radiative Forcing.

1.6.5 To determine the chemical composition of aerosol samples collected over different locations.

Chapter 2 provides a description of the study areas from the regions in Indian Ocean and Indian sector in the Southern Ocean, instruments used to generate data for the work carried out, details of the radiative transfer model and the methodology adopted.

Chapter 3 gives a detailed analysis of aerosol optical depth (AOD) and associated variation in Angstrom parameters (α, β). In case where the AOD spectra deviates from the Junge's power law, the first order derivative of α, α' was calculated. The chapter also provides an insight to the size variability of the aerosols over different regions between 15^{o}N and 55^{o}S obtained by

QCM and validating the satellite data of MODIS-AQUA for synoptic scale study over the remote regions of the Indian Ocean.

Chapter 4 provides the details of chemical analysis carried out on the aerosol samples obtained from different zones. The analysis of variability of black carbon (BC), over the region from Indian coast to 55^{o}S has also been discussed. This includes the relation of BC mass concentration with height of planetary boundary layer (PBL) over different regions.

Chapter 5 investigates the direct aerosol radiative forcing over different regions as a result of the variability of composite AOD, BC mass concentration and PBL height.

Chapter 6 Discusses the implications of intra-annual transformation processes of aerosols on radiative forcing over the Indian Ocean sector of southern ocean (South of 40^{o}S).

Chapter 7 summarizes the entire study, highlights the key points and presents the scope for future work that needs to be carried out for a better understanding of certain aspects of the aerosol interactions that may affect the climate of earth.

DATA AND METHODOLOGY

2.1 STUDY AREA

In order to understand aerosol processes over regions of different optical domains, different surveys were carried out and details are given below.

Cruise Name		Cruise Duration	Observation Location
Equator Cruise		14 September 2011 – 24 October 2011	Time Series at 0^o, 80^oE and 0^o, 80.5^oE
Southern Ocean Expedition (SOE)	6	25 December 2011 – 2 February 2012	Indian Coast (15^oN) to approximately 55^oS
	7	13 January 2013 – 25 February 2013	
	8	9 January 2015 – 26 February 2015	
32^{nd} Indian Scientific Expedition to Antarctica		23 January 2013 – 27th March 2013	Indian Antarctica stations Bharati (67.3^oS, 71.3^oE) and Maitri (70.7^oS, 11.7^oE)
South-West Tropical Indian Ocean (SWTIO)		29 May 2014 – 26 June 2014	Time Series at 8^oS, 68^oE
International Indian Ocean Expedition (IIOE) – 2		4 December 2015 – 23 December 2015	12^oN to 12^oS along 67.5^oE

Table 2.1 Details of cruises

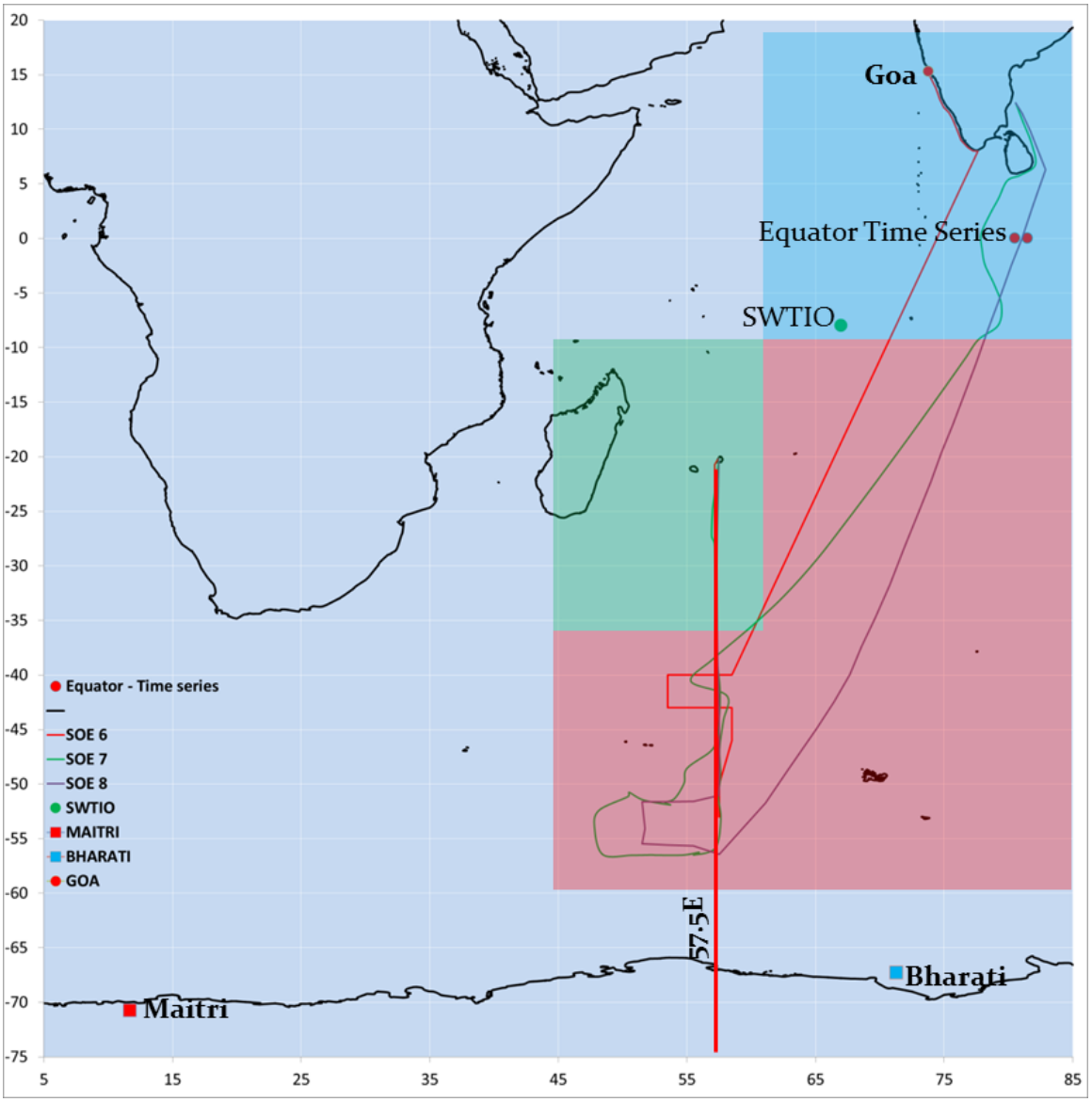

Fig 2.1 Study area displaying zonation and cruise tracks.

2.1.1 ZONATION

Since the distribution of aerosols in the study area is characterised by mesoscale phenomenon such as Inter-tropical Convergence Zone (ITCZ) and Sub-tropical Frontal zone (STF), it has been divided into different zones; Zone-1, Zone 2, Zone-3. The position of ITCZ during the latter half of December-January (i.e. during the SOE cruises) is around 8^{o}S; thereby creating a virtual atmospheric boundary separating the Zone 1 (where continental influence was observed) and rest of the oceanic region. An exception to this is the Equatorial cruise which

took place in the months of September-October, IIOE-2 cruise which took place in the first half of December and the SWTIO cruise which took place in May and June. Hence the mean position of ITCZ became a criterion to delineate Zone 1. The remaining zones were categorised on the basis of proximity of cruise track to coast and Subtropical front (STF).

Zone 1 (coloured in blue) essentially is in the close vicinity of the Indian and Sri Lankan coast. The northern boundary of the ITCZ marks the lower limit of this Zone. Due to the proximity to Indian subcontinent and Sri Lanka, the zone is seen to have the aerosol input from the continent (both from Indian subcontinent and Sri Lanka), mainly due to winds flowing from the north during the period of study. The southern boundary of the ITCZ marks the northern boundary of the Zone 2 (coloured in red). The aerosols prevailing in the zone are mainly of marine origin and a remotely transported small component originated from continent. Zone 3 (coloured in green) has the proximity to African continent, Madagascar, Mauritius and Reunion Islands. This makes the region to be considered as a separate zone though it is a subsection of Zone 2.

2.2 IN-SITU MEASUREMENTS

2.2.1 SUNPHOTOMETER

The portable instrument is equipped with five accurately aligned optical collimators, with a full field view of 2.5°. Internal baffles are also integrated into the device to eliminate internal reflections. Each channel is fitted with a narrow-band interference filter and a photodiode suitable for the particular wavelength range. The collimators are encapsulated in a cast aluminium optical block for stability. A sun target and pointing assembly is permanently attached to the optical block and laser-aligned to ensure accurate alignment with the optical channels. When the image of the sun is centred in the bull’s-eye of the sun target, all optical

channels are oriented directly at the solar disk. A small amount of circumsolar radiation is also captured, but it makes little contribution to the signal.

Radiation captured by the collimator and band-pass filters radiate onto the photodiodes, producing an electrical current that is proportional to the radiant power intercepted by the photodiodes. These signals are first amplified and then converted to a digital signal by a high resolution A/D converter. The signals from the photodiodes are processed in series. However, with 20 conversions per second, the results can be treated as if the photodiodes were read simultaneously. AOD and water vapour column are determined assuming the validity of the Bouguer-Lambert-Beer law.

$$F_\lambda = F_{o\lambda}\left(\frac{d_o}{d}\right)^2 e^{-m\tau_\lambda} \tag{2.1}$$

The sunphotometer provides voltage V_λ proportional to F_λ where F_λ solar flux reaching ground for nearly monochromatic radiation. Hence the equation becomes,

$$V_\lambda = V_{o\lambda}\left(\frac{d_o}{d}\right)^2 e^{-m\tau_\lambda} \tag{2.2}$$

In natural logarithmic form,

$$\ln V_\lambda = \ln V_{o\lambda}\left(\frac{d_0}{d}\right)^2 - m\tau\,(\ln e) \tag{2.3}$$

Since d_o and d are nearly constant for a given day,

$$\ln V_\lambda = \ln V_{o\lambda} - m\tau \tag{2.4}$$

This equation resembles the equation of line y=mx+c where the log $V_{o\lambda}$ is constant for a given wavelength and log V_λ is proportional to τ. This is the Langley plot method to estimate AOD.

The MICROTOPS-II calculates the AOD value at each wavelength based on the channel's signal, its extra-terrestrial constant, atmospheric pressure (for Rayleigh scattering), time and location. Solar distance correction is automatically applied. All optical depth calculations are based on the Bouguer-Lambert-Beer law. The AOD formula is as follows:

$$AOD_\lambda = \frac{\ln(V_{0\lambda}) - \ln(V_\lambda * SDCORR)}{m} - \tau_{R\lambda} * \frac{P}{P_0} \quad (2.5)$$

Where the index "$\boldsymbol{\lambda}$" references the channel's wavelength, $\ln(V_{o\boldsymbol{\lambda}})$ is the AOT calibration constant, V_λ is the signal intensity in [mV], SDCORR is the mean Earth-Sun distance correction, 'm' is the optical airmass, $\tau_{R\lambda}$ is the Rayleigh optical thickness, and P and P_0 are station pressure and standard sea-level pressure (1013.25mB) respectively. The optical depth due to Rayleigh scattering is subtracted from the total optical depth to obtain AOD. Optical depth from other processes such as O_3 and NO_2 absorption are ignored in MICROTOPS-II.

2.2.1.1 CALIBRATION

The instrument needs yearly calibration in order to eliminate the errors due to degradation of the filters used. To calculate the response of the filters in sunphotometer in the absence of atmosphere, or when air-mass m=0, the Langley plot extrapolation method is used. When m=0, the equation (2.4) becomes,

$$\ln V_\lambda = \ln V_{o\lambda} \quad (2.6)$$

This condition can occur if the change in AOD is minimal and air mass changes drastically (as typically seen in mornings or evening). The plot of $\ln V_{\boldsymbol{\lambda}}$ v/s m would be almost a straight line. This line when extrapolated to intersect y-axis, the point of intersection gives the $\ln V_{\boldsymbol{\lambda}}$ when m=0 i.e. $\ln V_{0\boldsymbol{\lambda}}$. The values of $\ln V_{0\boldsymbol{\lambda}}$ at different wavelengths present in the sunphotometer are required to ensure accurate measurements by the instrument.

An alternative method suggested by Adler-Golden, 2007 was used for calibrating the sunphotometer. The equation (2.4) can also be written as,

$$\ln V_\lambda/m = (\ln V_{o\lambda})m - \tau \qquad (2.7)$$

In order to find stable conditions with minimum variations in AOD data, the highest point in the Maharashtra, Mt. Kalsubai, with an altitude of 5400ft (1646 m) was chosen for generating the data required for calibration. With the help of weather forecasts, a clear sky morning was chosen.

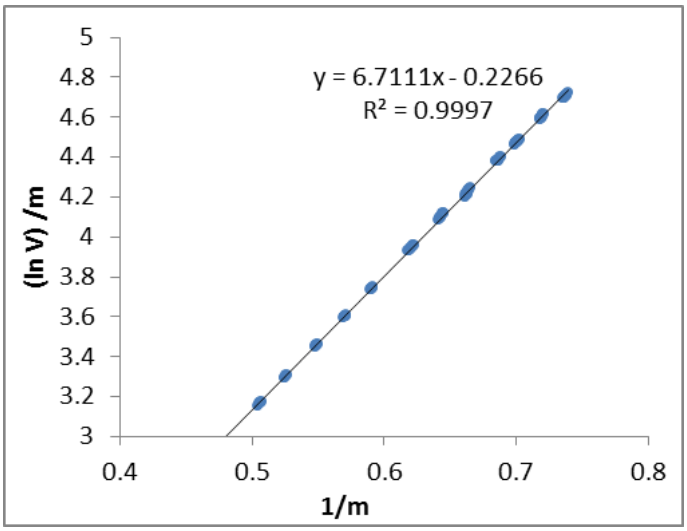

Fig 2.2: Estimation of ln $V_{0\ .0.5}$ using the alternative Langley plot method

In the fig 2.2, the estimation of ln V_0 for 0.5um is shown using the Alternative Langley plot method. The accuracy is high as evident from the value of R^2 which is 0.9997. The ln V_0 was calculated for all wavelengths for the sunphotometer before an expedition to ascertain that a freshly calibrated unit was used for data generation.

2.2.2 AETHALOMETER

The principle of the Aethalometer™ is to measure the attenuation of a beam of light transmitted through a filter, while the filter is continuously collecting aerosol sample. This measurement is made at regular intervals of a time-base period. By using the appropriate value of the specific attenuation for that particular combination of filter and optical components, the black carbon content of the aerosol deposit is determined at each measurement time. The increase in optical attenuation from one period to the next is due to the increment of aerosol black carbon collected from the air stream during the period. Dividing this increment by the volume of air sampled during that time, the mean BC concentration in the sampled air stream is calculated during the period. If the time base is short compared to the time scale of other variations in the air mass under study, the measurements appear to be continuous. If the mean concentration does not vary greatly from one measurement period to the next, the period average is a reasonable representation of the time behaviour of the actual BC concentration during the period.

The objectives of the Aethalometer hardware and software systems are thus as follows:

- To collect the aerosol sample with as few losses as possible on a suitable filter material;
- To measure the optical attenuation of the collected aerosol deposit as accurately as possible;
- To calculate the rate of increase of the BC component of the aerosol deposit and to interpret this as a BC concentration in the air stream;
- To display and record the data, and to perform necessary instrument control and diagnostic functions.

2.2.2.1 THE ALGORITHM TO ESTIMATE BC

The algorithm that the Aethalometer™ system uses to calculate the aerosol black carbon content of a sampled air stream is based on the following measurements:

(a) Measurements of the Reference and Sensing beam detector outputs with the lamps OFF, to determine their zero offsets;

(b) Measurements of the reference and sensing beam detector outputs with the lamps ON, to determine the transmitted light intensities;

(c) Measurement of the air flow through the system;

(d) Knowledge of the active collecting area of the spot on the filter, and of the specific attenuation of the particular combination of light source, detector, optical components and the filter medium in use.

Since the algorithm uses only ratios, with the 'zero' levels subtracted, the results are not dependent on any scaling, offset or proportionality constant of the photo detectors response. The only requirement is that the response be linear with respect to the incident light intensity.

If,

SB = Sensing Beam detector output with lamps on.

SZ = Sensing Beam detector Zero offset output with lamps off.

RB = Reference Beam detector output with lamps on.

RZ = Reference beam detector Zero output with lamps off.

A = Aerosol collecting spot area of filter, [cm^2].

F = Flow rate of air through filter, litres per minute.

T = Sampling time-base period, minutes.

ATN = Optical attenuation due to aerosol deposit on filter.

B = Surface loading of black carbon on filter, [g/cm²].

SG = Specific attenuation cross-section for the aerosol black carbon deposit on this filter, using the optical components of this instrument, [m²/gram].

BC = Concentration of black carbon in the sampled air stream, expressed in nanograms per cubic meter.

The 'true' detector responses to the light beam are (SB-SZ) and (RB-RZ). The correction to the sensing beam response for possible variations in light intensity output is performed by using the ratio (SB-SZ)/(RB-RZ). The optical attenuation is then defined as

$$ATN = -100 * ln \frac{(SB-SZ)}{(RB-RZ)} \quad (2.8)$$

The absolute value of this attenuation is not very important, as the determination of BC is calculated from its rate of change. The factor of 100 is introduced for numerical convenience. The increase of ATN is proportional to the increase of surface loading B of black carbon on the aerosol deposit spot, with the relation

$$d(ATN) = SG * d(B) \quad (2.9)$$

This increase of black carbon is the amount filtered from the air stream during the time-base interval T. If the air stream concentration is BC, the flow rate is F and the area of the filter onto which it is collected is A, then

$$d(B) = \frac{(BC*F*T)}{A} \quad (2.10)$$

2.2.3 QUARTZ CRYSTAL MICROBALANCE (QCM)

The Quartz Crystal Microbalance (QCM) is a mass-based inertial impaction system. It is a general-purpose analytical instrument which can be used for any application that has to do with airborne or gas-suspended particulates. It has a proprietary Quartz Crystal Microbalance (QCM) electronic mass sensors to provide air particle size distribution and mass concentrations in real-time. Since the sampling is based on inertial impaction, the system retains particles in size-segregated groups which can be saved for analysis to identify their morphology and elemental composition.

10-stage QCM cascade impactor covers particle size range of 25, 12, 6.4, 3.2, 1.6, 0.8, 0.4, 0.2, 0.1 and 0.05 microns. The inertial impactor has a flow rate of 0.24 lpm. The control unit provides printout of particle size distribution and mass concentration of the ten size fractions automatically in µg/m^3. The crystal's mass detection sensitivity is a function of the square of its resonant frequency. The sensitive region is restricted to the area of the metal electrode, within circle of 0.635cm diameter.

For a 10 MHz crystal used in the QCM, and for the mass deposition over the entire circular region, the mass detection sensitivity is,

$$\Delta F = (2.2 \times 10^{-6})\, f^2\, [\Delta M/A] \qquad \text{Hz-cm}^2/\text{g} \qquad (2.11)$$

Where,

ΔF = frequency change

ΔM = mass change

A = area of electrode = 0.317cm^2

f = crystal resonant frequency = 10^{7}MHz

$$\Delta F = (6.95 \times 10^{8}) \times \Delta M \quad \text{Hz/g} \quad (2.12)$$

$$\Delta M = (1.44 \times 10^{-9}) \times \Delta F \quad \text{g/Hz} \quad (2.13)$$

$$\Delta M = 1.44 \times \Delta F \quad \text{ng/Hz} \quad (2.14)$$

The equation 2.13 shows that a mass of 1.44ng deposited evenly over the entire electrode induces a change of 1Hz. However, the deposition might not be even nor the sensitivity of the crystal will be linear across the surface. In fact it is a bell-shaped curve tapering towards the edge of the crystal. The mass deposition is over a smaller region and sensitivity of found to be higher approaching 1ng/Hz.

2.2.4 AEROSOL CHEMISTRY

The aerosol samples obtained during the cruise were analysed using Ion Chromatograph (Dionex DX- 2500 cations and ICS-2000 for anions) and Inductively Coupled Plasma Mass Spectrometry (ICPMS) available at National Centre for Antarctic and Ocean Research (NCAOR) to determine the concentrations of elements present in the samples.

2.2.4.1 CHEMICAL CHARACTERISATION OF AEROSOL SAMPLES

The aerosol samples of the ambient atmosphere were generated using a high volume sampler during the 6th Southern Ocean cruise (SOE-6). The samples were obtained on a QM/A 90mm Quartz fibre filter paper by running the same at 400LPM for a period of 30 minutes. The samples were preserved in a desiccated container in plastic self-lock envelopes. The apparatus were acid-washed and oven-dried before used for the sample preparation and storage. The sampler was placed in bow of the ship in order to lead the incoming air straight in to the sampler inlet area. Precautions were taken to avoid any contamination from the various ship exhausts that may be present. The samples were analysed for presence of Na^{+}, $Mg^{+,}$ Ca^{+}, K^{+}, NH_4^{+}, Cl^{-}, SO_4^{2-}, NO_3^{-} and trace metals like Cu, Ti and Cd separately.

2.2.4.2 PROCEDURE FOR CATIONS AND ANIONS.

- A quarter of the filter paper was cut and then carefully sub-divided into fine pieces and then put into centrifuge tubes.
- These tubes were then filled with 10ml Milli-Q water and centrifuged at 2000rpm for 20minutes.
- The tubes were then decanted in correctly labelled plastic bottles.
- Steps 2 and 3 were repeated again to obtain 20ml of sample from a quarter of filter paper from every chosen station.
- Total 11 samples were generated from chosen stations and 1 blank sample for analysis using Ion chromatography.

2.2.4.3 PROCEDURE FOR TRACE METALS

- A quarter of the filter paper was cut and then carefully sub-divided into fine pieces and then put into Teflon tubes.
- About 20ml of conc. Nitric acid was added in the Teflon tube and then kept for digestion at approximately 200^{o}C for about 40 minutes.
- The Teflon tubes were then decanted into correctly labelled plastic bottles.
- Total of 11 samples were generated from chosen stations and 1 blank sample for analysis using ICPMS (Inductively coupled Plasma Mass spectrometry).

2.2.5 RADIO-SONDE

A radiosonde is a battery-powered telemetry instrument package carried by a weather balloon into the atmosphere that measures various atmospheric parameters and transmits them by radio to a ground receiver. It measures or estimates altitude, pressure, temperature, relative humidity, wind speed and wind direction and geographical position (Latitude/Longitude).

The Indian Space Research Organization's (ISRO)'s Vikram Sarabhai Space Centre (VSSC) has developed a GPS radiosonde, named Pisharoty sonde, with its ground station for atmospheric research and operational meteorology. The latest version of this radiosonde (B2/B3) uses a bead thermistor, a capacitive humidity sensor, and a GPS receiver module. The system provides lower-troposphere profiles at a cost than lesser its available counterparts in the international market. The Pisharoty sonde system comprises of two subsystems, viz., the sonde and the ground station (fig 2.3a).

2.2.5.1 PISHAROTY SONDE

The sonde consists of sensors for the measurement of temperature and relative humidity; a sigma delta analog-to-digital converter (ADC) to process sensor data; a GPS module to acquire the location parameters; a microcontroller for initialization, data acquisition, and frame formatting; a transmitter module for carrier generation, modulation, and transmission; an antenna; and a battery (fig 2.3b). Pressure is calculated from temperature and geo-potential height using software in the data processing and display system of the ground station.

The temperature sensor is a negative temperature coefficient glass bead thermistor with a base resistance of 1 kΩ at 25^{o}C (0.4- mm diameter and without anti-radiation coating). The humidity sensor provides an output voltage proportional to the relative humidity (sensor module covered by an aluminized plastic cap). The voltage outputs from the sensor circuits are collected and processed by the sigma delta ADC sequentially. The GPS receiver module with an integrated patch antenna provides altitude, time, location, and velocity of the balloon by processing the signals from GPS satellites. The output from the GPS receiver is in National Marine Electronics Association (NMEA) standard messages format.

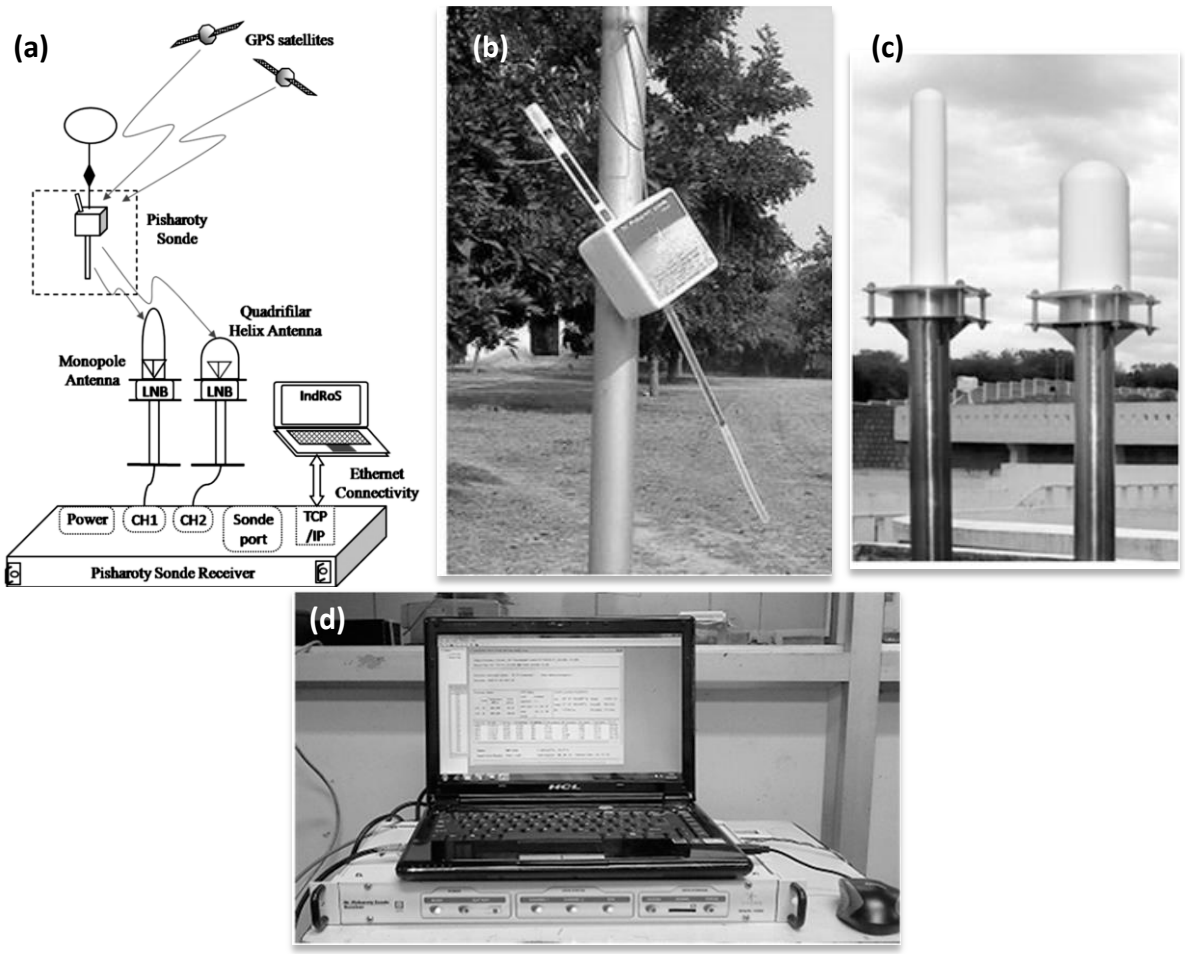

Fig 2.3 (a) Schematic diagram of Pisharoty radiosonde system (b) Pisharoty Sonde (c) LNB Antennae (d) Ground Station

The microcontroller acquires the data from ADC and GPS, multiplexes the data, and applies error corrective 'Reed-Solomon' coding. This coding is best suited for systems prone to burst errors. It is used in the sonde system for forward error correction. The telemetry frame with a frame synchronization pattern, multiplexed data, and error coding bytes are passed on to the transmission block. Telemetry data are frequency-shift keying (FSK) modulated on a carrier with frequency programmability in the range of 402-406 MHz, with central frequency of 403.5MHz. The package includes two AA lithium-thionyl chloride batteries allowing for operation for more than 6hrs. Sensor calibration coefficients are stored on chip. Initialization includes programming the transmission frequency to any desired 125-kHz step between 402 and 406 MHz.

The bead thermistor is subject to radiation errors, including heating by sunlight and cooling by radiation to space, as well as a lag in responding to temperature changes as the balloon ascends, with all errors being larger at high altitudes. A solar and IR radiation correction, varying with pressure and sun angle, is applied to compensate for all of these errors. For example, at 50 hPa the correction is 22.5^{o}C (the reported temperature is reduced) at high sun angles and 10.6^{o}C at night. While the RH sensor is similarly subject to errors, the RH data are currently not adjusted.

2.2.5.2 GROUND STATION

The ground station consists of three main systems:

2.2.5.2.1 ANTENNAS AND LOW NOISE BLOCKS (LNBS)

A full hemispherical coverage and high-quality signal reception is achieved by two independent antennas, a monopole antenna and a quadrifilar helix (QFH) antenna used for receiving signals emitted from the sonde. The output of each antenna is fed to the respective LNB, which contains a low noise amplifier (LNA) and a narrow band pass filter (BPF). The LNA gives sufficient amplification to the received signal to compensate the signal attenuation due to cable loss.

2.2.5.2.2 A PISHAROTY SONDE RECEIVER

The Pisharoty sonde dual-channel FSK receiver accepts signals from both the antennas simultaneously, demodulates, decodes independently, and sends the data from both the channels to the data processing and display system (fig 2.3c). The dual-channel receiver system with high sensitivity and Reed-Solomon decoding ensures a good telemetry link (even up to a range of 300 km), and the data loss is less than 0.2% (i.e., fewer than 12 frames out of a total of 6000 frames) in the high-resolution 1-s data file for most of the cases. Error

detection schemes, including checksum verification, ensure good-quality data throughout the ascent.

2.2.5.2.3 A DATA PROCESSING AND DISPLAY SYSTEM

The data processing and display system, developed by ISRO and called Indian Radiosonde Software (IndRoS), is installed on either a Windows XP, Windows-7, or Windows-8 desktop, or a laptop computer with Ethernet interface for Transmission Control Protocol/Internet Protocol (TCP/IP) connectivity to connect to the receiver for data collection or system configuration (fig 2.3d).

2.2.6 REMOTE SENSING OF AROSOL

2.2.6.1 AQUA – MODIS

The Moderate resolution Imaging Spectrometer (MODIS) instrument flies on the Earth Observation System's (EOS) Terra and Aqua satellites. Both satellites are polar-orbiting, with Terra on a descending orbit (southward) over the equator about 10:30 local sun time, and Aqua on an ascending orbit (northward) over the equator about 13:30 local sun time. From a vantage about 700 km above the surface and a ±55° view scan, each MODIS views the earth with a swath about 2330 km, thereby observing nearly the entire globe on a daily basis, and repeat orbits every 16 days. Each scan is 10 km along track. MODIS performs measurements in the solar to thermal infrared spectrum region from 0.41 to 14.235 μm (Salomonson et al., 1989). Detailed specifications and components can be found at http://modis.gsfc.nasa.gov. The aerosol retrieval makes use of seven wavelength bands listed in Table 2.2. Table 2.2 shows the estimates of the central wavelength in each band (obtained by integration of the channel-averaged response functions).

MODIS channels 1, 2, 3, 4, 5, 6 and 7 have the central wavelengths of 0.66, 0.86, 0.47, 0.55, 1.24, 1.64 and 2.12 µm respectively. The MODIS orbit is separated into 5-minute chunks called 'granules'. Each granule is about 2030 km (about 203 scans of 10 km) along the orbital path. Each scan line has a swath about 2330 km, and at nominal (nadir) 1 km resolution, is covered by 1354 pixels. Due to spherical geometry, the size of each pixel increases from 1km at nadir to nearly 2km at the swath edges. Each granule is 1354 by 2030 pixels in this '1 km' resolution. Only data from MODIS daytime orbits are considered for retrieval.

Band#	**Bandwidth(µm)**	**Weighted Central Wavelength(µm)**	**Resolution(m)**
1	0.620 – 0.670	0.646	250
2	0.841 – 0.876	0.855	250
3	0.459 – 0.479	0.466	500
4	0.545 – 0.565	0.553	500
5	1.230 – 1.250	1.243	500
6	1.628 – 1.652	1.632	500
7	2.105 – 2.155	2.119	500

Table 2.2 MODIS bands and resolution

2.3 METHODOLOGY

2.3.1 ANALYSIS OF ANGSTROM EXPONENT 'α'

Wavelength, optical thickness, and atmospheric turbidity (haziness) are related through Angstrom's turbidity formula,

$$\tau_\lambda = \beta\lambda^{-\alpha} \tag{2.15}$$

Where β is Angstrom's turbidity coefficient, λ is wavelength in microns, and α is the Angstrom exponent. α and β are independent of wavelength, and can be used to describe the size distribution of aerosol particles and the general haziness of the atmosphere.

For two different wavelengths λ_1 and λ_2,

$$\tau_{\lambda 1} = \beta{\lambda_1}^{-\alpha} \tag{2.16}$$

$$\tau_{\lambda 2} = \beta{\lambda_2}^{-\alpha} \tag{2.17}$$

From 2.8 and 2.9,

$$\frac{\tau_{\lambda 1}}{{\lambda_1}^{-\alpha}} = \frac{\tau_{\lambda 2}}{{\lambda_2}^{-\alpha}} \tag{2.18}$$

$$\frac{ln\,\tau_{\lambda_1}}{ln{\lambda_1}^{-\alpha}} = \frac{ln\tau_{\lambda_2}}{ln{\lambda_2}^{-\alpha}} \tag{2.19}$$

$$ln\left(\frac{\tau_{\lambda_1}}{\tau_{\lambda_2}}\right) = -\alpha\, ln\left(\frac{\lambda_1}{\lambda_2}\right) \tag{2.20}$$

So, α is equal to

$$\alpha = -\left(\frac{ln\frac{\tau_{\lambda_1}}{\tau_{\lambda_2}}}{ln\frac{\lambda_1}{\lambda_2}}\right) \tag{2.21}$$

A typical range for α is 0.5-2.5, with an average for natural atmospheres of around 1.3±0.5. Larger values of α, when the τ value for the larger wavelength is much smaller than the τ value for the smaller wavelength, imply a relatively high ratio of small particles to large (r > 0.5 μ) particles. As τ for the larger wavelength approaches the τ for the smaller wavelength, larger particles dominate the distribution and α gets smaller.(Iqbal, 1983)

2.3.2 ANALYSIS OF SECOND ORDER ALPHA (α')

King and Byrne (1976) observed that the aerosols do not follow the Junge's distribution in a natural scenario. Also, the radii of the aerosols in a given atmosphere have a size distribution within a limited range. This departure from the ideal conditions assumed by Junge (1955) introduces a curvature in the ln τ_a v/s λ plot.

The second-order polynomial fit to examine the curvature in the AOD spectra can be written as

$$\ln \tau = \alpha_2(\ln \boldsymbol{\lambda})^2 + \alpha_1(\ln \boldsymbol{\lambda}) + \alpha_0 \qquad (2.22)$$

where α_0, α_1, and α_2 are constants. Coefficient α_2 represents the curvature observed in the spectral distribution of AODs.

2.3.3 MARINE ATMOSPHERIC BOUNDARY LAYER (MABL)

Stull, 1988 defined the atmospheric boundary layer as the part of the troposphere that is directly influenced by the presence of the earth's surface, and responds to surface forcing with a time scale of about an hour or less. Typically, due to aerodynamic drag, there is a wind gradient in the wind flow just a few hundred meters above the Earth's surface—the surface layer of the planetary boundary layer. Wind speed increases with increasing height above the ground, starting from zero due to the no-slip condition (fig 2.4a) (Wizelius, 2007).

Flow near the surface encounters obstacles that reduce the wind speed, and introduce random vertical and horizontal velocity components at right angles to the main direction of flow. This turbulence causes vertical mixing between the air moving horizontally at one level and the air at those levels immediately above and below it, which is important in dispersion of pollutants (Hadlock, 1998). When the balloon attached with a radiosonde payload is launched, the ascent rate of the balloon is affected as a result of vertical shear, hence inducing deviation from the estimated ascent rate in absence of vertical velocity component.

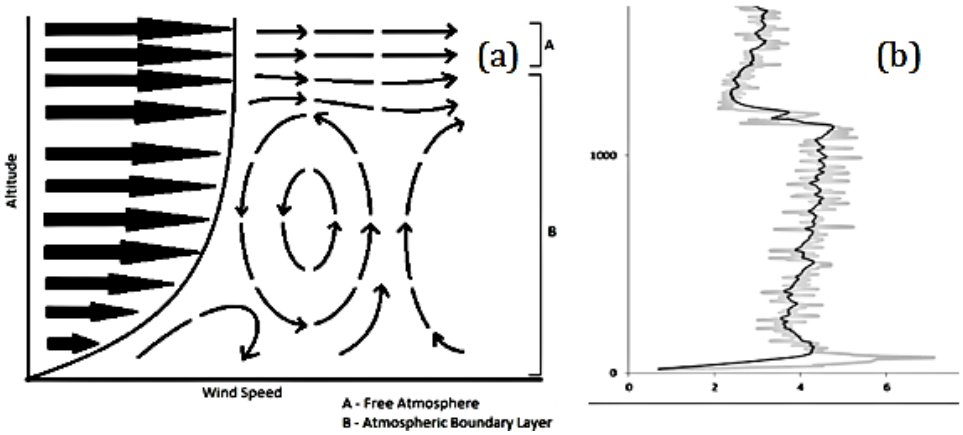

Fig.2.4: (a) Schematic of vertical mixing due to turbulence in boundary layer

(b) Ascent rate data from real radiosonde launch (0, 67^{o}E).

2.3.3.1 ESTIMATION OF ABL HEIGHT FROM 'θ', 'q', 'Γ_d'

Conventionally, the ABL height is estimated by computing the potential temperature 'θ', specific humidity 'q', dry lapse rate 'Γ_d', among a list of few other methods. In the current study, the above given parameters were calculated using the following equation.

Equation for Potential temperature,

$$\theta = T\,(p_0/p)^{k} \qquad (2.23)$$

where, θ is the potential temperature which is the temperature that an unsaturated parcel of dry air would have if brought adiabatically and reversibly from its initial state to a standard pressure, p_0 (typically 100 kPa) .

Equation for Specific humidity,

$$q = r_v / (1+r_v) \tag{2.24}$$

where 'q' is the specific humidity in a system of moist air, the (dimensionless) ratio of the mass of water vapour to the total mass of the system. It is related to the mixing ratio 'r_v' as given in the equation (2).

Equation for Dry lapse rate,

$$\Gamma_d = dT/dz \tag{2.25}$$

where Γ_d lapse rate is the rate at which atmospheric temperature T decreases with an increase in altitude 'z'. The individual profiles were generated to identify the capping inversion which marked the top of ABL.

2.3.3.2. TERMINAL VELOCITY OR RATE OF ASCENT FOR A RADIOSONDE BALLOON

The study carried out by Denny (2016), the terminal velocity of a weather balloon can be calculated using the equation (4)

Equation for terminal velocity,

$$(dz/dt) = \sqrt{(1 - M/M_{air}) \times (8r_0 g/3c_{D0})} \tag{2.26}$$

where, dz/dt is the terminal velocity achieved by a radiosonde of mass M. M_{air} is the mass of air displaced by the balloon of radius, r_0 with an aerodynamic drag coefficient, c_{D0}. This

velocity is found to be uniform in an ideal scenario where the atmosphere is uniformly dense and with an underlying assumption that there is no wind. But in a real scenario, the motion of air cannot be neglected.

2.3.3.3. ADJUSTMENT OF 'POSITIVE LIFT' FOR SLOWER ASCENT RATE OF RADIOSONDE BALLOON

A Pisharoty sonde weighs around 125g. The balloon used for the current study was a 600g latex balloon. Hence, in order to achieve a positive lift it is advisable to fill the balloon till it lifts approximately 1.5 times the total weight of the payload and the balloon itself. In this case would be 1.5 times of 725g (Balloon of 600g+ payload of 125g) which is approximately 1100g of lift. In this case, the balloon would steadily rise at a constant velocity of approximately 4m/s. A Pisharoty sonde generates and transmits data per second. Hence with a view to increase the number of point of observations, the balloon was filled 1.1times of the required lift, i.e. 800g which resulted in a much slower ascent rate of approximately 2.5m/s.

2.3.3.4. ESTIMATION OF MARINE ABL HEIGHT FROM 'w-PROXY' METHOD.

The slower ascent rate amplified the variations in the (dz/dt) of the balloon due to even minor variations in 'w' component of the wind motion vector which were caused due to the turbulence in wind. The turbulence being the inherent property of the ABL, gave an obvious and significantly higher values of the rate of ascent of the balloon within the ABL as compared to above the ABL (fig 2.4(b)). The reported value of the rate of ascent of the Pisharoty Sonde was exponentially smoothed with a damping factor of 0.9. This smoothed value is plotted for determination of ABL height. This method does not determine the 'w' component of the wind motion vector; rather it fundamentally depends on the effect of the presence of the 'w' wind vector. Hence, the name 'w-proxy' method.

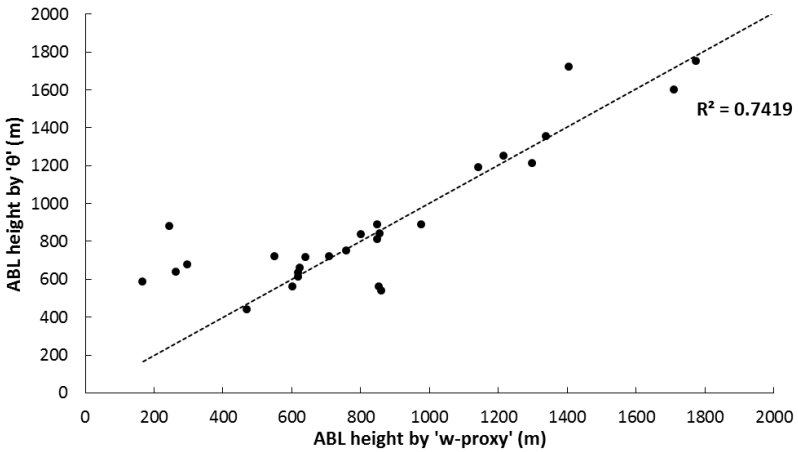

Fig. 2.5 (a) Correlation of the marine ABL height (m) potential temperature 'θ' and the 'w-proxy' method

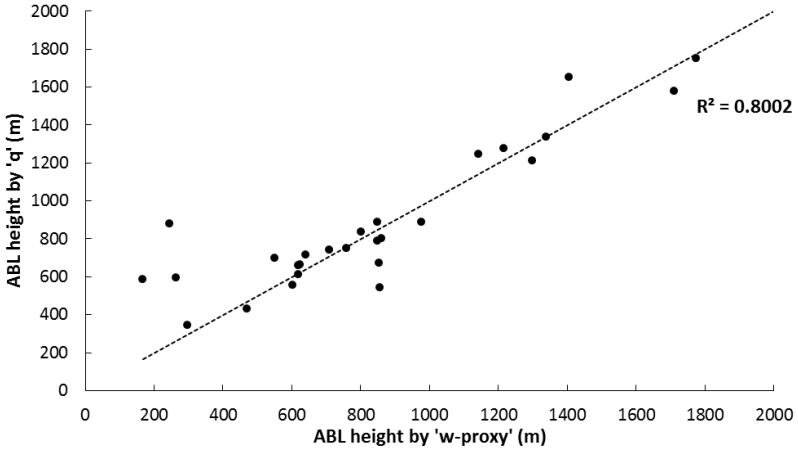

Fig. 2.5 (b) Correlation of the marine ABL height (m) specific humidity 'q' and the 'w-proxy' method

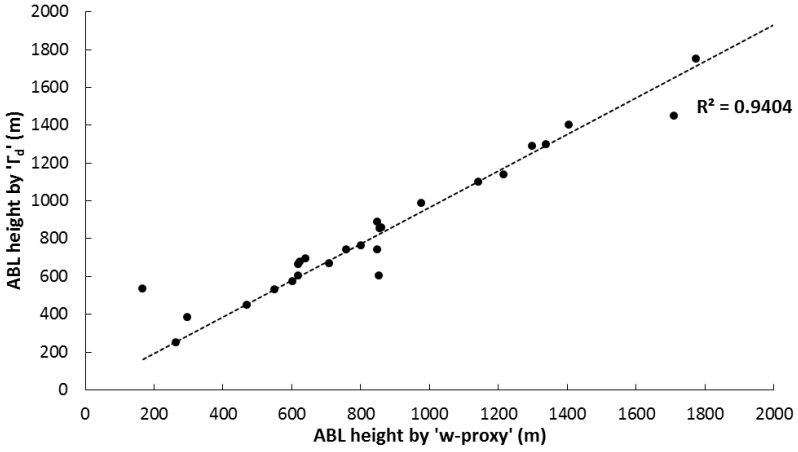

Fig. 2.5 (c) Correlation of the marine ABL height (m) dry lapse rate 'Γ_d' and the 'w-proxy' method

The marine boundary layer height was estimated using potential temperature 'θ', specific humidity 'q', dry lapse rate 'Γd' and the newly proposed 'w-proxy' method. The marine ABL height estimations using 'w-proxy' method correlated significantly with R^2= 0.74, 0.8 and 0.94 with the potential temperature (θ), specific humidity (q) and dry lapse rate (Γ_d) respectively making it a reliable method for ABL height estimations. (fig 2.5 (a), (b) and (c)). This method is used to find out the boundary layer height which was then used to estimate the aerosol radiative forcing.

2.3.4. RADIATIVE FORCING

Radiative forcing due to aerosols at any layer of the atmosphere is the net flux of upwelling and downwelling irradiances with and without aerosols at that layer (Charlson et al., 1992; Yu et al., 2001). An estimation of the difference in the flux at top of the atmosphere (TOA) and at the surface (SUR) with aerosol and without aerosol gives an estimation of forcing in the atmosphere.

$$ARF = Flux\ (NET)_{TOA/Surface\ with\ aerosols} - Flux\ (NET)_{TOA/\ Surface\ without\ aerosols} \quad (2.27)$$

And atmospheric forcing,

$$ARF_{ATM} = ARF_{TOA} - ARF_{SUR} \quad (2.28)$$

2.3.4.1 HEATING RATE

The net atmospheric forcing indicates the amount of radiant energy absorbed by the atmosphere caused by the presence of aerosols which is then converted into heat. The resulting atmospheric heating rate is (Liou 2002).

$$\frac{\partial T}{\partial t} = \frac{g}{C_p}\frac{\Delta F}{\Delta P} \quad (2.29)$$

where $\partial T/\partial t$ is the heating rate (s^{-1}), g is the acceleration caused by gravity, C_p the specific heat capacity of air at constant pressure (1006 J $kg^{-1}K^{-1}$), and P is the atmospheric pressure and ΔP is the pressure difference between the top and bottom layer of the atmospheric layer considered. The heating rate estimated in this study is a theoretical, static, 1D estimate, as a result of absorption of short wave flux. A realistic estimate would incorporate the effect of radiant energy in the long wave region and the boundary layer processes.

2.3.5 MODELS

2.3.5.1 OPTICAL PROPERTIES OF AEROSOL AND CLOUD (OPAC)

The model OPAC (M. Hess *et al*, 1998) consists of two parts viz; the first part is the data set of the microphysical properties and the resulting optical properties of cloud and aerosol component for different humidity conditions. This datasets are available for 6 types of water clouds, 3 ice clouds and 10 aerosol components for 61 wavelengths between 0.25 and 40 μm for aerosol and water clouds while at 67 wavelength between 0.28 to 40 μm for ice clouds. The second part consists of FORTRAN code, enabling the user to extract this dataset and subsequently to compute additional optical parameters and to calculate optical properties of mixtures of the stored clouds and aerosol components. All the data are stored as ASCII files and are for 1 particle cm^{-3} in each case which describes the effective properties of the mixture of all particles in the size distribution. All the values are multiplied by number density. To account for water uptake by aerosol component, data for eight values of relative humidity are given as 0%, 50%, 70%, 80%, 90%, 95%, 98% and 99%.

The input file to OPAC consist of five parts namely cloud or aerosol type, height profile, wavelength, relative humidity and optical parameters. In the cloud or aerosol type, it is possible to select one of the default clouds or aerosol types. However, a new mixture can also be defined by giving number density of up to five aerosol components from seventeen

components. In the height profile section, five height profiles have to be entered. If new mixture is chosen, measured height profile has to be incorporated. In the next section i.e. the wavelength section, desired wavelength can be selected by typing 1 (0 for deselect) against the wavelength.

2.3.5.2 SBDART

Santa Barbara DISORT Atmospheric Radiative Transfer (SBDART) model (Ricchiazzi et al., 1998) to compute the net flux at TOA and SUR. SBDART is a software tool that computes plane-parallel radiative transfer in clear and cloudy conditions within the earth's atmosphere and at the surface. All important processes that affect the ultraviolet, visible, and infrared radiation fields are included. The code is a combination of discrete ordinate radiative transfer (DISORT) module, low-resolution atmospheric transmission models (LOWTRAN), and Mie scattering results for light scattering by water droplets and ice crystals. The code is well suited for a wide variety of atmospheric radiative energy balance and remote sensing studies.

The model requires the input dataset as follows,

- Solar Geometry
    - Location (Lat. /Long.)
    - Date/Time of observation
- Spectral Range (0.25-4um)
- Atmospheric Profile
    - Tropical/Sub-tropical/Antarctic
    - Surface Albedo
- Aerosol Parameters
    - Background – Oceanic/Continental
    - Aerosol Optical Depth (0.5µm)

- Specific AOD due to BC at 0.5µm
- MABL height

The aerosol models previously available in SBDART 2.4 were typical rural, urban, maritime in lower atmosphere and fresh or aged volcanic, meteoric, and upper-tropospheric background aerosols from the upper atmosphere. In addition to these, aerosol models of mineral (coarse R_e=5.0 and fine R_e=1.0), Soot, (R_e=0.1 and R_e=0.2) and Sulphate (R_e=0.2 and R_e=0.4) are also included in the version of SBDART 4.36.

The SBDART 4.36 has the flexibility of adjusting 2 layers of aerosols in troposphere with lower and upper boundaries between 0 to 10Km and one layer in stratosphere with lower boundary and upper boundary at any altitude from 10 to 40Km. The model calculates the flux from top down, top up, bottom down and bottom up.

2.3.5.3 HYSPLIT

It is observed that the aerosols sampled at one location are a composite of locally generated aerosol and the one transported from long distances. This transported component can be studied using the Air Resources Laboratory's Hybrid Single-Particle Lagrangian Integrated Trajectory (HYSPLIT) model. HYSPLIT is a complete system for computing both simple air parcel trajectories and complex dispersion and deposition simulations. The model calculation method is a hybrid between the Lagrangian approach, which uses a moving frame of reference as the air parcels move from their initial location, and the Eulerian approach, which uses a fixed three-dimensional grid as a frame of reference. In the model, advection and diffusion calculations are made in a Lagrangian framework following the transport of the air parcel, while pollutant concentrations are calculated on a fixed grid.

2.3.5.3.1 THEORY

2.3.5.3.1.1 VERTICAL MOTION CALCULATION

In most circumstances the input meteorological data will contain a vertical motion field, usually in pressure units, and regardless upon which vertical coordinate system these input data are provided, the vertical velocity field is almost always relative to the meteorological model's native terrain-following sigma coordinate system. The trajectory and dispersion model calculations can use these data fields directly because the model's internal coordinate system will always be terrain following regardless of the form of the input data.

This is one of the primary reasons that the input data need to be remapped to a common vertical coordinate system. When the vertical motion fields are missing, or perhaps there are some special conditions required for a simulation, the dispersion model has an option to replace these fields with an internally calculated vertical velocity based upon an assumption that the pollutant parcel is transported on some other surface.

The input data can be remapped to various surfaces by computing the velocity ($W\eta$) required to maintain a parcel on the selected (η) surface, given the slope of the surface and its local rate of change and where the surfaces, η, can be isobaric (p), isosigma (σ), isopycnic (ρ), or isentropic (θ).

2.3.5.4.2 ADVECTION

The basis of any Lagrangian model is that the dispersion is computed following the particle or puff. That is, the advection of a particle is computed independently. Hence once the basic (u, v, w) velocity components of meteorological data have been processed and interpolated to the internal model grid, trajectories (the integrated advection term of a particle) can be computed to test the advection components of the model. The advection of a particle or puff

is computed from the average of the three dimensional velocity vectors for the initial-position P (t) and the first-guess position P'(t+Δt). The velocity vectors are linearly interpolated in both space and time.

The first guess position is

$$P'(t+\Delta t) = P(t) + V(P,t)\,\Delta t \qquad (2.30)$$

And the final position is

$$P(t+\Delta t) = P(t) + 0.5\,[\,V(P,t) + V(P',t+\Delta t)]\Delta t \qquad (2.31)$$

The integration method is very common (Kreyszig, 1968) and has been used for trajectory analysis (Petterssen, 1940; Draxler, 1996) for quite some time. Higher order integration methods were investigated and rejected because as long as the data observations are linearly interpolated from the grid to the integration point, higher order methods will not yield greater precision. Trajectories are terminated if they exit the model top, but advection continues along the surface if trajectories intersect the ground. The integration time step (Δt) can vary during the simulation. It is computed from the requirement that the advection distance per time-step should be less than the grid spacing. The maximum transport velocity U_{max} is determined from the maximum particle/puff transport speed during the previous hour. Time steps can vary from 1 minute to 1 hour and are computed from the relation, U_{max} (grid-units min-1) Δt (min) < 0.75 (grid-units).

2.3.5.4.3 TRAJECTORY FREQUENCY ANALYSIS

The trajectory frequency analysis is carried out with the help of multiple trajectories being calculated from the point of observation. The region under observation is divided in to user defined grid cell of dimensions e.g. 1^o X 1^o. Based on the residence time of the air parcel in each grid cell, a contour plot is generated showing the percentage contribution of each grid

cell to the air parcel reaching the point of observation (in case of back-trajectory analysis). Thus it becomes easy to demarcate the contribution from different regions to the total aerosol composition observed at the study area.

The Trajectory frequency analysis begins with counting the number of trajectories that fall within each grid cell that covers the area. The trajectory frequency (F) is the sum of the number of trajectories (T) that passed through each (i,j) grid cell divided by the total number (N) of trajectories analysed given by:

$$F_{i,j} = 100 \text{ X } (\Sigma \, T_{i,j} / N) \qquad (2.32)$$

2.3.6 FACTOR 'S'

In order to understand the role of chlorophyll-*a* in influencing the abundance of the fine mode aerosol particles, the coefficient of correlation (R^2) between the chlorophyll-*a* concentration and fine particle percentage has to be estimated. However, due to unavailability of above data, the estimation of R^2 is not possible. Hence, a factor 'S' is introduced, which has been estimated as follows.

S = Fine Particle Percentage X Chlorophyll-*a* Conc. (2.33)

It is seen in the data that the values of S normally vary between 2 to 12. 2 indicate minimum efficiency of chlorophyll-a in genesis of fine mode particles and 12 and above indicate high to very high efficiency.

2.4 GENERAL METEOROLOGY

The general meteorology of different zones of the study area is described, beginning from the northern most zone to southernmost ones.

2.4.1 TROPICAL INDIAN OCEAN

2.4.1.1 EQUATOR

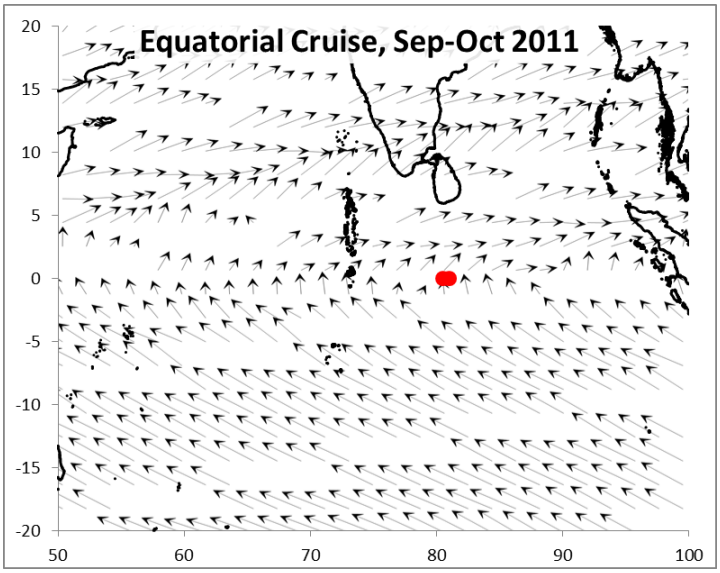

Fig 2.6(a) Wind pattern observed during the Equator cruise. Time series locations are marked.

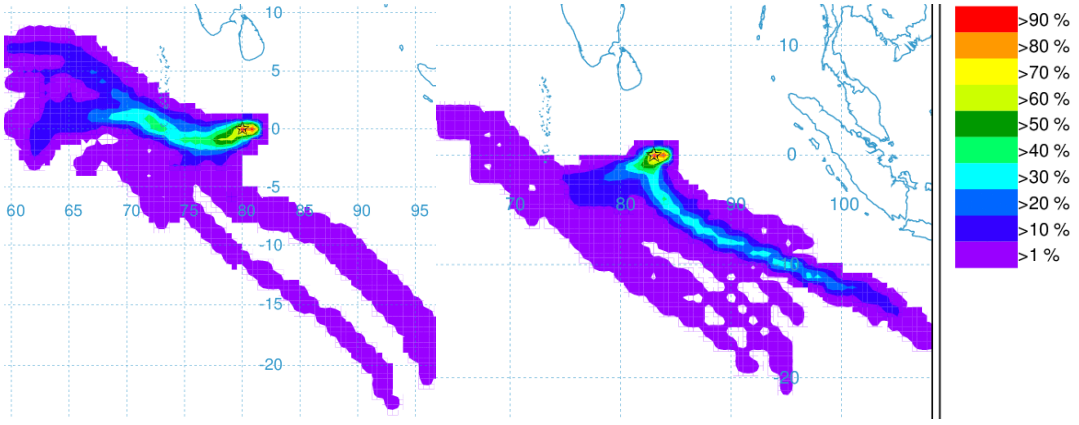

Fig 2.6(b) HYSPLIT back trajectory frequency analysis for the cruise in equatorial region.

The wind pattern over the Indian Ocean region during September-October 2011 is presented in the fig (2.6a, b). The wind pattern in Southern hemisphere shows South Easterly winds which change the direction approximately at the equator and maintain a general direction from Southwest to Northeast. During this period, South-west monsoon winds weaken over the Indian subcontinent. Hence predominant aerosol prevailing are maritime in nature.

The HYSPLIT trajectory frequency analysis was generated to identify the regions from where air parcels are originated. Fig (2.6b) shows that entire aerosol content is from oceanic region. More than 80% is locally generated from the grid of 1^{o} X 1^{o}. The contribution of dust and anthropogenic 'BC' from the Maldives islands is seen to be from 1% up to 30%.

2.4.1.2 SOUTH-WEST TROPICAL INDIAN OCEAN (SWTIO)

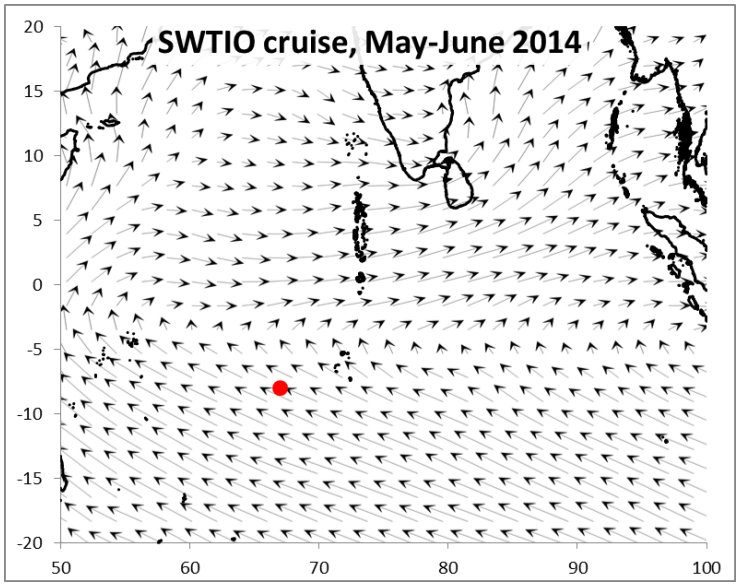

Fig 2.7(a) Wind pattern during the SWTIO cruise. Time series location is marked.

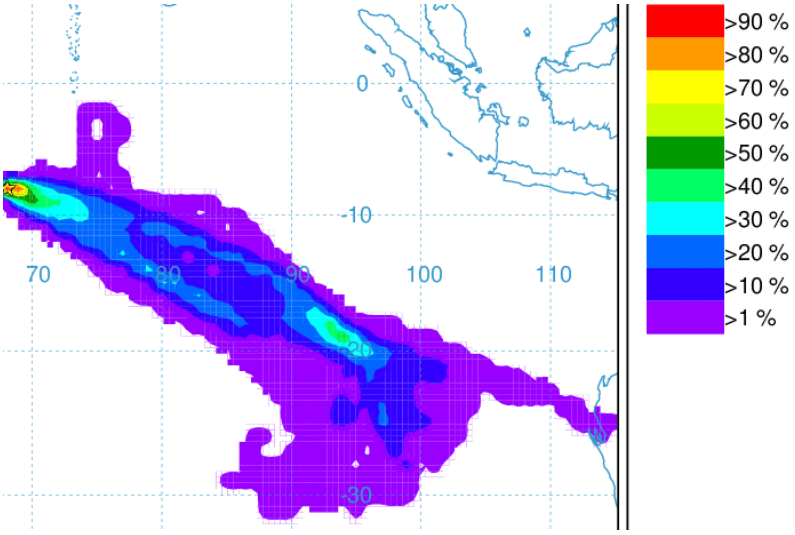

Fig 2.7(b) HYSPLIT back trajectory frequency analysis for the cruise in equatorial region.

The monsoon normally arrives at the southern tip of India by first week of June. Hence, the monsoon wind is experienced during this cruise. As a result, in the southern hemisphere, the wind is from south-east which then forms south-west monsoon winds. Although major contribution is from the oceanic region, a remote contribution of greater than 1% from Australian coast is also being present (fig 2.7a, b).

2.4.1.3 INTERNATIONAL INDIAN OCEAN EXPEDITION-2 (IIOE-2)

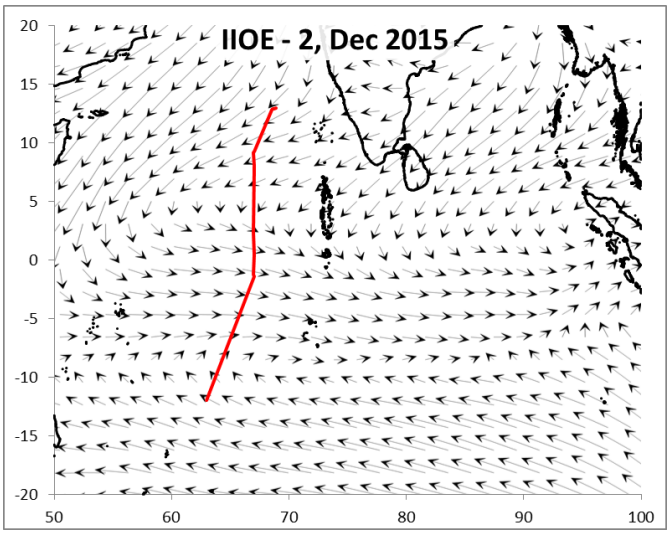

Fig 2.8(a) Wind pattern during the IIOE-2 cruise. Cruise track is shown.

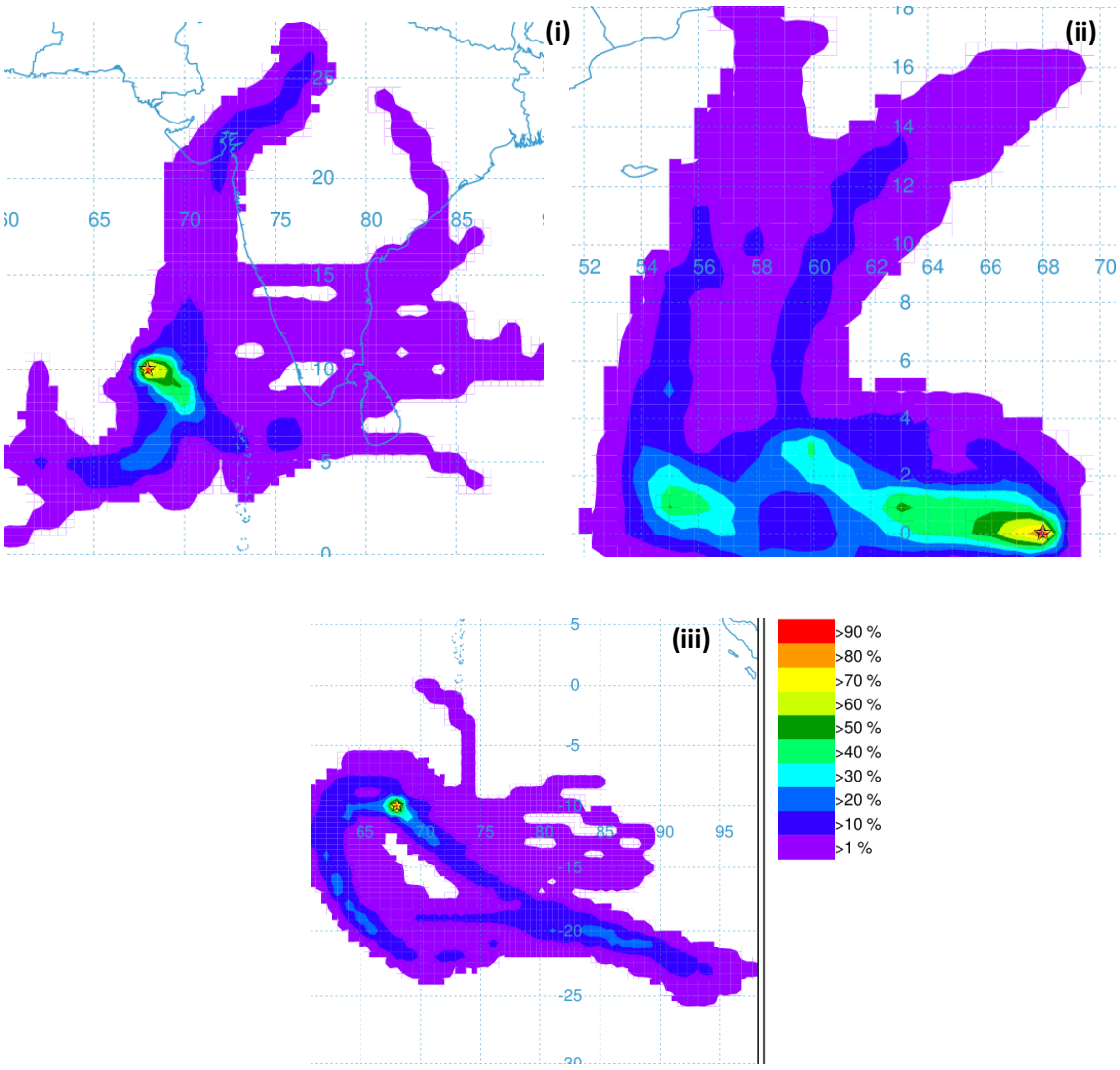

Fig 2.8(b) HYSPLIT back trajectory frequency analysis for the cruise in (i) Zone 1 (ii) Equator (Zone 1) (iii) Zone 2 during IIOE-2 expedition.

During the IIOE-2 cruise, the ITCZ is seen to be present at approximately 4^{o}S (fig 2.8a). The trajectories reaching the location in the north of equator and the equator show continental input of up to 20% for the location nearer to the land (fig 2.8b). As the cruise proceeds away from the land, the effect of continentally produced aerosol reduces to 1-10% near the equator. The location to the south of the ITCZ shows major contribution of oceanic region. Hence it is appropriate to assume that the aerosols encountered in this region are of oceanic origin.

2.4.2 SOUTHERN OCEAN EXPEDITION

The three zones were traversed up to approximately 55^{o}S during all the SOE cruises. SOE 6 started from Goa and has traversed along a track on the west coast of India, where the effect of retreating monsoon was not as effectively experienced as on the east coast. SOE 7 and SOE 8 were initiated from Chennai. This is the reason for different wind patterns in different Zones though the study period was somewhat similar. In Zone 1, it is clear that the wind flowing from Indian mainland is the major contributor. As one proceeds towards the northern edge of ITCZ, the contribution from the continent is reduced to 1-10% (fig 2.9(a), (b), and (c)), (fig 2.10(a), (b), (c)).

In Zone 2, the wind pattern and HYSPLIT confirm the contribution of marine aerosol to the composite aerosol (fig 2.9(a), (b), and (c)), (fig 2.11(a), (b), (c)). The aerosol content in Zone 3 is almost similar to that of Zone 2 with an exception of dust from Kerguelen Islands, which amounts to an order of 1 to 10% (fig 2.12(a), (b), (c)). Moreover, the region also falls under diesel powered-ships trade routes; which implies the presence of BC mass concentration.

The wind pattern encountered over the Indian Ocean region during the time of SOE cruises is shown in fig 2.9(a), (b), and (c). The first most noticeable feature seen in the wind pattern is the delineation of ITCZ. The approximate position of ITCZ ranges from 10^{o}S to 15^{o}S depending on the time of the SOE cruises. SOE-6 and SOE-8 witnessed wind from north-eastern direction which gradually changed into westerly winds as the cruise approached ITCZ (fig 2.9(a), (c)). During the SOE-7 (fig 2.9(b)), rainfall of 150-200mm (TRMM data, neo.sci.gsfc.nasa.gov) was reported at the eastern coast of India. A cyclonic circulation of wind is seen off eastern Indian coast over the Bay of Bengal. The region to the south of ITCZ mainly witnessed easterly winds up to approximately 40^{o}S beyond which the region is dominated by westerly winds. This observation holds true for SOE-6 and SOE-8. During

SOE-7, an anti-cyclonic circulation is seen over the region centred on approximately 35^{o}S, 82^{o}E.

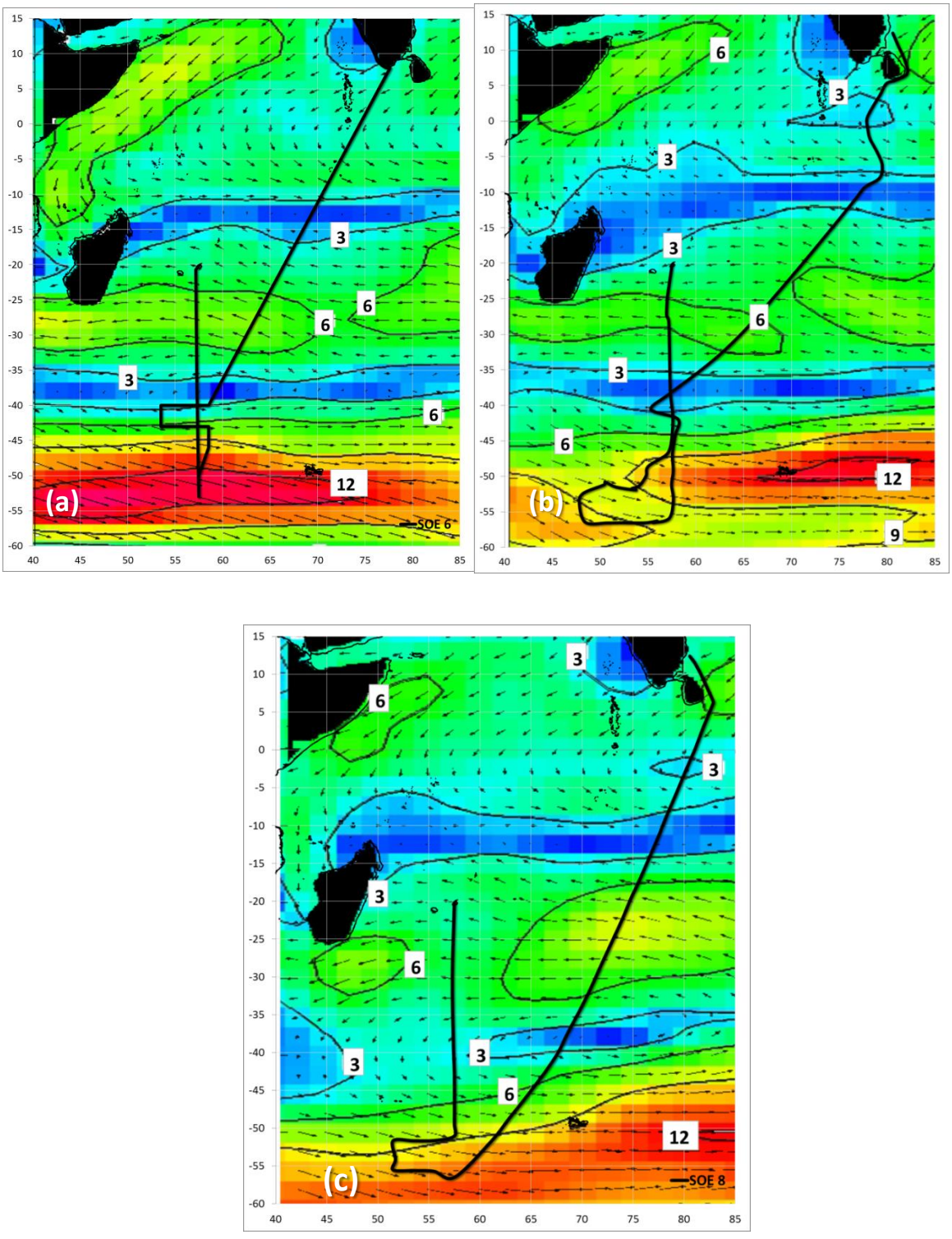

Fig 2.9 Wind pattern during the (a) SOE-6 (b) SOE-7 (c) SOE-8 cruises. The length of wind vectors represents the wind speed; the boxes shown for each of the contours indicate wind speed in m/s.

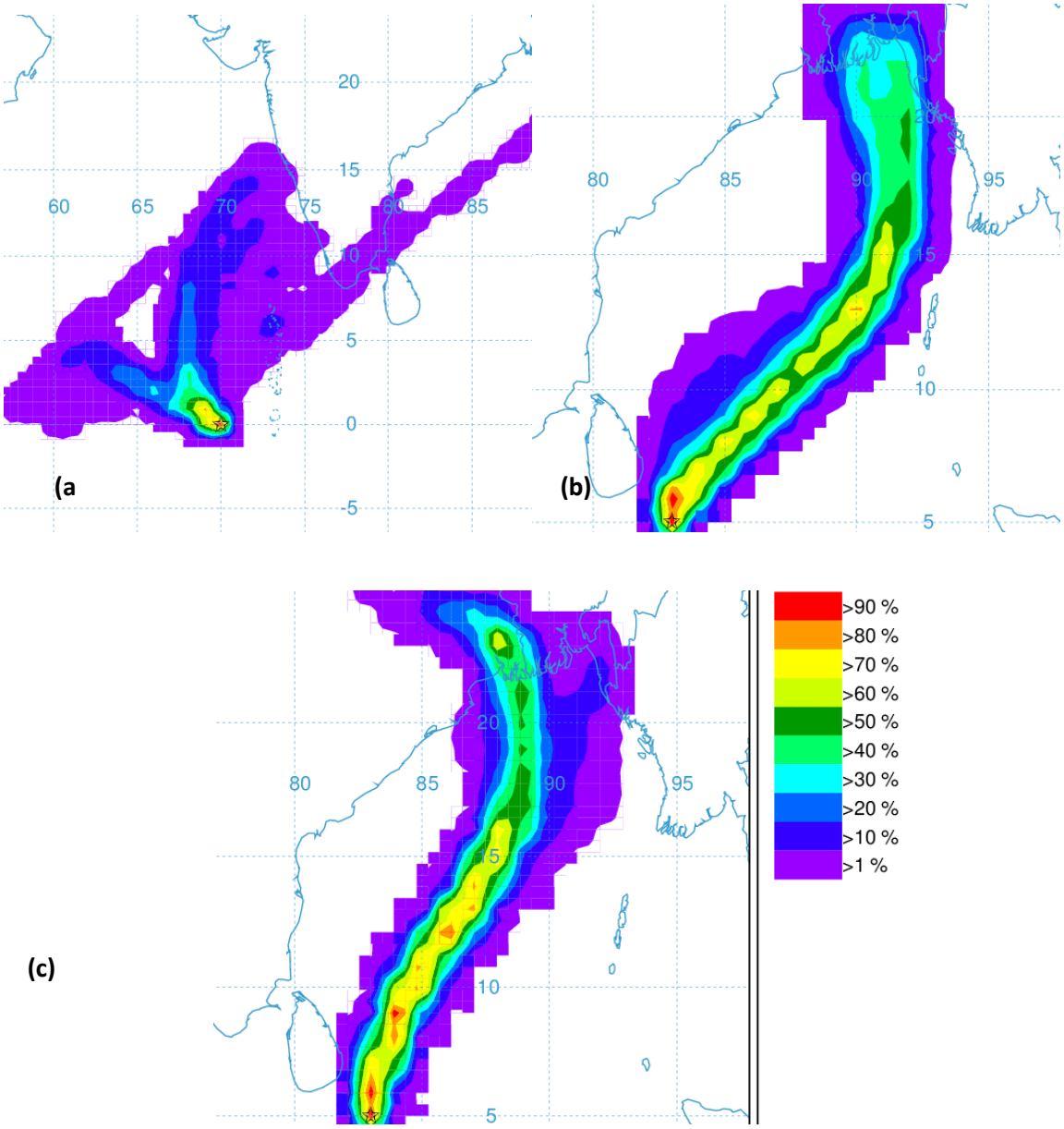

Fig 2.10 HYSPLIT back trajectory frequency analysis carried out in Zone 1 during (a) SOE-6 (b) SOE-7 (c)SOE-8 cruises.

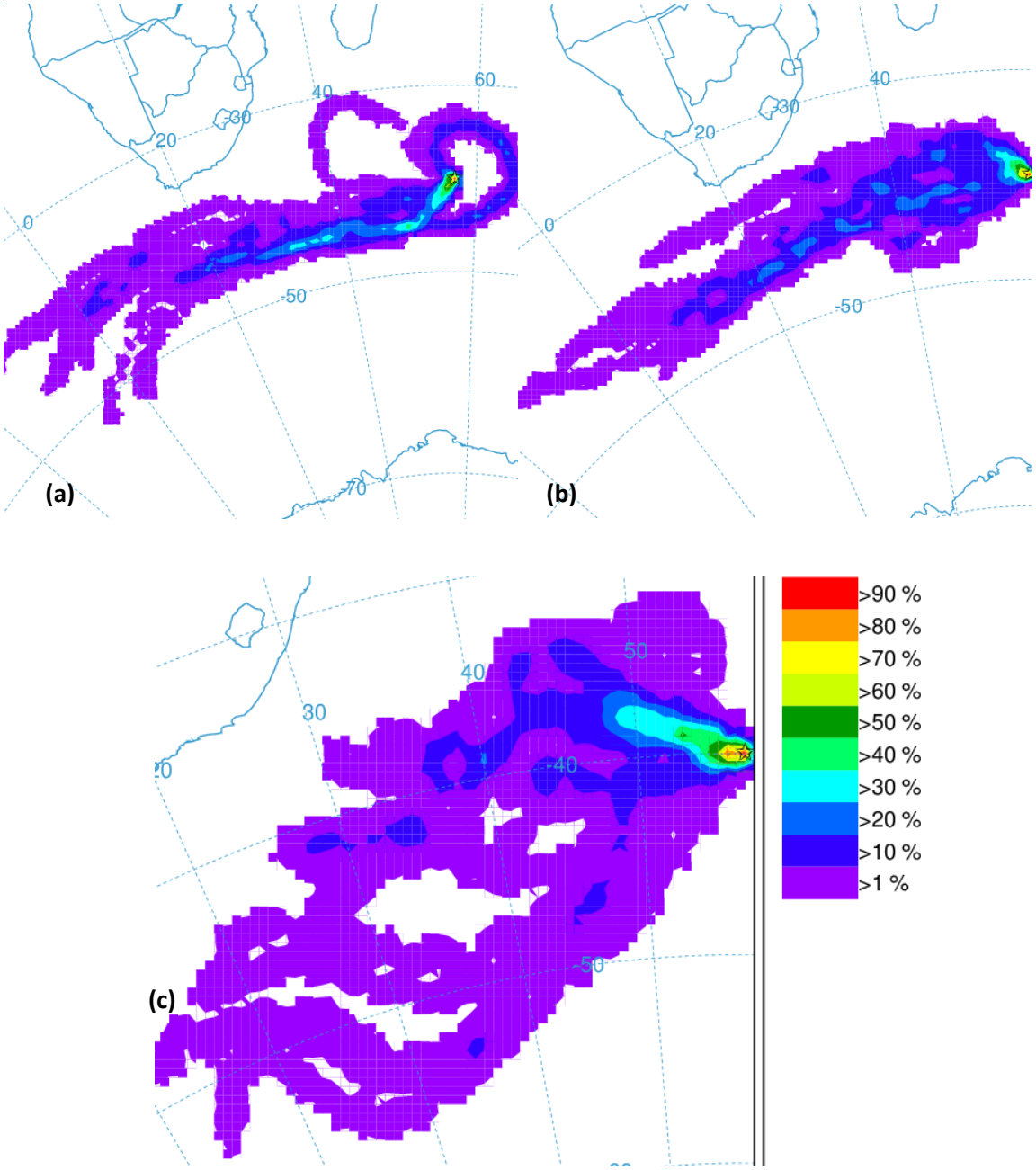

Fig 2.11 HYSPLIT back trajectory frequency analysis carried out in Zone 2 during (a) SOE-6 (b) SOE-7 (c)SOE-8 cruises.

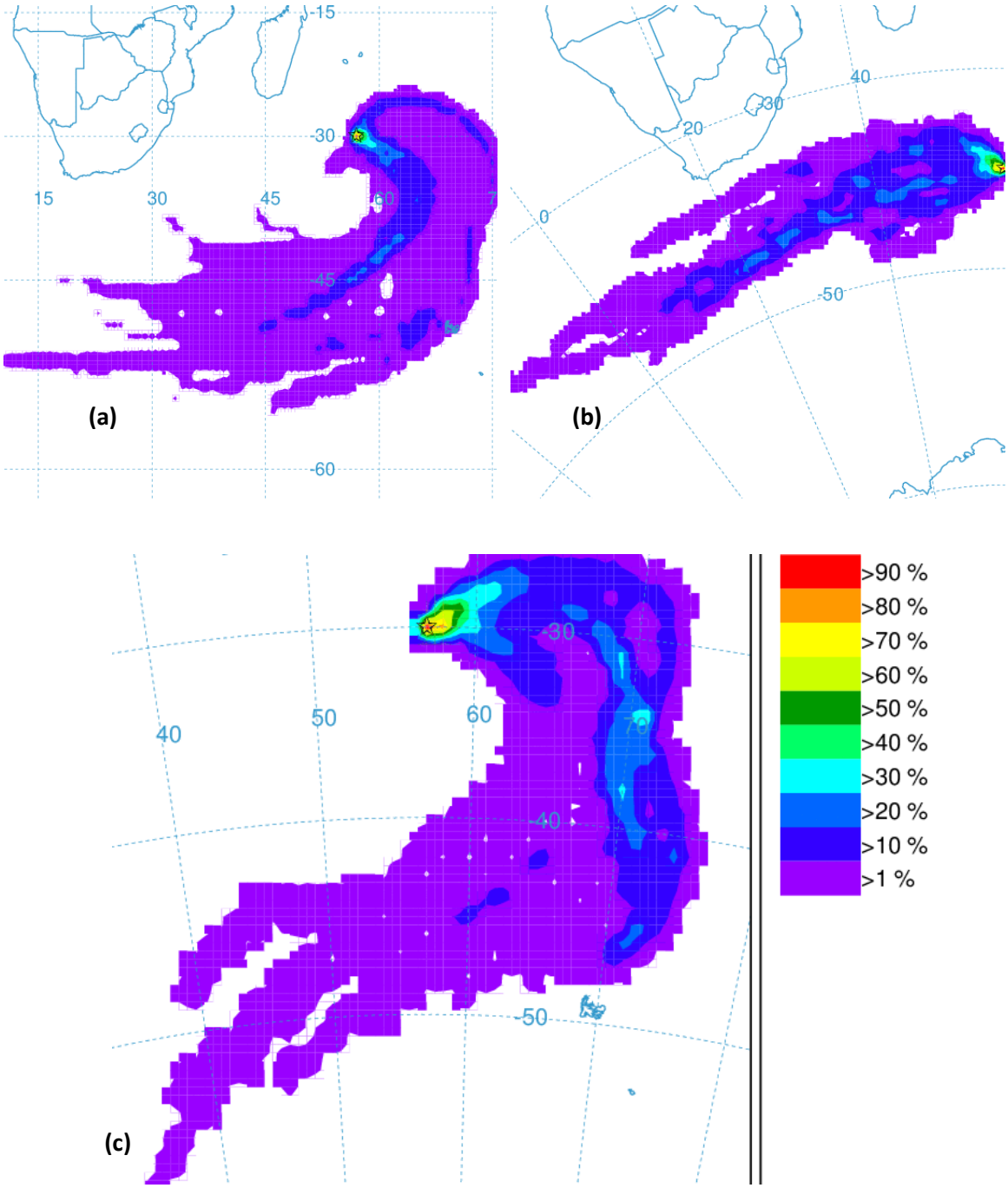

Fig 2.12 HYSPLIT back trajectory frequency analysis carried out in Zone 3 during

(a) SOE-6 (b) SOE-7 (c) SOE-8 cruises.

2.4.3 ANTARCTICA

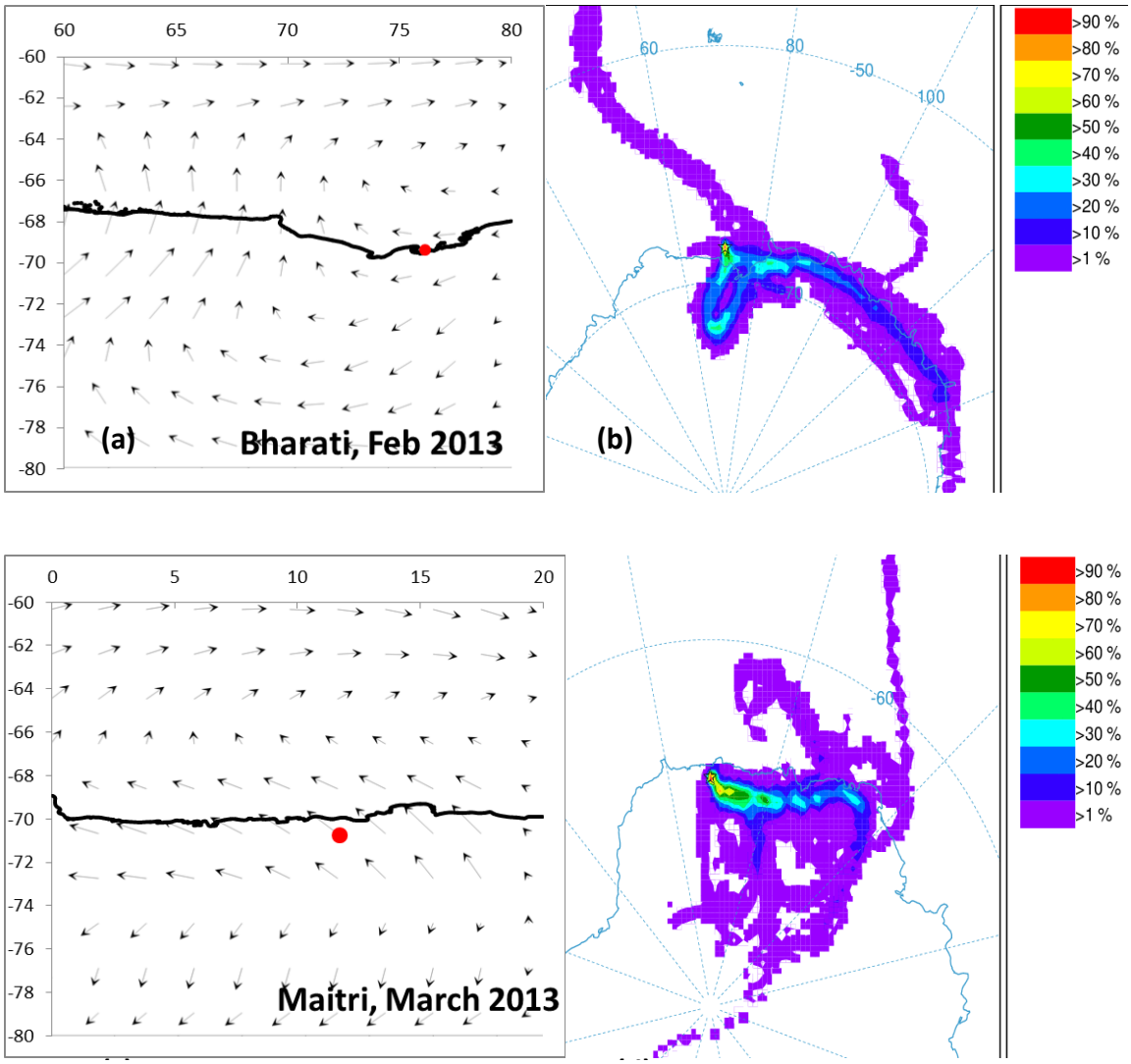

Fig 2.13 Wind pattern during the 32nd Expedition to Antarctic (a) Bharati (b) Maitri stations. HYSPLIT back trajectory frequency analysis carried out at (c) Bharati (d) Maitri stations.

The wind in Bharati region mainly blows from the east to west along the Antarctic coast (fig 2.13 (a)). Since Bharati is situated on the coast with a bay to its South and East, the wind might be carrying aerosols of maritime origin. However in Maitri region, the case is different. The major wind direction observed is from South-east to north-west (fig 2.13 (c)). Since Maitri is situated about 125km to the south from Antarctic coast, the south-east winds might be considered to transport only the continent based aerosols. An important point to note here

is the continent based aerosols will comprise of sulphate droplets and sea salt particles (Hess et al., 1998). In addition to that, mineral dust can also be present since the point of observation i.e. Maitri station is situated in Schirmacher oasis which has exposed land surface during the summer.

The trajectory frequency analysis of Bharati and Maitri provides the evidence of minimum intrusion of wind from north of Antarctic continent. In fact the contribution from the coastal oceanic region is up to 1-10% (fig 2.13(b)). The Bharati station is situated near the coast with a bay to its south. Hence, presence of oceanic aerosols would be predominant which contribute up to 30-40% to the total aerosol content. The air parcel circulates along the coast and inland before reaching the point of observation. Maitri station is built on the Schirmacher oasis about 125Km away from the coast. However, it has an equal contribution from ocean as well as inland regions(fig 2.13(d)).

MICROPHYSICAL CHARACTERISITCS OF AEROSOLS

3.1 INTRODUCTION

Wavelength dependence of aerosol optical depth (AOD) is governed by the physical and chemical properties of aerosols. In addition, when the columnar AOD is a result of multimodal distribution of aerosols, a curvature is introduced in the relationship between ln (AOD) and ln (λ). This is accounted by applying second order polynomial fit to the Angstrom equation by applying a second order polynomial fit to the ln (AOD) and ln (λ) data. Schuster et al. (2006) found that the concentrations of fine mode aerosols strongly change sign of curvature from negative to positive.

Moorthy et al. (1991) have studied the seasonal variability of bimodal size distributions over the west coast of India. Following which, the curvature effect on AOD retrieval over different regions of Indian subcontinent and over the Indian Ocean was extensively investigated (Beegum et al., 2009; Kalapureddy et al., 2009; Kaskaoutis et al., 2011; Kedia et al., 2011; Soni et al 2011; Gularia et al., 2012). The results from Integrated Campaign of Aerosols, gases and Radiation Budget (ICARB) marked the importance of several factors affecting AOD such as proximity to the coast, meteorological parameters, in-situ and long range transport (Moorthy et al., 2008; Kedia et al., 2008; Nair et al., 2008).

Several studies were carried out to understand the spectral dependence of aerosols; most of them concentrating over the Indian subcontinent and Indian Ocean sector north of equator. However, the information on the spectral dependence of aerosol in the sub-tropical and Southern ocean region, south of 40^{o}S, is inadequate due to inaccessibility and non-availability of data.

The zonation is essential due to two important factors. The first is that the surveys were carried out in different times and the second the area has been subjected to mesoscale phenomena like ITCZ and Subtropical convergence.

The size distribution of aerosols is one of the most conspicuous properties of atmospheric aerosols in course of learning their impact on insolation and hence climate. The knowledge of aerosol size distribution alone provides insight to many processes in the Earth's atmosphere. Consequently it becomes crucial to understand the size distribution of aerosols to clearly understand their effect on both climate (Charlson et al., 1987; Russell et al., 1994) and human health (Künzli et al., 2000).

The effect of aerosols on the climate is classified usually into direct effect; the ability of aerosols to scatter and absorb the incoming short wave and outgoing long wave solar radiation (Charlson et al., 1992) and indirect effect, the ability of aerosols to act as cloud condensation nuclei; thereby affecting the cloud droplet size distribution, droplet concentration, optical properties, precipitation rate and lifetime of clouds (Twomey, 1977; Ackerman et al., 2000; Rosenfield, 2000).

The aerosol size studies are mainly focussed on locations that consist of either urban/semi-urban landmass or oceans adjacent to densely populated and polluted coastal belt (Moorthy et al., 1997; Nair and Moorthy, 1998; Moorthy and Satheesh, 2000; Srivastava et al., 2008). In the Indian context, the area nearby Indo-Gangetic Plains are given special attention (Day et al., 2004; Singh et al., 2004). However, the comparatively lesser focus was given to open ocean; specifically the Indian Ocean sector of Southern Ocean region owing to its remote nature. The site specific nature of aerosol properties is clearly reported by Ganesh et al. (2008); Gadhavi et al.,(2004) and Chaubey et al., (2011) from the surveys carried out in the coastal areas of Antarctic and the interior Antarctic region, which are basically pilot dataset.

In order to understand the microphysical characteristics of aerosols over different regions, the spectral variations of AOD have been studied during the expeditions SOE-6,

SOE-7, SOE-8 and during the 32nd Indian Scientific Expedition to Antarctica at Bharati and Maitri stations(fig 2.1). The Angstrom exponent '**α**' and the second order derivative of **α**, viz. **α'** were analysed. The measurements of size segregated mass concentration of aerosol were also carried out in the Indian Ocean sector of Southern ocean, using the QCM model PC-2X.

In this chapter, microphysical properties of aerosols based on spectral dependence of AOD inferred from the data obtained during the expeditions to the Equator, SOE-6, SOE-7, SOE-8 and IIOE-2 and 32nd Indian Scientific Expedition (fig 1) and the size characterisation of aerosols are presented.

3.2 Zonal Variability of Aerosol Optical Depth

The AOD spectra obtained during different cruises are shown in the fig 3.1. The data obtained near the equator shows usual AOD spectra following the Angstrom's equation. Since the position of ITCZ is a major decisive factor for demarcating zones as explained in Chapter 2, Section 2.1.1, the data from the Equator (fig 3.1a) is categorized as Zone 2 data. In fig 3.1b, c, d, e and f, the origin of data is indicated.

The observation closest to the land lying to the north of ITCZ (Zone 1) depicts the highest AOD, whereas the values drop down drastically as one proceeds towards south (Zone 2) (fig 3.1 b, c, d, e). This is due to the wind pattern prevailing during the Southern Ocean cruises in the month of December, as shown in Chapter 2.

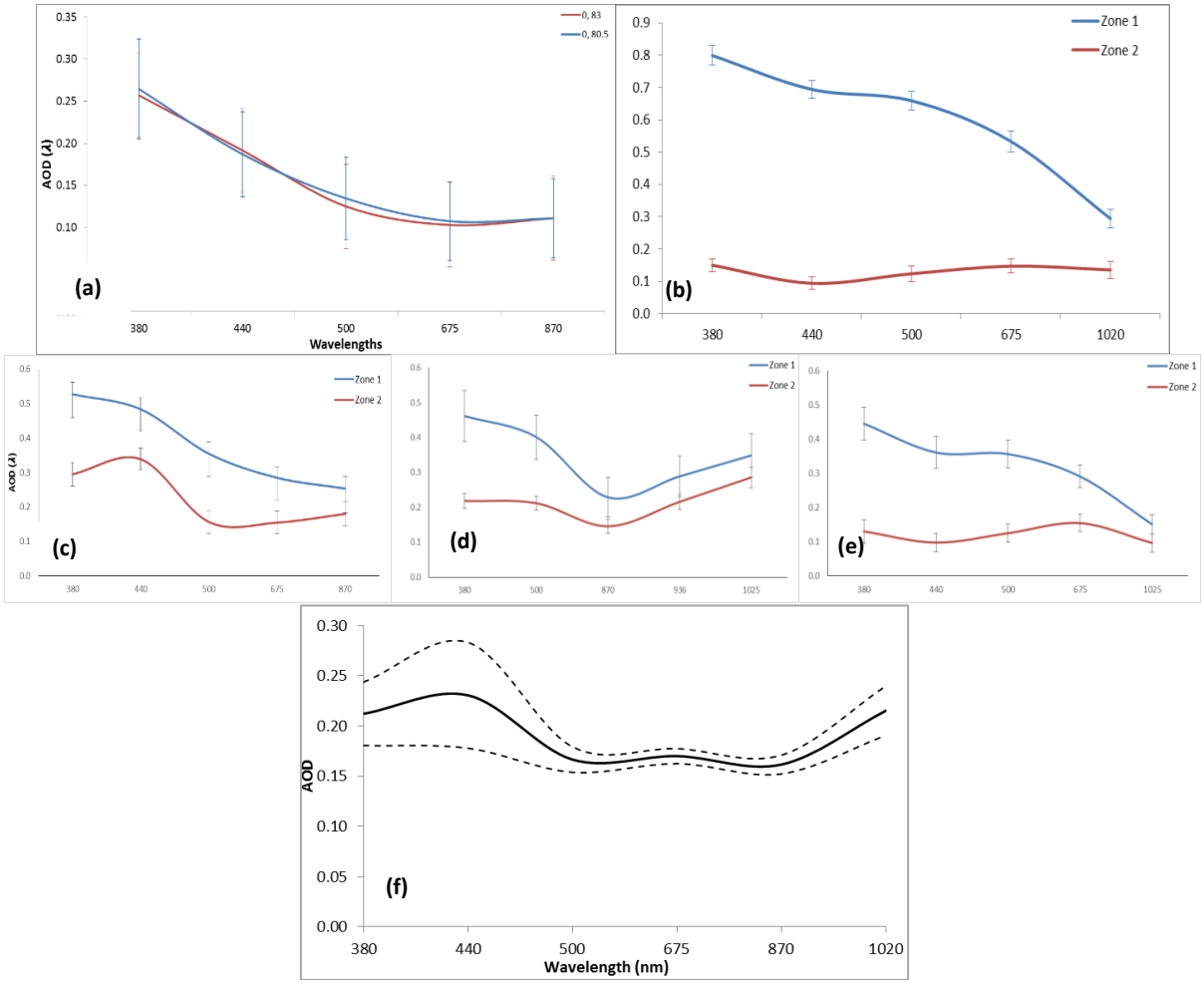

Fig 3.1: Spectral variability of AOD obtained from different cruises traversed across different zones
(a) Equator Cruise (b) IIOE-2 (c)SOE – 6 (d)SOE – 7 (e) SOE – 8
(f) Composite results of SOE-6, SOE-7 and SOE-8

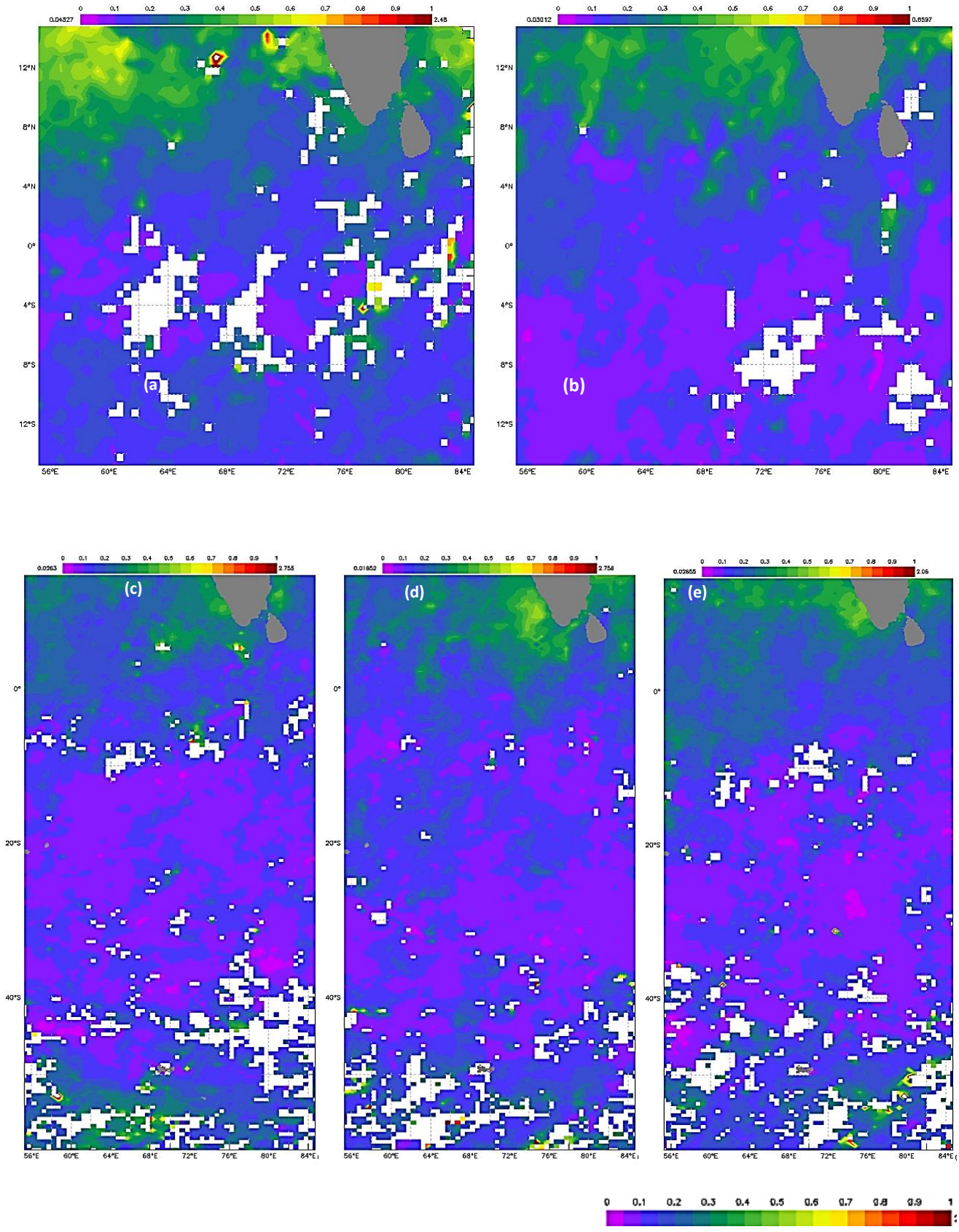

Fig 3.2: Satellite derived $AOD_{0.5}$ obtained during the period of different cruises.
(a) Equator Cruise (b) IIOE-2 (c) SOE – 6 (d) SOE – 7 (e) SOE – 8
The white patches indicate unavailability data

3.2.1 Zone 1

The Zone 1 was surveyed during IIOE-2, SOE-6, SOE-7 and SOE-8. Hence, the data shown below as 'Zone 1, comprises of those obtained during the months December and January (2011-2015). (Fig. 3.1b, c, d, e)

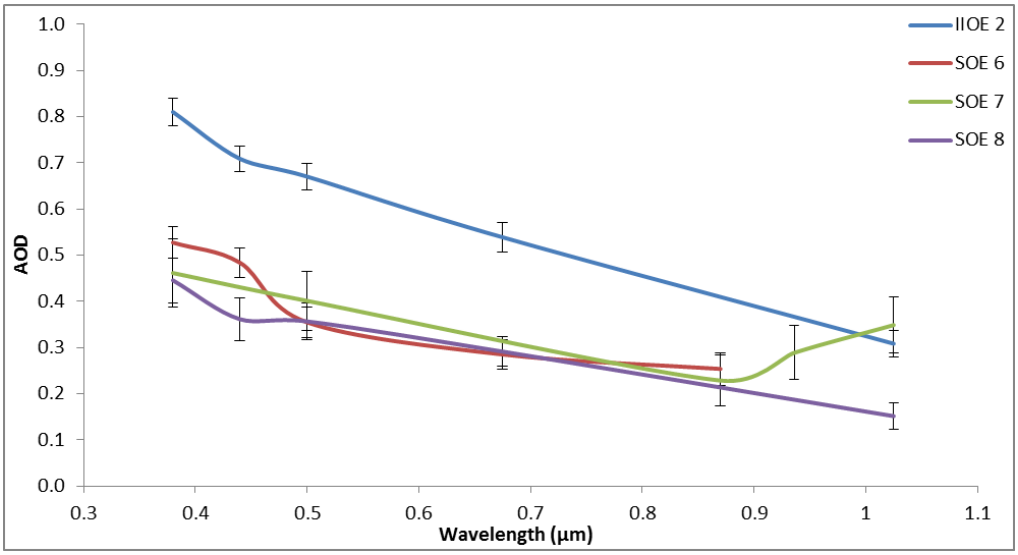

Fig. 3.3 Mean and standard deviation of Spectral AOD in Zone 1

It is observed that AODs at different wavelengths derived in three SOE cruises are similar and overlapping each other (fig 3.3). However, the spectral variability of AODs generated during IIOE-2 revealed higher values than those of SOE cruises. An exception to this is at $AOD_{1.025um}$ wherein the value measured during the IIOE-2 is comparable to that of SOE-7. The value of $AOD_{0.38um}$ during IIOE-2 is around 0.8 which gradually decreases to 0.67 ($AOD_{0.5}$) and further down to 0.3 ($AOD_{1.025um}$).

The $AOD_{0.38um}$ values in Zone 1 during the three SOE cruises range from 0.45 to 0.52 while $AOD_{0.5}$ ranges from 0.35 to 0.4. The $AOD_{1.025}$ value during SOE-7 was 0.35 which is noticeably higher than that seen during the SOE-8 (0.15).

The general wind pattern during the study period clearly explains the reason behind the low or high AOD values obtained in the cruises (fig 2.7, 2.8). The wind pattern during

IIOE-2 was north-easterly from Indian mainland to Oceanic region north of equator, while during SOE cruises; it was from marine environment.

Naturally, the continental aerosol increased AOD values during IIOE-2 cruise. SOE cruises on the other hand depict a mixture of oceanic and continental aerosols with dominant oceanic aerosols reducing the overall spectral AOD values. The increase in AOD at higher wavelengths during the SOE-7 could be justified by the presence of coarse mode particles of marine origin, due to wind speeds in the range of 10-12 m s^{-1} with gusts up to 14 m s^{-1} in the region.

The satellite data shows a plume of higher $AOD_{0.5\mu m}$ values near the coastal region and Arabian Sea with small patches extending up to $4^{o}N$ (fig 3.2(b)). The wind pattern during the study period explains the possible reason for the higher values. In-situ data from Zone 1 derived during the SOE cruises are in a good agreement with those of satellite data of respective time periods (fig 3.2 (c), (d), (e)). In fig 3.2 (d), the bright green aerosol plume seen along the western coast of India is larger with higher magnitudes as compared with fig 3.2 (c) and fig 3.2 (e). The higher AOD values near the coast are also seen in the in-situ data. The region experiences retreating monsoon during this period. Hence it would be ideal to assume higher ambient relative humidity, which in turn supports gas to particle conversion followed by hygroscopic growth of particles.

3.2.2 Zone 2

Since position of ITCZ was considered to be a determining factor in designating zones across the study area, majority of data generated during different cruises are categorised as those from Zone 2. A characteristic of this zone is that the overall AOD values tend to be the lowest than the other two zones, owing to dominance of marine aerosols in the total aerosol load. Most interesting features with respect to spectral AOD variations are seen

in Zone 2. The spectra depict anomalous spectral variation of AOD in the Southern Ocean as seen in January (SOE-6) data and the composite data of SOE cruises (fig 3.4).

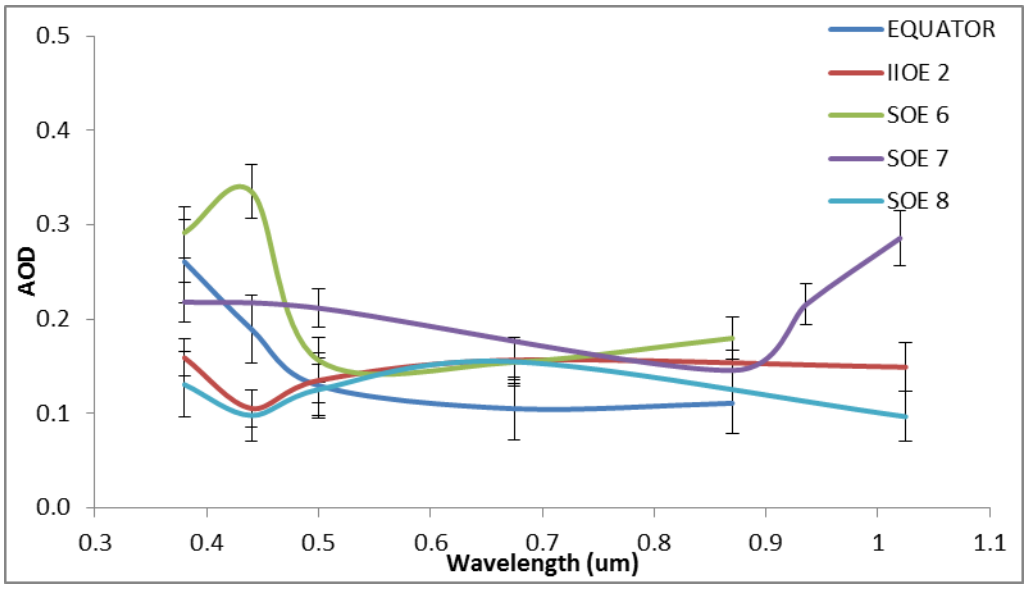

Fig 3.4 Mean and standard deviation of Spectral AOD in Zone 2

The AODs generated during different cruises mentioned above reveal almost similar values, though the time of observations are different as explained in Chapter 2, Table 2.1. The spectral AOD values of all the cruises are higher at shorter wavelengths with exceptions during IIOE-2 and SOE-8. The cruise in the equatorial region was undertaken during September – October 2011 when the region experienced south-westerly winds (Chapter 2, fig. 2.5b). Due to such a wind pattern, the sea-salt aerosols generated over the ocean would get transported towards mainland. The coarse sea spray aerosols hence would become dominant in the total aerosol content, resulting in lower AOD values from 0.5µm onwards.

Satellite data obtained from the same period of observation agree well with the observations of IIOE-2 and SOE-8. The satellite imagery shows that northern boundary of ITCZ actually acting as the boundary between Zone 1 and Zone 2. This is seen as a region of lower AOD to the south of approximately 8^{o}S (which is the northern boundary of ITCZ during the time of SOE cruises) in fig 3.2 (c), (d) and (e).

In January 2012, during the SOE-6 cruise, an unusual spectral variation of AOD was noticed in Zone 2 (fig 3.1c). Primary and secondary maxima of AOD have been observed at 0.44µm and 0.675µm, respectively. Such a signature over an oceanic environment is primarily due to chlorophyll-a. Hence a similar signature in the aerosol spectra pointed that chlorophyll-a is could be the main source of aerosol. However, such a signature is not seen in the spectra obtained during SOE-8, measurement for which was carried out in February (fig 3.2(e)). An analysis of mean and standard deviation reveals that variability of all AOD data taken south of 40^{o}S is higher at the shorter wavelengths and minimum at 0.675um and 0.87um with a further increase toward long wavelengths (fig 3.2(f)). This result depicts primary and secondary maxima more distinctly. The higher standard deviation in the spectral data at shorter wavelengths is attributed to the data from January (SOE-6) when the anomalous data was obtained while that at higher wavelengths was associated with the coarse mode aerosol – sea-salt which is abundant in marine atmosphere.

Subsequent analysis of AOD spectra of different zones revealed that drastic departure from the normal spectrum is observed only in the Zone 2. A comparison between chlorophyll-*a* absorption (generated from analysing the water sample) spectra with AOD spectra in Zone 2 helped in understanding the effect of chlorophyll-*a* on aerosols (fig 3.5(a), (b)).

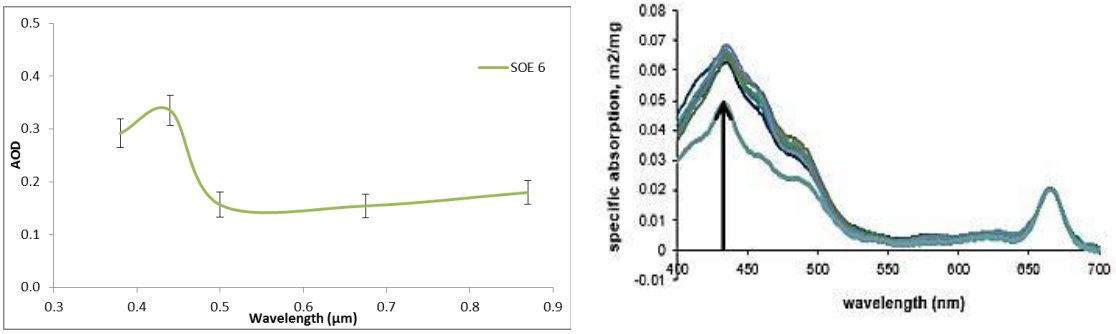

Fig 3.5 (a) Comparison of Zone 2 AOD spectra and (b) typical chlorophyll-*a* spectra

The AOD value at 0.44µm was estimated using a model OPAC (Hess et al, 1998) to understand the role of chlorophyll-*a* in AOD. The difference between AOD values estimated and measured at 0.44µm were correlated with chlorophyll-*a* concentrations, which results in a coefficient of correlation (R^2) 0.79 (fig 3.6). This indicated that the chlorophyll-*a* had a significant role in affecting the overall abundance of fine mode particles in Zone 2.

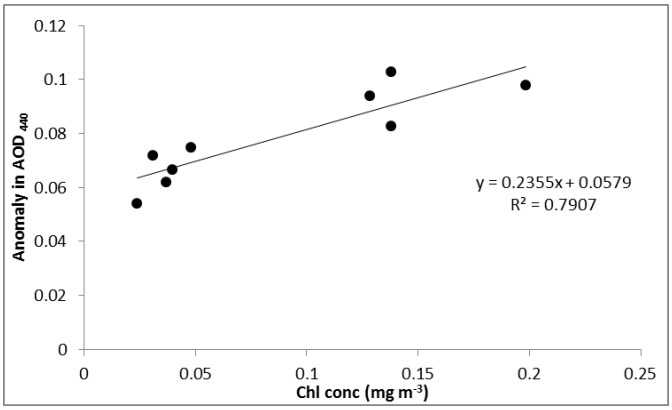

Fig 3.6: Anomaly in AOD440 correlated to chlorophyll-*a* concentration

3.2.3 Zone 3

As explained in the Chapter 2, Sect 2.1.1.2, Zone 3 is essentially a part of Zone 2 with the African continent and the island of Madagascar as its western boundary. Zone 3 was visited only during the SOE cruises. However, owing to bad weather, the only in-situ dataset present in this zone is the data from SOE 6.

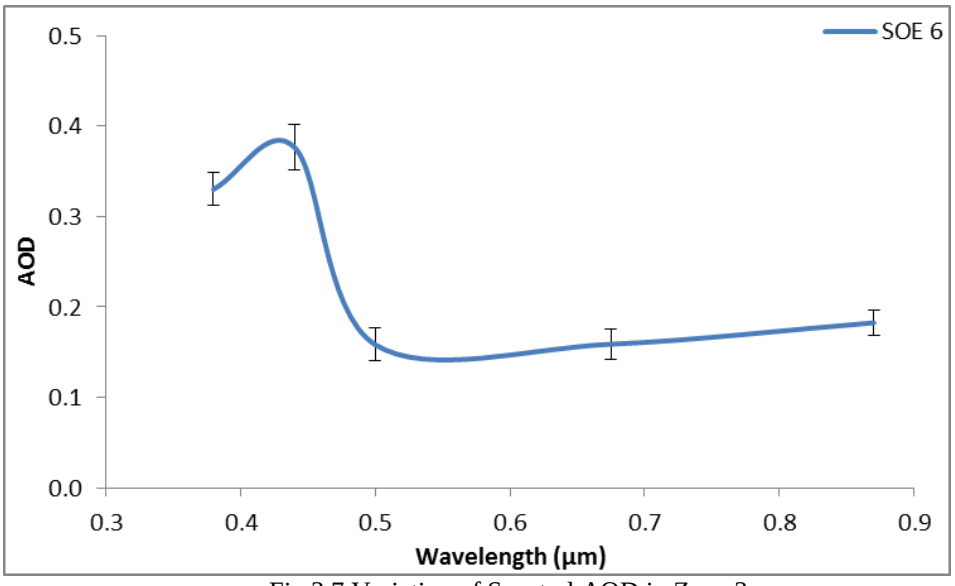

Fig 3.7 Variation of Spectral AOD in Zone 3

Since Zone 3 is essentially a subset of Zone 2 which is separated out owing to its vicinity to land, the AOD spectra is similar to that seen in Zone 2. An increase in AOD at longer wavelengths due to influx of coarse mode marine aerosol was prominent in Zone 3. Though the wind pattern supports the dominance of marine aerosol in the total aerosol load, a poor regression of R^2 (0.02) between wind speed and $AOD_{0.87}$ indicated a small influence of wind on $AOD_{0.87}$. This has been probed by examining the surface salinity along the entire track, as salinity is a decisive factor while analysing wind transported marine aerosols. Wind generates coarse-mode sea-salt particles, due to bursting of bubbles at wave crests (Monahan et al., 1986; Fitzgerald, 1992) over saline waters with salinity 35 PSU or above. O'Dowd et al., (1999) and Martensson et al., (2003) studied the role of salinity and wind acting as an external mechanism for the marine aerosol flux and surface salinity. These play a crucial role in the aerosol droplet formation and hence the aerosol size distribution.

The salinity increases towards the Sub-Tropical Front (STF), increasing the viscosity. But more than salinity, SST plays a dominant role in determining the viscosity. A decrease in SST towards STF and further south increases the viscosity. Since the viscosity increases towards high latitude the wind prevailing over there produces coarse mode aerosols, which is clearly depicted by an increase of $AOD_{0.87}$.

Since the STF in Zone 3 was stronger due to the confluence of the Agulhas retroflection (Anilkumar et al., 2006), an increased chlorophyll-*a* concentration might have been responsible for higher DMS and high non-sea-salt sulphate generation in this zone. Since the observations carried out during the return leg of SOE-6 were from low chlorophyll-*a* waters to high chlorophyll-*a* waters (as the ship approached STF), predominance of fine mode particles of marine origin formed as a result of gas to particle conversion responsible for increasing AOD at short wavelength.

3.2.4 Aerosol characteristics over Antarctic continent

During the 32nd Indian Scientific expedition to Antarctica, measurements of AOD were carried out from the two Indian stations viz., Bharati and Maitri. Since the data generated are from a region which is pristine in nature and absolutely different from all other regions dealt in this study, it is treated as a separate zone altogether.

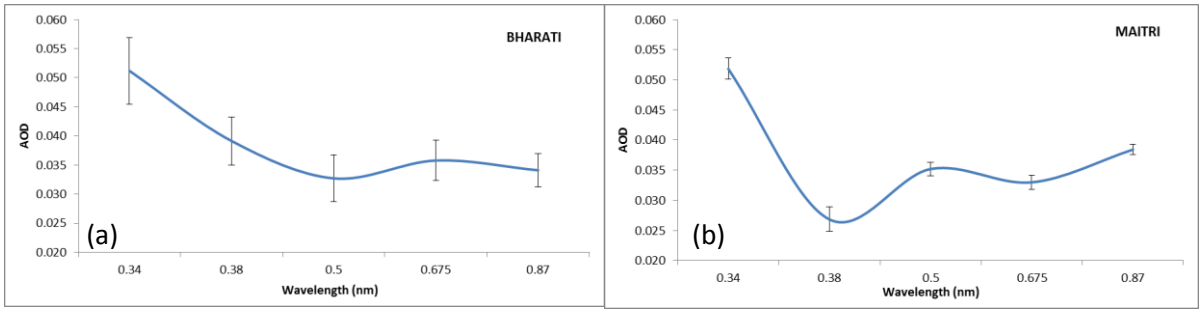

Fig 3.8 Mean and standard deviation of spectral AOD in (a) Bharati and (b) Maitri

The AOD values clearly exhibit the pristine nature of the environment over Antarctica, as clear from $AOD_{0.5um}$ value, which is close to 0.035. It can be observed that the values in the shorter wavelength region are almost similar in both the regions though the stations are located far apart with one on the coast and the other far away from the coast, also seen in Chapter 2, Sect. 2.2.3. However, the AODs towards the higher wavelength are greater in Maitri than those encountered in Bharati station. This could be due to the presence of the mineral dust as a result of exposed land surface in the Schirmacher oasis.

It is also observed that the standard deviation in Bharati station is consistently higher than that at Maitri station. This is a result of Bharati being in the vicinity of sea, atmosphere contains more maritime aerosol. The contribution of sea spray generated in the bay near Bharati greatly affected the variability of the spectral AOD in that region.

3.3 Angstrom exponent 'α'

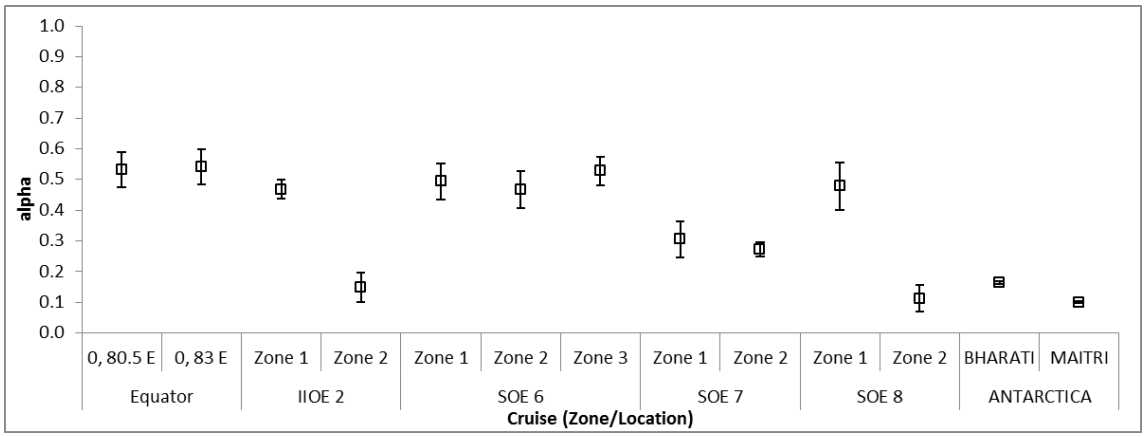

Fig 3.9 Angstrom exponent derived from in-situ data for different field campaigns

The variation of alpha in different zones is shown in fig 3.9. During the IIOE-2 and the SOE cruises, the period when the ship was in Zone 1 coincides with Indian north-east monsoon. Particularly during SOE-7, moderate rainfall was encountered off Indian coast. Due to rainfall, wet deposition resulted in significant reduction in aerosol concentration, thus removing most of anthropogenic input of sulphates and nitrates, essentially contributed to fine mode particles. The low alpha values are a result of the measurements obtained during that time (considering average α for natural atmosphere to be 1.3±0.5 (Iqbal, 1983)).

The highly dynamic nature of Zone 2 is clear from the aerosol size spectrum. During the observation in the equatorial region, the wind was flowing from south to south-east. The aerosol content would be mainly of maritime origin i.e., coarse mode aerosols. This resulted in lower α value of 0.53±0.11. Zone 2 data was obtained from the tropical Indian Ocean during the IIOE-2. The wind pattern showed the presence of only oceanic wind and hence oceanic coarse mode sea-spray was present in higher numbers as compared to fine particles. Hence a very low value of 0.15±0.1 was observed.

Indian ocean sector of Southern Ocean reveals a completely new scenario in the aerosol dynamics. The AODs of Zone 2 generated from SOE cruises depict a large variability depending on the time of observation. The AODs generated during SOE-6 were mainly during January 2012. The α value obtained have been 0.47±0.12. Measurements taken during

SOE 7, during the period from January to February 2013, resulted in α values of 0.27±0.05. This is further reduced to 0.11±0.09 in February 2015, measurements carried out during SOE-8, depicting the overall reduction of fine particles in the region.

The data from Antarctic region exhibits negligible deviation from the mean α values of 0.1647±0.0038 (Bharati) and 0.1003±0.0028 (Maitri). The low α values indicate a distribution highly inclined towards coarse mode particles. This could be due to the sea spray and mineral dust present at both Bharati and Maitri region, the reasons for which are discussed in Chap 2, Sect 2.2.3.

3.4 First order derivative of α (α')

In order to understand the microphysical characteristics of aerosols, α' was calculated for the data generated over the entire area of study. If the values of α' tend to be near zero, it indicates compliance with Angstrom relation, while higher α' values suggest non-compliance to Angstrom relation. Positive α' values indicate the dominance of fine-mode particles, while near zero to negative α' values suggest the dominance of coarse mode aerosols in the bimodal aerosol distribution (Eck et al, 1999).

Since the spectral shape of AOD in Zones 2 and 3 were similar, α' values in these two zones were put together. The results of time series studies (α' values) carried out at two locations of the equatorial region range from -1 to -8. This undoubtedly indicates the dominance of coarse mode aerosols (fig 3.10(a)), hence lower AODs.

All the α' values generated during IIOE 2 show a clear separation of aerosol characteristics in different zones. The values in zone 1 are clustered around 1, while those binned as zone 2 range between 0.5 and -3. Zone 1 being in the vicinity of continent, dominance of fine mode particles were observed; whiles those from Zone 2 being far away from the coast have coarse mode dominance with bimodal distribution. (fig 3.10(b)).

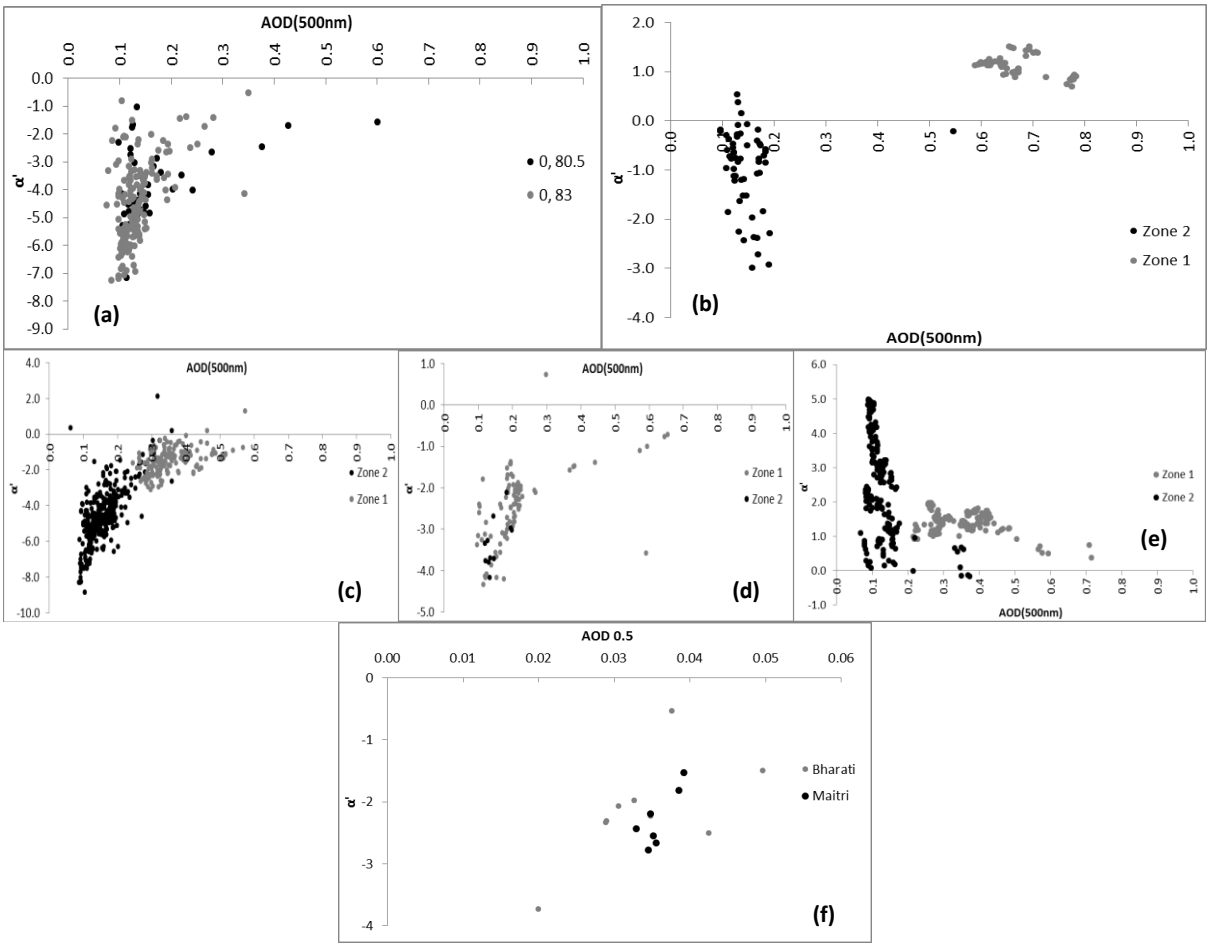

Fig 3.10: Second order derivative α'from spectral AOD obtained from different field surveys. Equator Cruise (b) IIOE-2 (c) SOE – 6 (d) SOE – 7 (e) SOE – 8 (f) Antarctica

During the SOE-6, most values of α' in Zone 1 were near zero and the minimum value was ~ -3. Among them only two values were positive. Since the cruise was conducted during the period of north-easterly winds, the continental advection as described in Chapter 2, Sect. 2.2.2, submicron aerosols would greatly contribute to the aerosol leading to a steeper AOD spectrum in Zone 1. However, In Zone 2, most of **α'** values were in the range -2 to -8, suggesting a bimodal aerosol size distribution with dominant coarse mode particles of maritime origin.

The analysis of α' from SOE 7 showed values similar to SOE 6 in the different zones. However, the magnitudes during SOE-7 were seen to have increased from -1 to -4. This showed that the compliance with the Angstrom relation was higher as compared to SOE 6. The projected size distribution was similar to SOE 6.

α’ values during SOE 8 in Zone 2 ranged from 0 to 5. This shows a complete opposite picture with dominance of fine mode particles and mere presence of coarse mode particles. This however, for the reasons unknown, is in complete disagreement with α derived from in-situ spectral AOD data and the size segregated mass concentration data obtained from QCM and satellite observations. All point towards coarse mode dominance and mere presence of fine mode discussed further.

The analysis of α’ from Bharati and Maitri both support the presence of coarse mode with values ranging from -0.5 to -4 in Bharati region and from -1.5 to -3 in Maitri region. The broader range at Bharati is clearly noticeable as compared to Maitri indicating wide range of particles present at Bharati while narrower range at Maitri indicating lesser variety of particle size.

3.5 Size segregation from in-situ analysis using Quartz Crystal Microbalance (QCM)

3.5.1 SOE-6

The size segregated mass concentration data generated during SOE-6 across all the zones are presented in fig (5.1(a)). The drastic increase in fine mode (Aitken and accumulation modes) from Zone 1 (~25%) to almost 55% in Zone 2 is the most prominent feature. However, this has been decreased to 40% in Zone 3. Considering only the fine mode fraction, the accumulation mode noticeably increased from 15% to around 40% from Zone 1 to Zone 2. This further reduces to about 30% of total aerosol mass concentration. The aerosols in Aitken mode in Zone 1 and Zone 3 are comparable (12% - 15%), whereas those in Zone 2 are slightly lesser than 10%.

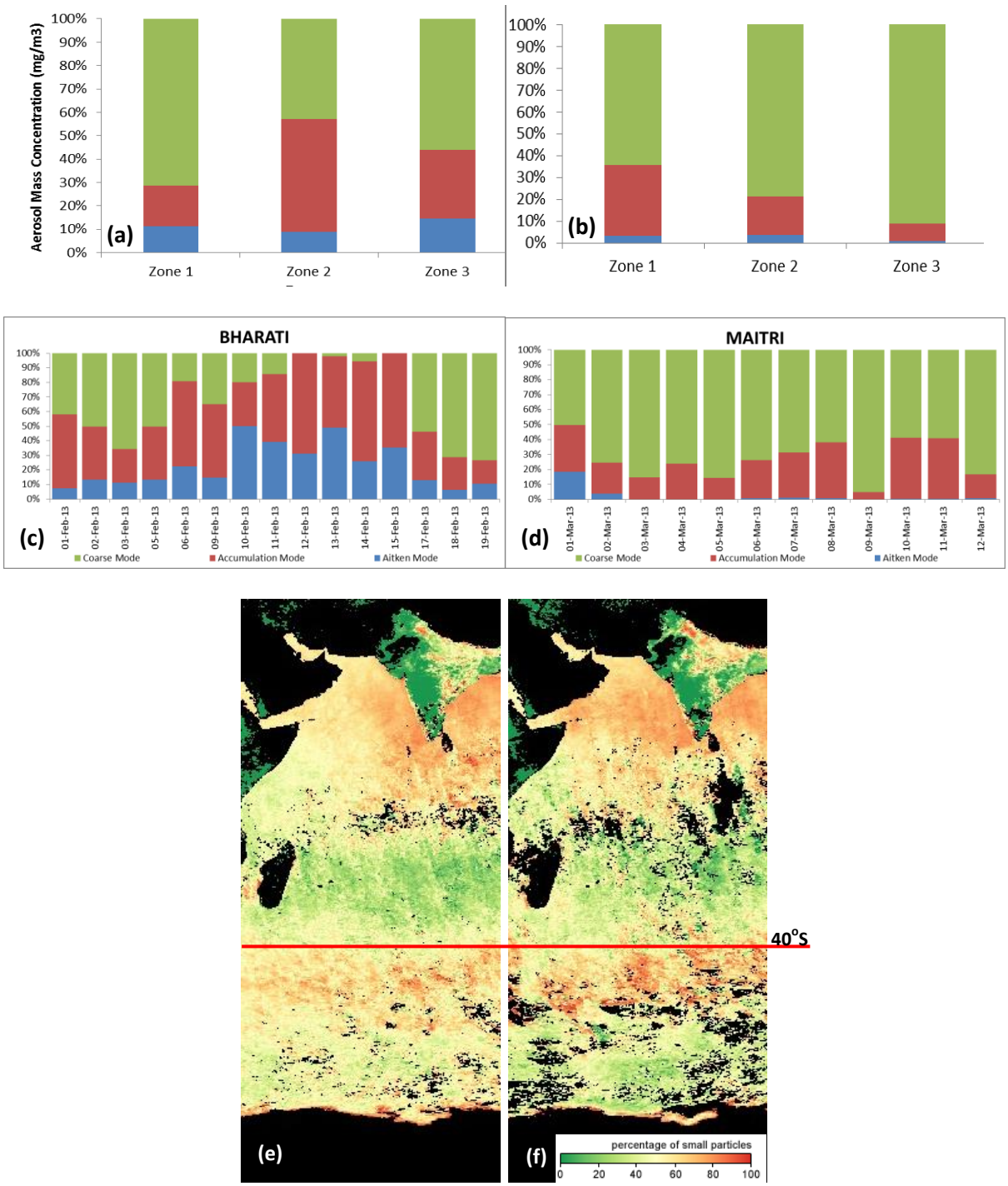

Fig 3.11 Fig 2.1: In-situ QCM data obtained from different cruises.
(a) SOE – 6 (b) SOE – 8 (c) Bharati – Antarctica (d) Maitri – Antarctica
(e) Satellite aerosol particle size during the SOE – 6 (f) Satellite aerosol particle size during the SOE – 8

After examining the composite picture for each zone, it is clear that the distribution in Zone 1 has dominance of fine mode while that in Zone 2 and Zone 3 shows a bimodal distribution of aerosols. This fact is also verified using the optical characteristics of aerosol

discussed in Chapter 3, Sect. 3.2 and 3.3. The distribution is in good agreement with the outcome of analysis of alpha and second order alpha which points towards coarse dominance with bimodal distribution.

3.5.2 SOE-8

The data generated during SOE 8 in all three zones is presented in fig 3.11(b). A gradual decrease in fine mode (Aitken and accumulation modes) (~35%) from Zone 1 to almost 20% in Zone 2 is clearly seen. In Zone 3, this further reduced to about 10%. Observing the variations in the fine mode fraction, the accumulation mode decreased from 30% to around 15% from Zone 1 to Zone 2 which reduced to less than 10% of total aerosol mass concentration. The aerosols in Aitken mode in Zone 1 and Zone 2 are less than 5%, whereas in Zone 3, the Aitken mode is almost absent.

Examination of the dataset for each zone revealed that the coarse mode predominance in Zone 1 has further increased in Zone 2. A bimodal distribution of aerosols is observed with the balance tilted more in favour of coarse mode. However, when this fact was verified using the optical characteristics of aerosol (Chapter 3, Sect. 3.2 and 3.3) it is seen that the distribution is in good agreement with the outcome of analysis of α but completely disagrees with second order alpha which points towards fine mode dominance.

3.5.3 Satellite Data for Aerosol Particle Size

The satellite data acquired from MODIS – AQUA for the SOE-6 and SOE-8 are shown in the fig 3.11(c), (d). A noticeable change in the fine particle percentage is seen while comparing the SOE-6 and SOE-8. The satellite data testifies the presence of higher fine mode in bimodal distribution during SOE-6 and the higher coarse mode in the SOE-8 in the region south of 40^{o}S.

3.5.4 32nd Indian Scientific Expedition to Antarctica

The particle size distribution at Bharati in general indicated high percentage of accumulation and Aitken mode particles, which even exceeds 90% (fig 5.1(c)). While an opposite picture was seen in the Maitri station with maximum coarse mode particles (fig 3.11(d)). It is also noticed that the particles in Aitken mode are present only in Bharati region while absent in Maitri region apart from two instances. However, in Bharati station, it should also be noted that some days, the dominance of coarse mode particles (contribution to total aerosol mass greater than 60%) is also observed. Hence, the results of alpha and second order alpha indicate major contribution of aerosols in coarse mode even in Bharati region (Chapter 3, Section 3.2 and 3.3).

The presence of Aitken mode particles in the Bharati region could be an indicator for the gas to particle conversion as a result of photosynthesis in the coastal waters. In Maitri region, as a result of long range transport, the possibility of such a process extending over up to this region due to favourable wind pattern cannot be overlooked (Chapter 2, Section 2.2.3, fig 2.9 (b)).

AEROSOL CHEMISTRY AND BLACK CARBON

4.1 Introduction

A clear understanding of the chemical composition of aerosols is imperative in recognizing their sources, sinks and their impact on insolation. The variety in the sources, their concentrations and compositions show substantial spatial and temporal variability which makes it challenging to assess the radiative forcing by aerosols on global scale. It is known that aerosols of continental origin get transported to oceanic environments and the marine aerosols get advected to continental regions owing to the wind patterns (Prospero et al 1989a, b; Charlson et al, 1992).

The chemical analysis of the aerosol samples collected at different regions over the oceanic environment can provide evidence on the advection of continental aerosols and their relative contribution (Carmichael et al, 1997; Prospero et al 1989a, b). Studies carried out during the INDOEX have shown that marine aerosols comprising of sea-salts, non-seasalt (nss) sulphates, mineral dust and a variety of other organic and inorganic components getting transported from distant locations (Krishnamurti, et al, 1998; Jha, et al, 1998).

Atmospheric black carbon (BC) is an important aerosol species with respect to climate change and human health studies. It absorbs the solar radiation over a wide spectral band (Rosen, H., 1978; Ramanathan, et al 2008; Tiwari, et al 2013) significantly contributing to atmospheric forcing. BC is produced as a result of incomplete combustion (Chen, L.W.A., 2001; Latha, K.M. et al, 2005). Substantial rise in fuel demand in the daily energy needs for domestic, industrial and transport sectors has caused a historical alteration in BC emission in the past decades (Sreekanth, V.et al, 2007). Significant amount of BC in the clouds may heat up and cause ‘cloud burn off’ (Ackerman, A.S.et al, 2000; Babu, S.S. et al, 2002). Conversely, it has a cooling effect at the surface, which affects the temperature profile in the troposphere and eventually the rainfall mechanism (Safai et al, 2007; Menon et al, 2002).

Being hydrophobic, BC is not significantly removed by precipitation. However, BC particles get transformed into hydrophilic when coated with sulphate (SO_4^{2-}), which then act as cloud condensation nuclei (CCN) and get removed due to precipitation (Twomey, S., 1977; Linhong, K., 1996).It has been reported that BC shows certain pattern of variations in association with boundary layer dynamics (Latha et al, 2003; Safai et al., 2007; Sreekanth, V.et al, 2007; Saha, et al, 2009).

In this chapter, the spatial distribution of BC from 15°N to approximately 55°S is discussed. The dataset comprise of values generated in-situ by aethalometer during SWTIO, IIOE-2, SOE-6, SOE-7 and SOE-8 from Zone 1, Zone 2 and Zone 3. The aerosol samples of the ambient atmosphere were collected using a high volume sampler during SOE-6. These were processed using an Ion Chromatograph (IC) and the Inductively Coupled Plasma Mass Spectroscopy (ICPMS). The samples were named in the format SN-61-XX where SN-61 is the cruise number and 'XX' represents the station number.

4.2 Results and Discussion

4.2.1 Analysis of Ions and Trace Elements

Station Code	Latitude		Longitude	
SN - 61 - 5	6	S	75	E
SN - 61 - 6	11	S	73	E
SN - 61 - 7	17	S	70	E
SN - 61 - 9	34	S	62	E
SN - 61 - 10	43	S	57	E
SN - 61 - 12	53	S	58	E
SN - 61 - 13	50	S	58	E
SN - 61 - 15	43	S	58	E
SN - 61 - 21	27	S	57	E
SN - 61 - 23	25	S	57	E

Table 4.1 Station name and location of the aerosol sampler.

Na^+ and Mg^+ were found to be the most abundant cations in the region followed by Ca^+ and K^+. NH_4^+ were the least in the region except at the stations SN-61-10 and SN-61-12 where the values were higher. Though the location SN-61-10 and SN-61-15 are nearly same, SN- 61-13 was surveyed after 10 days. Hence the values depicted a large variability.

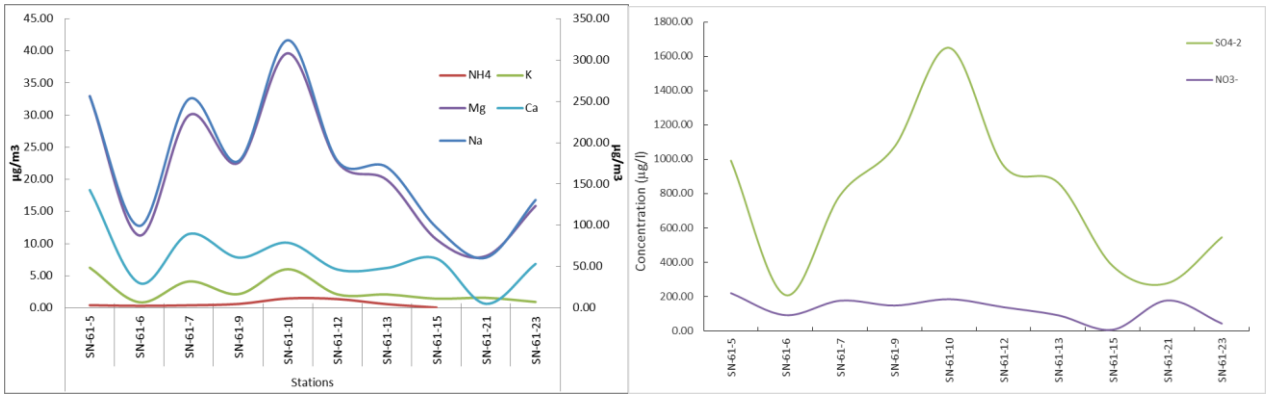

Fig 4.2: Spatial variation of (a) Cations and (b) Anions over the Indian Ocean and Southern Ocean during the SOE-6

Cl^- was found to be the most abundant anion followed by SO_4^{2-}. NO_3^- was observed to be present in a uniform concentration throughout the cruise track except at station (SN-61-15) where it showed the least value. Along the cruise track variations of both cations and anions were similar.

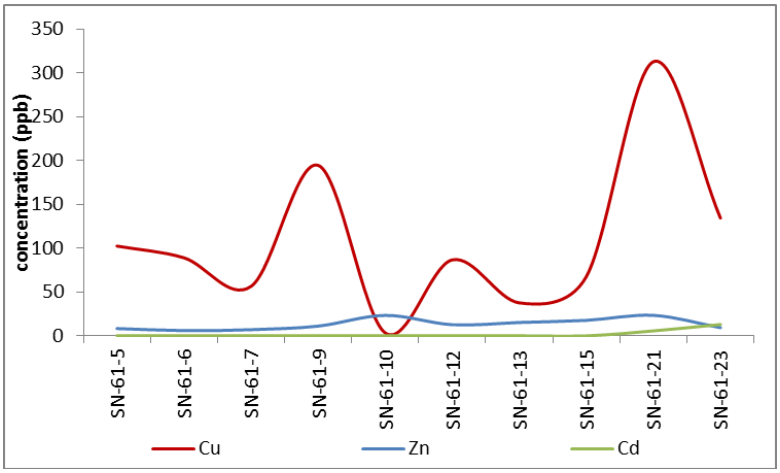

Fig 4.3: Spatial variation of the trace metals over the Indian Ocean and Southern Ocean during the SOE-6

The most abundant trace metal in the study area was copper (Cu). The least abundant trace metal was cadmium (Cd) which showed a slightly higher value at station (SN-61-23). At station SN-61-10, however, Zn was found to be more in concentration than Cu. Peak

values of Cu were seen at SN-61-21 and SN-61-9 which mainly have the wind coming from the South American peninsular region, as confirmed by HYSPLIT back-trajectory analysis, The South American region is known to have copper mines which may be a reason for increased copper content in minerals transported.

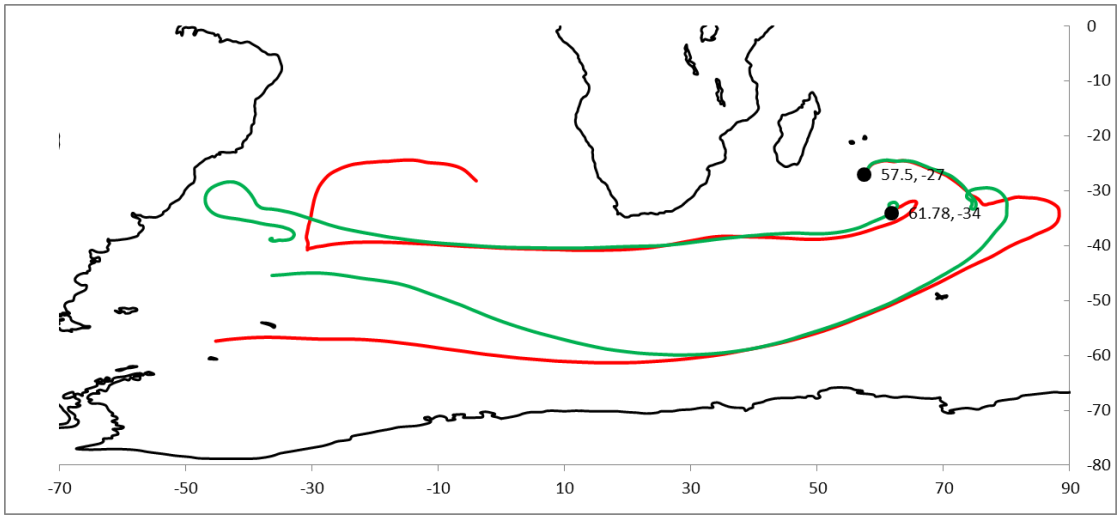

Fig 4.4: 315HRS HYSPLIT back-trajectory

In chapter 3, the effects of chlorophyll-a presence over the fine mode particles is discussed. Trace metals like Cu, Zn, Cd can inhibit metabolism if present in elevated concentrations. If they are bound to the wrong metabolic sites, which are normally occupied by other essential nutrient ions, the overall effect on cellular rate processes such as growth, and productivity of the phytoplankton community, decreases. (Sunda, 1989).

It implies that if the chlorophyll-*a* concentration gets affected by the trace metals which were transported by natural or anthropogenic process, the fine mode particle mass concentration will be affected. Since fine mode particles are responsible for scattering of high energy shortwave radiation, the consequence of variability of fine mode will be instantaneously observed in the Radiative forcing calculation. Hence, this forms a pathway through which the indirect effect mineral dust could be observed on the Direct Aerosol Radiative Forcing (DARF).

The concentration of sulphate was found to be lower at stations SN 61 -21 and SN-61-9, where Cu was higher. The source of sulphate at these stations is mainly associated with Dimethyl sulphide (DMS) resulting from photosynthesis, which means presence of Cu in high concentration directly affect sulphate aerosol generation, which eventually affects DARF through the pathway explained above.

4.2.2 BC Mass concentration

The BC mass concentration data presented in the figure 4.5 comprises of those obtained from three expeditions carried out under Indian Southern Ocean program and from the IIOE-2. The distribution of BC mass concentration from Indian coast to approximately 50^{o}S has been analysed. The concentration decreases drastically from south of ITCZ and an average value of 79.6 ±31 ng m^{-3} has been observed throughout Zone 2. Hess et al., 1998 stated the value of the open ocean atmosphere to be 0 ng m^{-3}.

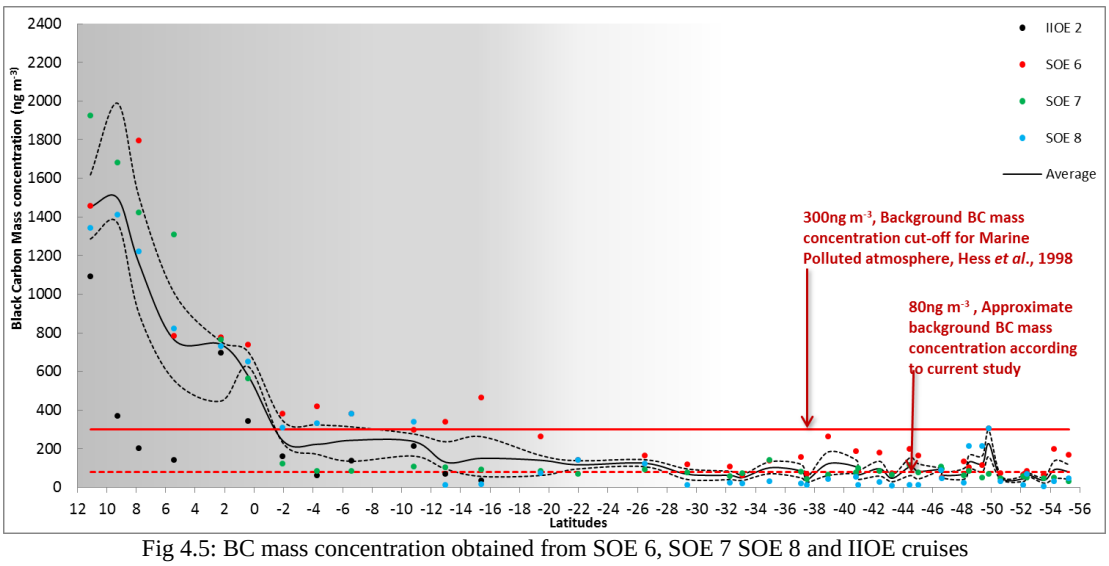

Fig 4.5: BC mass concentration obtained from SOE 6, SOE 7 SOE 8 and IIOE cruises

4.2.2.1 Zonal distribution of Black Carbon aerosols

The data generation in the Zone 1 took place during the month of December, Zone 2 during September, October, December and January and in Zone 3 during January and February.

4.2.2.1.1 Zone 1

The highest BC was encountered in Zone 1 with an average value of 1700 ng m^{-3} at around 10^{o}N (Fig 4.1). This is mainly due to the proximity of the Indian sub-continent and Sri Lanka. The Zone 1 is subjected to the north-easterly winds during December. Hence the aerosol load from the continent is carried towards the equatorial region increasing the average BC mass concentration.

4.2.2.1.2 Zone 2

The ITCZ forms a major mesoscale phenomena separating Zone1 from Zone 2. The concentration gradually decreased and a minimum value of 670 ng m^{-3} was observed at equator. In Zone 2, BC ranged in between 37 and 132ng m^{-3}, with an abnormal peak of 226ng m^{-3} at 50^{o}S. An irregular distribution pattern with high and low BC mass concentration is observed. Two possibilities attributed to such a distribution of BC mass concentration are either in-situ source or remote forcing. The in-situ source is emission from the ship while the remote forcing is those from the continent.

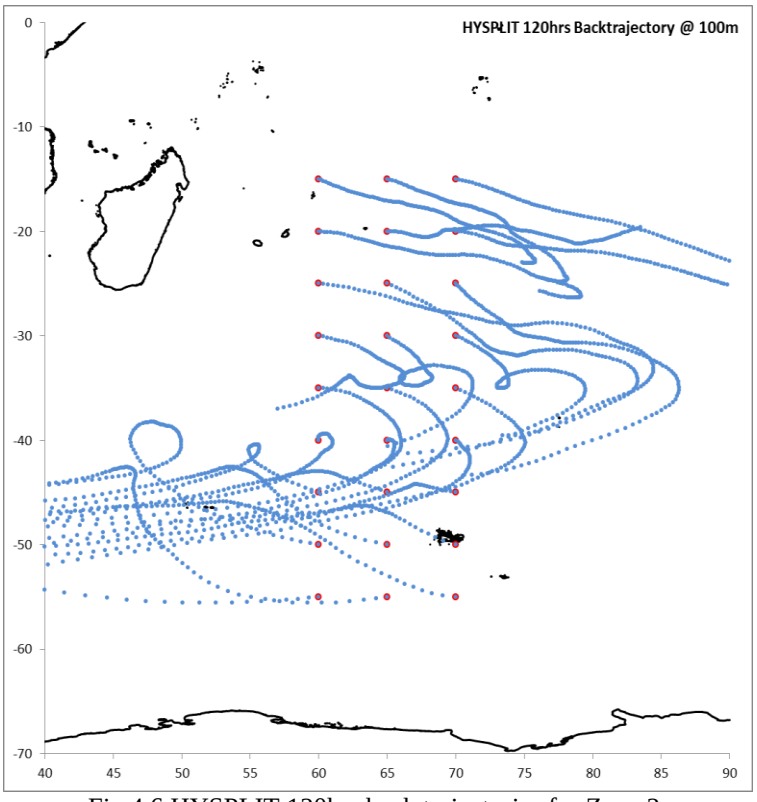

Fig 4.6 HYSPLIT 120hrs back trajectories for Zone 2.

The HYSPLIT 120 hrs back trajectory analysis was carried out to address the remote forcing. The back-trajectories reaching the location at 100 m show the aerosols being transported from the oceanic region. Necessary precautions were taken in order to remove the effect of ship exhaust fumes thereby reducing the possibility of in-situ source. Hence, the BC mass concentration in Zone 2 could be a result of the aerosol already present accumulated in the atmosphere or a result of remote advection.

4.2.2.1.3 Zone 3

Zone 3 is essentially a part of Zone 2 partitioned owing due to vicinity of the African continent. Though most of the HYSPLIT back trajectory analysis point towards dominance of the oceanic aerosols, sea routes often used by cargo carrying ships are present in this region which my contribute to the total BC mass concentration in this region. The effect of the same is clearly observed as slightly higher values of 93.8±21.7 ng m^{-3} of BC as observed compared to Zone 2.

4.2.3 Effect of MABL on BC mass concentration

The Marine atmospheric boundary layer (MABL) plays an important role in altering the volume concentration of the aerosols. Hence an understanding of the MABL proves to be essential in studying the distribution over a large geographical area.

During IIOE-2, it was observed that there is an inverse relation between the height of MABL and BC mass concentration in the region south of ITCZ, where BC was mainly due to remote advection of aerosols. A correlation coefficient of R^2= 0.67 is observed between the height of MABL and BC mass concentration in Zone 2, while such a relation is absent in in the region north of ITCZ (Zone 1) where the coefficient of correlation , R^2 is found to be 0.14.

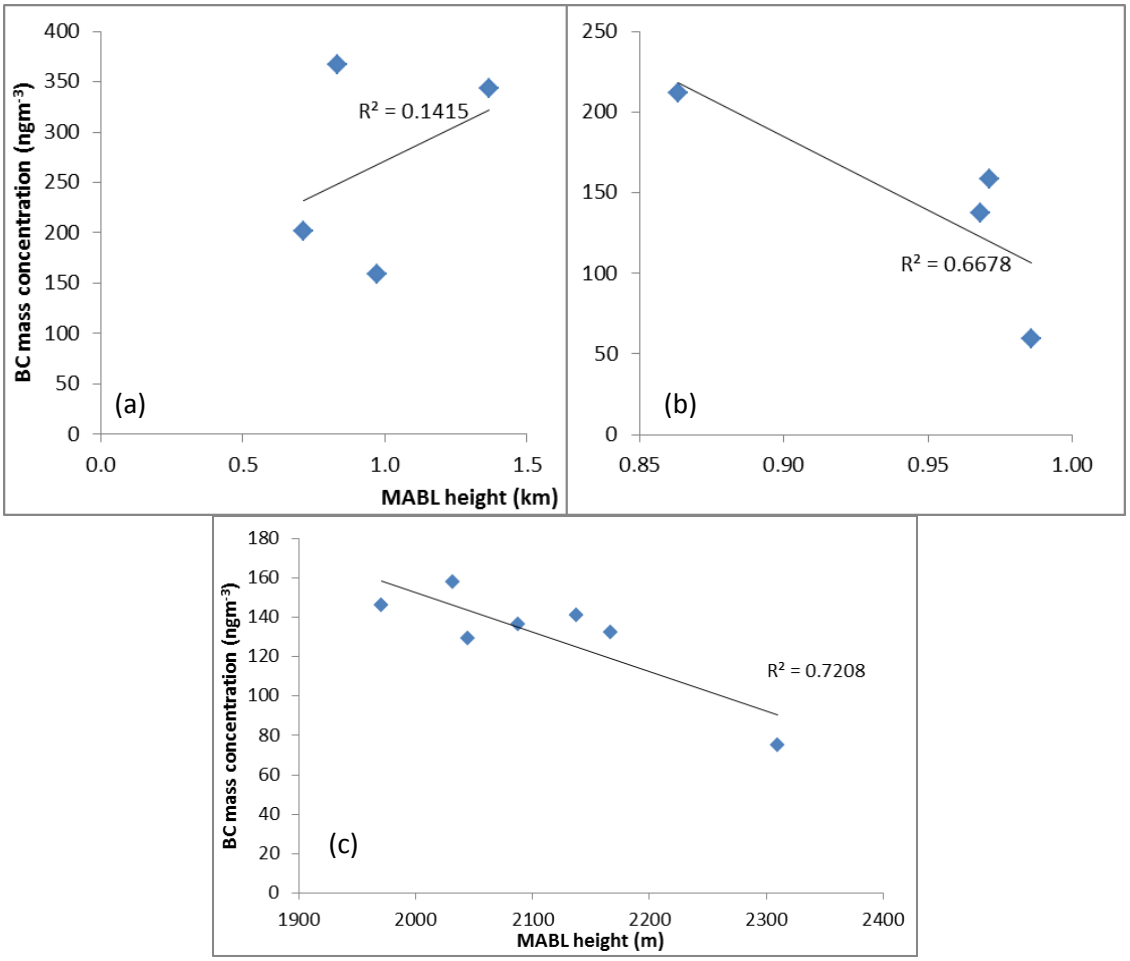

Fig 4.7 Relation between MABL and BC mass concentration as seen during the IIOE-2
(a) Above and (b) below ITCZ (c) SWTIO cruise – Time series

During the SWTIO cruise, MABL height data estimated using the balloon data was generated. It was linearly correlated with the BC mass concentration as shown in fig 4.7 (c) which resulted in R^2=0.72. This result will also fall in the region to the south of ITCZ.

In conclusion, two of the studies showed a higher correlation of BC mass concentration with MABL height. However, this needs to be probed further with enough data to comment statistically on the exact nature of relation between BC mass concentration and the MABL height.

DIRECT AEROSOL RADIATIVE FORCING AND HEATING RATE

5.1 Introduction

Aerosols affect climate by absorbing and scattering incoming solar radiation (direct effect) or by acting as cloud condensation nuclei (CCN), thus affecting cloud albedo and its lifetime (indirect effect). Species of aerosols like black carbon (BC) absorbs sunlight efficiently and heat the atmosphere, which can lead to cloud-burn-off. A metric to express the possible impact on climate is radiative forcing expressed in W m^{-2}.

An estimation of the net flux at the top of the atmosphere (TOA) and the surface (SUR) with and without aerosols provides the difference between respective forcing. The difference reveals the effect of aerosols on the atmosphere (ATM) also known as the Direct Aerosol Radiative Forcing (DARF). The DARF considers the changes in radiation due to the optical properties of aerosol – the scattering of incoming solar radiation (cooling) and the absorbing (warming). The indirect RF considers feedbacks resulting from interactions between clouds and aerosols. Since the data generation was undertaken only on cloud free days, indirect RF stays out of the scope of this study.

The direct aerosol short wave radiative forcing was computed using the SBDART model (Ricchiazzi et al., 1998). An important factor influencing radiative forcing is the surface reflectance (Haywood and Shine, 1995). Since the study area is atmosphere over Ocean, DARF was estimated using the standard sea surface albedo model (surface albedo=0.06) built in SBDART model.

Some of the studies limited over the Indian Ocean and the Indian Ocean sector of the Southern Ocean. (Babu et al., 2010; Chaubey et al., 2013) focussed on the continental impact and sea spray aerosols on climate. These studies proved to be the pilot database for this region. For the current study, the measurements taken during the three expeditions to the Southern Ocean and the IIOE-2 were used to estimate the Direct Aerosol Radiative Forcing (DARF).

5.2 Results and Discussion

The estimated forcing at TOA, SUR and the ATM or DARF values observed during the SOE-6, SOE-7, SOE-8 and IIOE-2 reveal negative SUR and TOA forcing. Since locations in Zone 1 had remote influence of north-easterly monsoon winds as seen in Chapter 2, the aerosol load from the Indian sub-continent resulted in high surface forcing (Fig 7(b-ii)). This is also evident from the HYSPLIT trajectory frequency analysis carried out in Chapter 2. The enhanced BC associated with continental outflow and reduced precipitation during this period is responsible for the high atmospheric forcing. The observation locations during the SOE-6 and IIOE-2 were both on the west coast of India. But, the locations visited during the IIOE-2 were away from the coast while during the SOE-6, they were along the coast.

Hence, in spite of near-about same time and in the path of influence of the continental outflow, the values obtained during different cruises showed a wide spatial variability in atmospheric forcing.

5.2.1 Zone 1

The aerosol composition in this zone is primarily a mixture of sea spray accompanied with the sulphates, nitrates and BC mass concentration. The atmospheric forcing ranged from 12 W m^{-2} for further off-shore locations during the IIOE-2 cruise (December 2015) to 25 W m^{-2} at stations near the coast carried out during the SOE cruises (end-December 2011), (fig 5.1 (a), (b-i)). Babu et al (2010) observed the atmospheric forcing to be in the range of 6 – 13W m^{-2} during their study in the first half of January 2004.

The higher atmospheric forcing values in Zone 1 and comparatively lower values in Zone 2 and 3 were primarily because of the influence of the wind carrying the aerosol mass from the Indian and African continent to Zone 1. The effect is observable till 4^{o}S during IIOE-2 cruise and 10^{o}S during SOE cruises, both marking the southern boundary of the ITCZ during the respective periods.

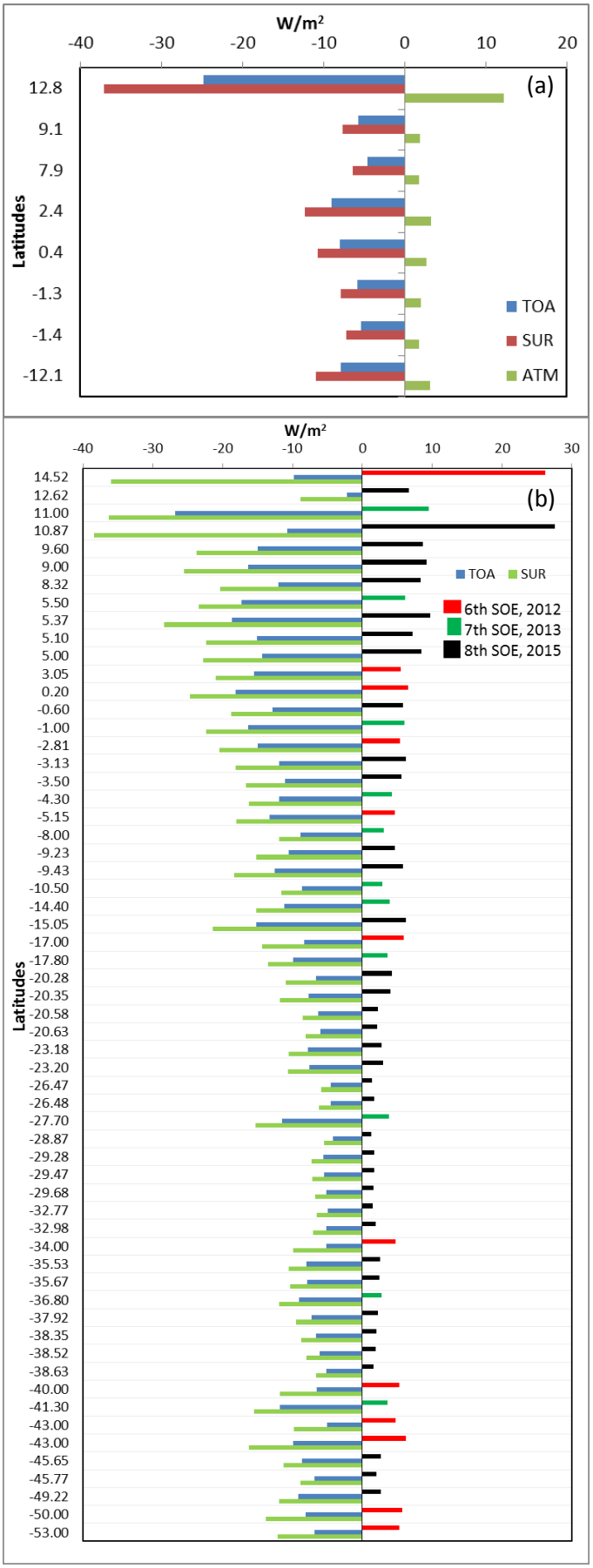

Fig 5.1: Radiative forcing seen over the Indian Ocean and the Indian Ocean sector of Southern Ocean at (a)IIOE-2 and (b) SOE6, 7 and 8 in the Atmosphere, at Surface and at Top of atmosphere

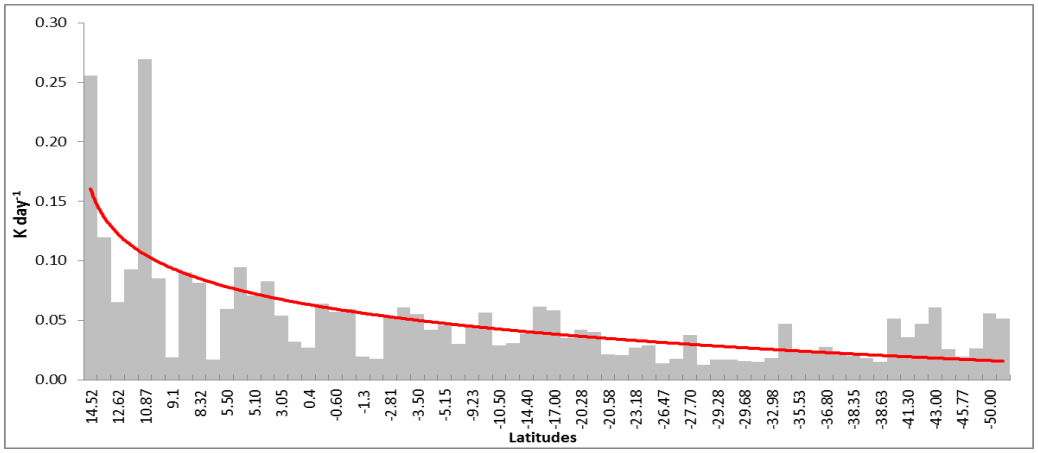

Fig 5.2: Heating Rate estimated over the Indian Ocean and the Indian Ocean sector of Southern Ocean at IIOE-2 and SOE-6, 7 and 8 shown with its logarithmic trendline.

5.2.2 Zone 2

In Zone 2, the aerosol composition is purely of oceanic origin. A few locations towards the south are exception where an influence of the South American peninsula was observed from the HYSPLIT trajectory frequency analysis explained in the Chapter 2. As a result, the average AODs of the region are lower than those in Zone 1 and 3 resulting in lower atmospheric forcing. The sea spray, BC mass concentration and sulphate values in this zone were incorporated in the SBDART model to estimate the forcing. The atmospheric forcing values seen in Zone 2 ranged from 1.5W m^{-2} (during February 2015, SOE 8) to 5W m^{-2} (during January 2012, SOE 6) as compared to 0.8-1.4 W m^{-2} as seen during the month of February by Babu et al 2010 (fig 5.1(b)).

5.2.3 Zone 3

In Zone 3, the confluence of the Agulhas retroflection (Anilkumar et al., 2006) with STF could be responsible for increased albedo and surface forcing, resulting in a higher ATM, which is in the range from 5-7 W m^{-2}. The analysis of microphysical characteristics indicate higher fine mode particles present near the surface as mentioned in Chapter 3. These can also contribute to the higher reflectance at the surface level other than the surface itself, which directly affect the surface forcing.

The proportionate variability of SUR and TOA forcing at each location away from the coastal waters suggest a restricted effect of anthropogenic aerosols while moving towards the Southern Ocean. The variation in DARF could also be attributed to an intra-annual process explained in Chapter 6. This process occurring in the Indian sector of the Southern Ocean region results in drastic variations in fine particles mass concentration with respect to time over the region south of 40^{o}S.

5.2.4 Variability of Radiative forcing and Heating Rate

It was noticed that the main source of variations in the DARF were due to the variability in the MABL and the variations in BC mass concentration which in turn could be due to variations in MABL as explained in Chapter 4. The DARF at TOA in the Zone 1 was in the range of –26.8 to –8.62 W m^{-2} and corresponding forcing at the surface was in the range –38.38 to –11.56 W m^{-2} resulting in the atmospheric forcing to be in the range of 2.9 to 27.6 W m^{-2}. In Zone 2, the top of atmosphere (TOA) forcing stayed approximately close to -7.3 Wm^{-2} while the surface forcing (SUR) increased from -12Wm^{-2} to -9Wm^{-2} as the season advanced from summer to winter in the southern hemisphere. The resultant variations of the TOA and SUR lead to much lower DARF values during the month of February (2-3 Wm^{-2}) as compared to January (4-6 Wm^{-2}).

The heating rate varies from an average value of 0.15 K day^{-1} from near the Indian coast to around 0.03 K day^{-1} in the Indian Ocean Sector of Southern Ocean. The heating rate in Zone 1 reduced from 0.124 K day^{-1} during the SOE 6 (December 2011) to 0.07 K day^{-1} in SOE 8 (January 2015), while in Zone 2 the values reduced from 0.053 K day^{-1} during SOE-6 (January 2012) to 0.022 K day^{-1} SOE-8 (February 2015). The higher heating rate seen off Indian coast could be attributed to the BC outflow from the Indian mainland owing to the wind pattern as explained in the Chapter 2, fig 2.7(b)(i), fig 2.8(a), (b) and (c). The data

points to the south of ITCZ, show lower heating rate values in the range 0.013 – 0.061K day^{-1} with an average value of 0.03K day^{-1} approximately.

A cyclic process emerged after analysing the dataset for the three SOE cruises. The process could induce variation in DARF observed in the region. The details of this process and the consequent variations in DARF are discussed in the Chapter 6.

IMPLICATIONS OF INTRA-ANNUAL TRANSFORMATION PROCESSES OF AEROSOLS ON RADIATIVE FORCING OVER THE INDIAN SECTOR OF SOUTHERN OCEAN

6.1 Introduction

Atmospheric aerosols play a vital role in Earth's radiation budget. Nevertheless, aerosols remain one of the greatest sources of uncertainty in climate modelling. The interaction with solar and terrestrial radiation by aerosols perturbs the radiative budget via scattering and absorption of sunlight. One of the greatest challenges in studying aerosol impacts on climate is their diversity, not only in terms of particle size, composition, and origin, but also spatial and temporal distributions (IPCC Report, 2014).

Major processes generating aerosol include emission of biogenic compounds from phytoplankton, surface winds and anthropogenic activities to list a few. The main source of cloud-condensation nuclei (CCN) over the oceans appears to be dimethyl sulphide (DMS), produced by Oceanic phytoplankton. It oxidizes in the atmosphere to form sulphate aerosol (Charlson et al., 1987). However, less emphasis has been laid to understand aerosol sinks since 2007 (IPCC Report, 2013).

A process has been discovered based in-situ data (from cruises) generated during the austral summers of 2011-2012, 2012-2013 and 2015 and concurrent MODIS data (onboard the satellite Aqua) derived during the same period, before and after the cruises. This process is responsible for the apparent generation and removal of natural aerosols in the Indian Ocean sector of Southern Ocean. The details of the processes and their implications on direct aerosol radiative forcing are given below.

6.2 Analysis of spectral variation of AOD, angstrom exponent and percentage of fine particle

The variations and anomalies seen in the AOD spectra, the resultant angstrom exponent ‘α’ and the percentage of fine mode particles in the total aerosol load are well

documented in Chapter 3. Primary and secondary peaks were seen in AOD spectra at 0.44μm and at 0.675μm respectively, which represent the general absorption characteristics of chlorophyll-a , pointing towards the effect of presence of phytoplankton derived products in the atmosphere.

The data from SOE-6, SOE-7 and SOE-8 was used for further analysis particles which represent January, End-January to February and February data respectively. The size segregated mass distribution of aerosols generated onboard during January from QCM data revealed abundance of fine mode particles (~55%). However, the percentage of fine mode aerosols reduced drastically to 20% in February during SOE 8 (fig 6.1b). The α values estimated from spectral AOD obtained during SOE-6, SOE-7 and SOE-8 are also seen to reduce from ≈0.5 to ≈0.1 indicating the large reduction in fine mode particles between January and February (fig 6.1c).

The satellite derived percentage of fine mode aerosols and α for 10 year period have been analysed for verifying the presence of a regularly occurring process. The mean and standard deviation of these parameters for 10 years during September to March have been presented in fig 6.1(d) and fig 6.1 (e). The figure clearly indicates a steady increase in percentage of fine mode particles (15% to 50 %) and α (0.45 to 0.9) from September to December. Subsequently it decreases to around 25% fine mode and α = 0.5 in February-March.

A comparison of α and percentage of fine mode particles derived from satellite data with those derived in-situ revealed that satellite derived values are consistently high. However, a good correlation is observed between the in-situ and satellite derived values of the above parameters during January, February and March. Since an increase in fine mode aerosols has been observed from September, the satellite data from September is considered.

These observations point to a cyclic process that exists in the region which is responsible for the variability of the fine mode particles in the given time frame.

Further investigating the cyclic process, a climatological survey was undertaken using the satellite data for past 10yrs from 2006-2015. The fig 6.1d and fig 6.1e present the 10-year climatological average of the satellite data of fine mode particle percentage and angstrom exponent for each month from September to March with its standard deviation.

The fine mode percentage values were in the range of 40-50% of the total aerosols size fraction (fig 6.1d). The satellite data (fig 6.1e) shows angstrom exponent values from 0.8 to 1 in December-January in the Southern Ocean. This indicates increasing dominance of fine mode aerosols during this period. The angstrom exponent values go as low as 0.4 to 0.6 fast during the month of February. It reaches a low value during March and remains constant for the rest of the year till the following austral summer. Every year, an increase in fine mode particles from September onwards and a subsequent decrease is observed from the in-situ as well as satellite data.

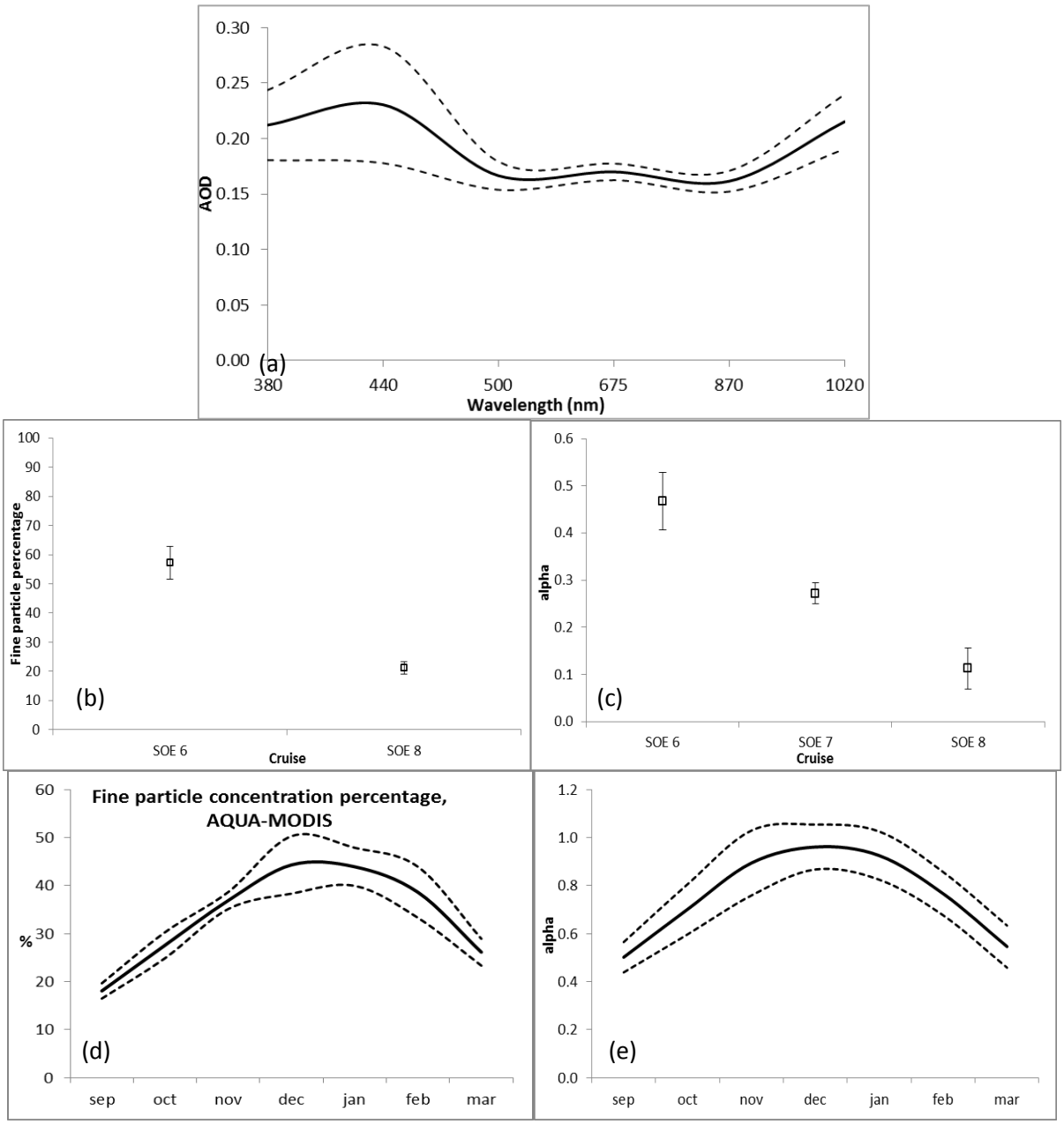

Fig 6.1: (a) Composite spectral AOD from SOE-6, SOE-7 and SOE-8; (b) In-situ fine particle percentage concentration derived from QCM during SOE-6 and SOE-8; (c) α derived from in-situ spectral AOD during SOE-6, SOE-7 and SOE-8; 10 year average of percentage (d) concentration of fine mode particles and (e) satellite derived alpha for months of September to March with their standard deviation.

6.3 Temporal variations in the solar insolation and surface chlorophyll-*a* concentration

The solar insolation over the region gradually increases from September onwards marking the beginning of austral summer essentially due to the annual axial tilt of the earth. The insolation peaks is in January and then rapidly decreases to March as the season advances towards winter (fig 6.2a). The satellite data show a gradual increase in chlorophyll-*a* concentration during October and November and peaks in January (fig 6.2b). The concentration begins to decline thereafter owing to the decrease in solar insolation.

The solar insolation is one of the factors influencing the growth of phytoplankton and hence primary productivity in the Southern ocean region. Other factors such as nutrients, reproduction and grazing also affect it. But in the present study, the effect of solar insolation is taken into consideration as this is the factor influencing the temperature, relative humidity and hence supports coagulation of finer particles to form coarse particles.

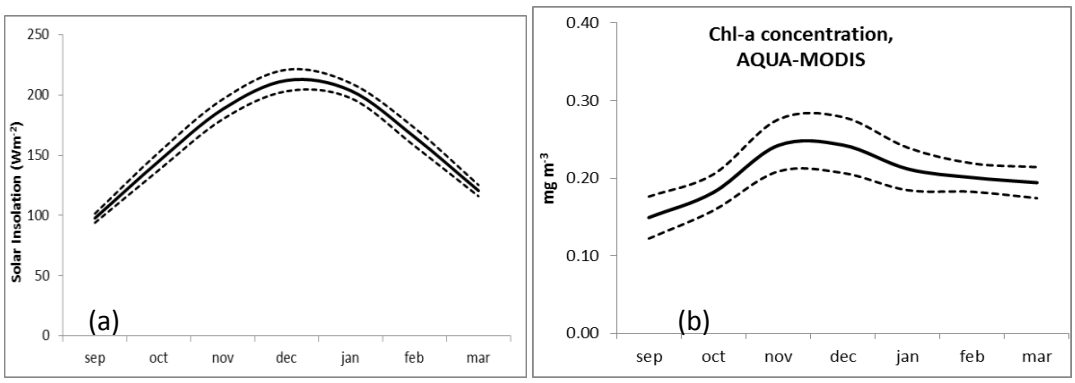

Fig 6.2: 10 year average of percentage (a) solar insolation for months of September to March and (b) chlorophyll-a concentration with their standard deviation.

6.4 Radiative forcing during the period of expeditions

The direct aerosol radiative forcing estimated during the SOE-6, SOE-7 and SOE-8 and the probable reasons thereof are discussed in Chapter 5. The average values of atmospheric forcing estimated during the SOE 8 are shown in Chapter 5 (fig 5.1). The surface forcing during January (SOE-6) is -12Wm^{-2} which is lower than that of February (SOE 8)

which is -9.3Wm^{-2}. The TOA forcing increased from -7Wm^{-2} to -7.3Wm^{-2} as the season advanced from summer to winter. The variation in the combination of the two resulted in lowering of atmospheric forcing values during the month of February as compared to January.

6.5 THE CYCLIC PROCESS OF SOUTHERN OCEAN

The solar insolation over the region increases from September (fig 6.2a) resulting in the growth of phytoplankton subsequently, increasing the primary productivity of the region. This resulted in an increase in the chlorophyll-a concentration (fig 6.2b). DMS produced as a by-product is released to atmosphere where it oxidises forming sulphate and methane sulphonate (MSA) aerosols (Charlson et al., 1987). The aerosols thus formed are either in nucleation or in Aitken mode. Due to favourable atmospheric conditions prevailing for a hygroscopic growth, aerosols convert from Aitken to accumulation mode and finally lead to further coagulation to form coarse mode aerosols (Seinfeld and Pandis, 1986).

However, the satellite data show higher α values during December-January in certain regions on the southern ocean indicating increasing dominance of fine mode aerosols during this period (fig 6.1b, 6.1c, 6.1d, 6.1e). As the austral summer advances to winter, the solar insolation reduces, directly influencing the growth of phytoplankton and primary productivity, as seen evident from the decrease in chlorophyll-a concentration (fig 6.2a and 6.2b). Thus the major source of DMS weakens, reducing the generation of aerosols in fine mode.

The fine to coarse conversion however, continues resulting in reduction of overall fine mode concentration. These observations are in conformity with Babu et al, (2010), a study based on data obtained in February 2004, showing lower α values and lower DARF. Hence,

if the cyclic process was known, it could have been predicted that the data obtained in February would yield such results.

It is a possibility that the mass concentration of aerosols might not be changing; rather it might only be the relative concentration of fine mode aerosol that changes. Consider a scenario where, a layer of mist that is present in the surface of ocean has an $AOD_{0.5}$ = 0.01 and it remains constant. Since the location under consideration is Southern Ocean, the most likely aerosol components constituting the mixture would be the water soluble particles originating from gas to particle conversion consisting of various kinds of sulphates, nitrates, organics and the sea spray in accumulation and coarse mode as a result of higher wind speed (Koepke et al. 1997). Since the back-trajectory analysis indicated presence of mineral transportation, the mineral dust will also form a part of aerosol mixtures.

The model OPAC was run considering the above conditions. The result showed that the mixture would have an average Single Scattering Albedo (SSA) of 0.996. Using this mixture in the model SBDART, the surface forcing estimated was -1.36Wm^{-2} and the top of atmosphere forcing was -1.08Wm^{-2}. The resulting atmospheric forcing would be 0.28Wm^{-2}. After simulating the variations in sulphate aerosol content of the mixture in SBDART, the variations observed in atmospheric forcing were up to 0.17Wm^{-2}. In other words, the sulphate aerosol variations contribute up to 0.17Wm^{-2} discrepancy in the estimation of atmospheric forcing.

The CLAW hypothesis is hence quantified through a pathway in cloud-free scenario through which the incoming radiation is altered right at the surface before it becomes available for the phytoplankton due to the DMS generated by the phytoplankton. The pathway as described by the hypothesis in which DMS forms the CCN and form clouds which obstruct the radiation might also hold true.

Higher surface forcing have been reported during the month of January (Menon et al., 2015) while those values obtained in the month of February, during the cruise SK200 (Babu et al, 2010) and 8th SOE, were lower. Depending on the characteristics of the surface layer of aerosol, the error in calculating the actual surface forcing would vary.

6.5.1 INTRODUCTION OF A FACTOR 'S' TO UNDRSTAND THE EFFECT OF CHLOROPHYLL-*a*

Analysing the variations in the fine mode percentage as a result of variations in chlorophyll-*a* concentrations, it is seen that the chlorophyll-*a* has a significant role in increasing the fine mode concentration (R^2=0.95) (fig 6.3a). The decline of fine mode particle concentration is only partially due to the decreasing chlorophyll-*a* concentrations (R^2=0.52) (fig 6.3b). The decline is attributed to the decrease in DMS generation which was responsible for the input of fine mode particles. On the whole, a climatological relation between chlorophyll-*a* and fine mode particles in Southern Ocean is significant (R^2=0.79) as seen in chapter 3, fig 3.6.

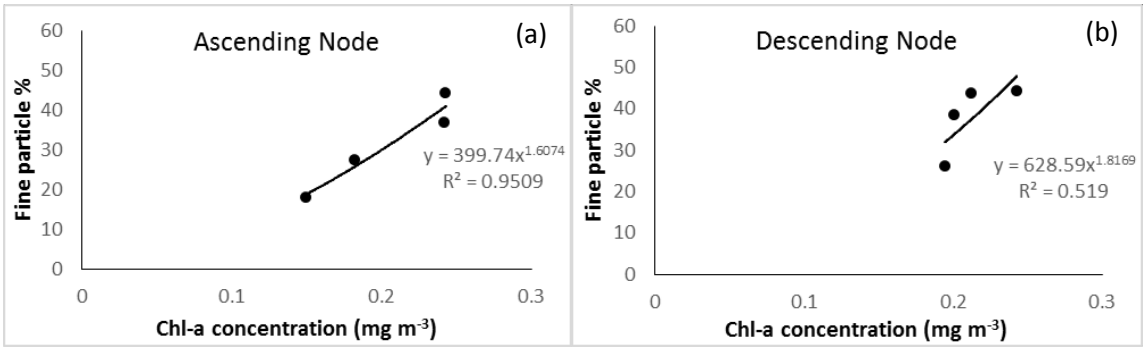

Fig 6.3: 10-year exponential correlation between chl-a concentration and fine particle percentage during the austral summer
(a) Ascending node – Increase in Fine mode aerosols (b) Descending Node – Decrease in Fine mode aerosols

In the process of analysing the correlation during the study period, it was noticed that the correlation between chlorophyll-*a* concentration and the percentage of fine mode particle oscillates giving a higher coefficient of correlation (R^2) every alternate year from 2006 to 2015 (fig 6.4). It was also noticed that during the austral summer of 2012-13 (Nov 2012 –

March 2013), the expected peak was not observed. This may have resulted in lowest R^2= 0.27 seen in past 10 years during austral summer of 2013-14 (Nov 2013 – March 2014).

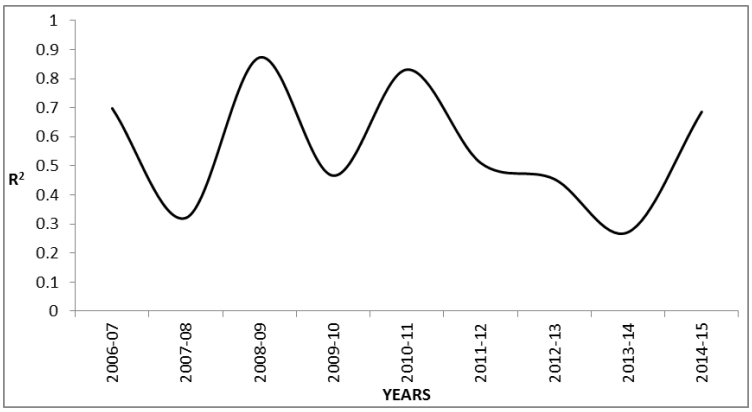

Fig 6.4: The oscillating nature correlation between chl-a concentration and percentage of fine particle during Sept 2006 to March 2015.

In order to understand the efficiency of chlorophyll-*a* in increasing fine mode particles in the Southern Ocean, south of 40^{o}S, a factor **'S'** is introduced, which has been estimated as follows.

S = Fine Particle Percentage X chlorophyll-*a* conc. **(6.1)**

The resultant Hovmoller plot is shown in fig 6.5, which clearly indicates that the highest efficiency has been achieved during December-January window of every year. It also shows an oscillation as seen in the figure, which is for a period of 10 years (2006 – 2015).

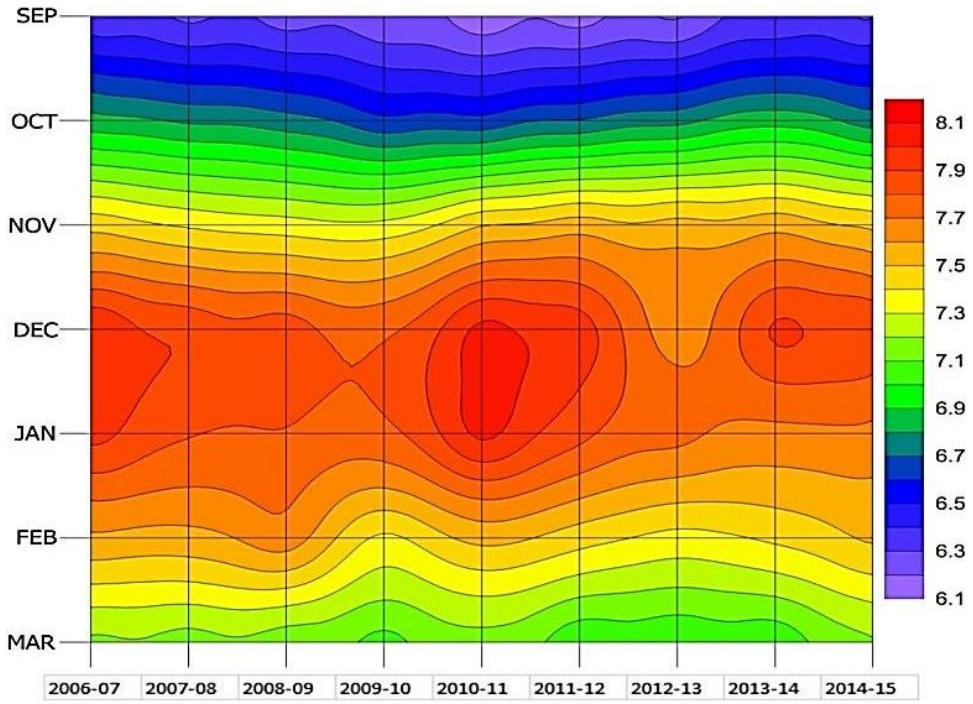

Fig 6.5: Hovmoller plot of the factor 'S'

The cruise SK200 to the Southern Ocean held during the February of 2004 falls in the time slot 2003-04. Analysing the result of this cruise as discussed in Babu et al 2010, with the help of factor 'S', a simple extrapolation would place the value of 'S' in the lower range during the period of 2003-04. That would imply a lower value of R^2 of the regression between chlorophyll-*a* and fine particles percentage be expected. As a result, a lower DARF would be expected. Since, the R^2 would be lower, the influence of variations in chlorophyll-*a* concentration would have lower effect on the fine mode particles concentration, resulting in lower values and deviation in the DARF values of the study.

SUMMARY AND FUTURE SCOPE OF THE STUDY

7.1 Summary

The present study has been carried out to characterize physical properties of aerosols based on their optical properties over the Indian Ocean, specifically over equatorial region, South-west Tropical Indian Ocean (SWTIO) region, area covering 15^{o}N and 55^{o}S (SOE) and Antarctica. SWTIO and Equator cruises were during June and September while, Southern Ocean Expedition (SOE), second International Indian Ocean Expedition (IIOE-2) and Antarctica cruises were carried out during the period December to February. Major focus was given to the spatial and temporal variability of composite aerosols with a special reference to black carbon (BC) mass concentration. Since the area of study includes those in the proximity of land and remote areas of the ocean, the entire study area had been divided in to three different zones viz., Zone 1, Zone 2 and Zone 3 (as explained in Chapter 2).

A unique study of this research work is the chemical analysis of aerosols to characterize the trace elements, samples for which were collected during SOE-6. This addressed some of the key issues related to generation of aerosols over the oceanic environment. An attempt to identify the source has been performed to all the observations from different cruises. Implications of the variability of aerosols over the study area on the incoming solar radiation were also studied by estimating the direct aerosol radiative forcing (DARF) and its associated heating. This was done using the models, Optical Properties of Aerosols and Cloud (OPAC) and Santa-Barbara DISORT Atmospheric Radiative Transfer (SBDART), to understand their potential to perturb the radiative budget of the atmosphere system.

The Important results of the study are summarized below.

- On the basis of Microtops II measurement, the aerosols parameters studied include columnar AOD, α, ’ and QCM based size segregation. The columnar $AOD_{0.5um}$ in Zone 1 is ranging between 0.35 an 0.4 which reduces to 0.06 to 0.25 with an average value of 0.15 in Zone 2 with a further increase to 0.2±0.04 in Zone 3.
- Subsequent analysis to understand the components of composite aerosols revealed that fine mode particles are more predominant in Zone 1 which reduces further in the remote oceanic region, Zone 2. The intra-zonal variability analysed over Zone 2 revealed a large seasonality in this zone. Based on 10yrs of MODIS derived AOD, it is observed that the fine mode particles increased from September to December and decreased as the austral summer advances towards winter from December to March. To delineate the source of such variability, 10 yrs of MODIS Angstrom exponent, chlorophyll-*a* concentration, and solar insolation were also studied.
- A distinct feature seen in the spectral AOD is the non-compliance with the Angstrom turbidity formula in Zone 2 and Zone 3 wherein the spectra revealed a primary peak at 0.44 µm and a secondary peak at 0.675µm. The only possibility of such an anomaly in the spectral AOD is the dominance of aerosol from the phytoplankton. This has been examined from OPAC model by estimating $AOD_{0.44um}$ and comparing the difference between measured and modelled $AOD_{0.44um}$ with chlorophyll-*a* concentration. The R^2 is around 0.8.
- Since this result was only of one cruise, the 10yrs of MODIS-AOD during the period 2006-2015 have been examined along with the rest of the MODIS data mentioned before. An important result obtained from this analysis is that the coefficient of correlation between fine mode particles and chlorophyll-a concentration oscillates in alternate years from 2006 to 2015. This means that in first year a strong correlation is vivid while in

second year, the correlation is weak. However, this relation was weak during the austral summer of 2012-2013 which could be ascribed to of the phytoplankton cell as revealed by a study on pigment packaging effect in Southern Ocean by Tripathy et al 2014, carried out during this period.

- In order to understand the efficiency of chlorophyll-*a* in increasing fine mode particles in the Southern Ocean, south of 40^{o}S, a factor **'S'** is introduced, which has been estimated as follows.

S = Fine Particle Percentage X chlorophyll-*a* conc.

- An ICPMS based trace metal analysis of the aerosol samples collected during SOE 6 sampled from Zone 2 showed that the main components are Cu, Zn and Cd. Cu ranges from 50 ppb to100 ppb while Zn has a maximum value of around 25ppb at two locations. Cd showed overall low values except for one location where it increases to approximately 20 ppb. An interesting result observed is the inverse relation between trace element Cu and sulphate aerosols which could be explained as follows. Generally, the source of sulphate aerosols are anthropogenically derived, those from industrial output, and naturally produced from phytoplankton. The area of study being a remote region of the ocean, the only source of sulphate aerosol is phytoplankton. It is observed that, when Cu increases, sulphate decreases which clearly indicates effect of anthropogenic derived trace elements such as Cu on the metabolism of phytoplankton. HYSPLIT trajectories have been analysed and it was found that the trace elements transported from South American continent, which is abundant with copper mines, are the major source.
- The aethalometer derived BC mass concentration depicted a large variability, from Zone 1 to Zone 3. In Zone 1, concentration is around 1700 ng m^{-3} while in Zone 2 the values ranged from 37 and 132ng m^{-3}, with an abnormal peak of 226 ng m^{-3} observed at 50^{o}S and in Zone 3 it is 93.8±21.7 ng m^{-3}. The BC mass concentration in Zone 2 had an

average of 80 ng m^{-3}, revealing the fact that the atmosphere is not clean, devoid of BC as per the definition of Hess et al, 1998.

- It was observed that to the south of ITCZ, the BC concentration is controlled mainly by the Marine Atmospheric Boundary layer (MABL) dynamics.
- The information on spatial and temporal variability of aerosols and BC mass concentration had been used in SBDART to estimate DARF. The DARF at TOA in the Zone 1 was in the range of –26.8 to –8.62 W m^{-2} and corresponding forcing at the surface was in the range –38.38 to –11.56 W m^{-2} resulting in the atmospheric forcing to be in the range of 2.9 to 27.6 W m^{-2}. In Zone 2, the top of atmosphere (TOA) forcing stayed approximately close to -7.3 Wm^{-2} while the surface forcing (SUR) increased from -12Wm^{-2} to -9Wm^{-2} as the season advanced from summer to winter in the southern hemisphere. The resultant variations of the TOA and SUR lead to much lower DARF values during the month of February (2-3 Wm^{-2}) as compared to January (4-6 Wm^{-2}).
- Heating rate has been estimated and it is found to be varying between, 0.124 to 0.052 K day^{-1} in Zone 1, while lower heating rate values are seen in Zone 2 with values in the range of 0.013 – 0.061K day^{-1} with an average value of 0.03K day^{-1} approximately. The heating rate varies from an average value of 0.15 K day^{-1} from near the Indian coast to around 0.03 K day^{-1} in the Indian Ocean Sector of Southern Ocean. The heating rate in Zone 1 reduced from 0.124 K day^{-1} during the SOE 6 (December 2011) to 0.07 K day^{-1} in SOE 8 (January 2015), while in Zone 2 the values reduced from 0.053 K day^{-1} during SOE-6 (January 2012) to 0.022 K day^{-1} SOE-8 (February 2015).
- The process similar to the one described by CLAW hypothesis is quantified in cloud-free scenario wherein the solar insolation is altered at the surface by up to 0.17 Wm^{-2} only due sulphate aerosol directly related to DMS and 0.28 Wm^{-2} considering the composite

aerosol of the region before it is available for the phytoplankton due to the aerosols present as a result of DMS generated by the phytoplankton.

7.2 Scope for Future work

The present research work was initiated due to lack of concurrent measurements of optical and physical properties of aerosols over the North Indian Ocean (15^{o}N to equator), the Indian Ocean and Indian Ocean sector of Southern Ocean (equator to 55^{o}S). Based on the current study, it is observed that phytoplankton derived DMS is the main source of sulphate aerosol over the study area. The chemical analysis of aerosol samples provided important information about the trace metals prevailing in the region and detrimental effect on the phytoplankton, if present in higher concentration. However, additional instrumentation is required for in-depth knowledge to establish the hypothesis of formation of sulphate aerosol from phytoplankton and the adverse effect of the trace elements. Thus, the detail mechanism of the sulphate aerosol formation from phytoplankton and chemical characterisation of aerosol are necessary for future atmospheric research to infer their role as CCN and radiative impact. This is probably the only study, dealt with the chemical composition of aerosol linking it to the phytoplankton and subsequent formation of aerosols.

The objective of present study was to enhance accuracy of estimating DARF using SBDART by incorporating aerosol chemistry. In course of understanding the variability in chemistry data viz., spatial variation of sulphate ion, the role of trace elements in altering the fine mode aerosol concentration was revealed. While estimating DARF with the help of SBDART using the $AOD_{0.5um}$, BC mass concentration and chemical composition measurements at the surface, it was assumed that concentrations of different species of the aerosol mixture are uniformly distributed till the top of the local MABL which may not be

always true. Therefore, further improvement in the estimation of optical properties of aerosols and hence DARF calculations can be achieved by augmenting the instrumentation.

The co-located measurements of aerosol parameters can be improved using the LIDAR, Nephalometer measurements and unmanned Aerial Vehicle Systems (UAVS) as a part of future studies. In addition, it is also proposed to procure 'Particle In Liquid Sampler' (PILS) for generating aerosol samples for chemical analysis improving sample handling and avoiding the sample degradation associated with filter papers. Since most of the aerosol characteristics have a direct link to the evolution of boundary layer, to have a better understanding of the different atmospheric process related to aerosols generation, advanced meteorological measurements using higher resolution radiosonde observations need to be initiated.

Finally, using the dataset generated a better estimate of DARF and thus a better understanding of the climate could be achieved.

REFERENCES

References

Aloysius, M., Mannil Mohan, S. Suresh Babu, Vijayakumar S Nair, K. Parameswaran and K. Krishna Moorthy, Influence of circulation parameters on the AOD variations over the Bay of Bengal during ICARB, 2008, Journal of Earth System Science, 117, S1, 2353-360.

Andreae, M.O., Jones, C.D., Cox, P.M., (2005). Strong present-day aerosol cooling implies a hot future. Nature 435 (3671), 1187–1190.

Babu, S.S., K.K. Moorthy and S.K. Satheesh, "Latitudinal gradient in aerosol properties over the Indian and Southern oceans during the austral summer", 2010, Current Science, 99 (10).

Beegum S.N., Moorthy K.K. and Babu S.S. (2009) Aerosol microphysics over a tropical coastal station inferred from the spectral dependence of Ångström wavelength exponent and inversion of aerosol spectral optical depth; Journal of Atmospheric and Solar-Terrestrial Physics, 71, 1846–1857.

Carmichael, G. R., M.-S. Hong, H. Ueda, L.-L. Chen, K. Murano, J. K. Park, H. Lee, Y. Kim, C. Kang, and S. Shim, (1997), Aerosol composition at Cheju Island, Korea, J. Geophys. Res., 102, 6047 – 6061,.

Charlson R. J., Schwartz S. E., Hales J. M., Cess R. D., Coakley J. A., Jr., Hansen J. E. and Hofmann D. J. Climate forcing by anthropogenic aerosols. Science 255 (1992) 423-430.

Charlson, R. J., Lovelock, J. E., Andreae, M. O. and Warren, S. G. (1987). "Oceanic phytoplankton, atmospheric sulphur, cloud albedo and climate". Nature. 326 (6114): 655–661. Bibcode:1987 Natur.326..655C. doi:10.1038/326655a0

Chaubey, J.P., Krishnamoorthy, K., Suresh Babu, S., Gogoi, Mukund M., 2013. Spatiotemporal variations in aerosol properties over the Oceanic regions between coastal India and Antarctica. J. Atmos. Solar-terr. Phys. 104, 18–28.

Collins, D. R., Jonsson, H. H., Seinfeld, J. H., Flagan, R. C., Gasso, S., Hegg, D. A., Russell, P. B., Schmid, B., Livingston, J. M., Öström, E., Noone, K. J., Russell, L. M., and Putaud, J. P. 2000. In-situ aerosol size distributions and clear column radiative closure during ACE 2. Tellus 52B, 498-525.

Covert, D. S., Gras, J. L., Wiedensohler, A., and Stratmann, F. (1998). Comparison of directly measured CCN with CCN modeled from the number-size distribution in the marine boundary layer during ACE 1 at Cape Grim, Tasmania. J. Geophys. Res. 103, 16597-16608.

Durkee, P. A., Nielsen, K. E., Smith, P. J., Russell, P. B., Schmid, B., Livingston, J. M., Holben, B. N., Tomasi, C., Vitale, V., Collins, D., Flagan, R. C., Seinfeld, J. H., Noone, K. J., Öström, E., Gasso, S., Hegg, D., Russell, L. M., Bates, T. S., and Quinn, P. K. 2000a. Regional aerosol optical depth characteristics from satellite observations: ACE 1, TARFOX and ACE 2 results. Tellus 52B, 484-497.

Eck, T.F., Holben, B.N., Reid, J.S., Dubovik, O., Smirnov, N.T., O'Niel, Slutsker, I., Kinne, S., (1999). Wavelength dependence of the optical depth of biomass burning, urban and desert dust aerosols. J. Geophy. Res. 104 (D24), 349 31,333–31.

Forster, P., Ramaswamy, V., Artaxo, P., Berntsen, T., Betts, R., Fahey, D. W., Haywood, J., Lean, J., Lowe, D. C., Myhre, G., Nganga, J., Prinn, R., Raga, G., Schulz, M., and Van Dorland, R.: Radiative Forcing of Climate Change, in Climate Change 2007: The Physical Science Basis. Contribution of Working Group I to the Fourth Assessment Report of the Intergovernmental Panel on Climate Change, edited by S. Solomon, D. Qin, M. Manning, Z.

Chen, M. Marquis, K. B. Averyt, M. Tignor, and H. L. Miller, (2007), pp. 129–234, Cambridge Univ. Press, Cambridge, United Kingdom and New York, NY, USA,.

Guleria R.P., Kuniyal J.C. and Dhyani P.P. (2012) Seasonal variability in aerosol optical and physical characteristics estimated using the application of the Angstrom formula over Mohal in the northwestern Himalaya; India Journal of Earth System Science, 121, 697– 710.

Hadlock, Charles (1998). Mathematical Modeling in the Environment. Washington: Mathematical Association of America. ISBN 0-88385-709-X)

Haywood J, Boucher O, (2000) Estimates of the direct and indrirect radiative forcing due to tropospheric aerosols: a review. Rev Geophys 38: 513-543

Haywood, J. and Schulz, M.: Causes of the reduction in uncertainty in the anthropogenic radiative forcing of climate between IPCC (2001) and IPCC (2007), Geophys. Res. Lett., 34, doi:10.1029/2007GL030749, l20701, 2007.

Hoppel, W. A. 1988. The Role of Non-Precipitating Cloud Cycles and Gas-to-Particle Conversion in the Maintenance of the Submicron Aerosol size distribution over the tropical Oceans. P. V. Hobbs and M. P. McCormick (Ed.), In Aerosols and Climate. A. Deepak Publishing, Hampton, Virginia: 9-19.

Huebert, B. J., Howell, S. G., Zhuang, L., Heath, J. A., Litchy, M. R., Wylie, D. J., Kreidler-Moss, J. L., Cöppicus, S., and Pfeiffer, J. E. 1998. Filter and impactor measurements of anions and cations during the First Aerosol Characterization Experiment (ACE 1). J. Geophys. Res. 103, 16493-16509.

Iqbal, Muhammad, (1983) An Introduction to Solar Radiation. Academic Press, Toronto.

Jaenicke R. (1993) Tropospheric aerosols. In: P.V. Hobbs (Ed), Aerosols cloud-climate interaction, Academic Press, San Diego, pp. 1-27.

Jayaraman, A., D. Lubin, S. Ramachandran, V. Ramanathan, E. Woodbridge, W. Collins and K.S. Zalpuri. Direct Observations of Aerosol Radiative Forcing Over the Tropical Indian Ocean during the Jan-Feb 1996 Pre-INDOEX Cruise, J. Geophys. Res., 103(D12), 13827-13836, 1998. C4 publication #180.

Jha, B. and Krishnamurti, T. N., Real-time meteorological reanalysis atlas during pre-INDOEX field phase-1998, FSU Report #98-08, Department of Meteorology, Florida State University, Tallahassee FL 32306-4520, USA, August, 1998.

K. Krishna Moorthy, Influence of circulation parameters on the AOD variations over the Bay of Bengal during ICARB, 2008, Journal of Earth System Science, 117, S1, 2353-360.

Kalapureddy, M.C.R., Ernest Raj, P. and Devara, P.C.S., Total columnar ozone variations over oceanic region around Indian sub-continent during pre-monsoon of 2006 , 2008, Atmos. Chem. Phys. Discuss., 8, 3143–3162,

Kaskaoutis D.G., Kharol S.K., Sinha P.R., Singh R.P., Badarinath K.V.S., Mehdi W. and Sharma M. (2011) Contrasting aerosol trends over South Asia during the last decade based on MODIS observations; Atmospheric Measurements Techniques Discussion, 4, 5275–5323, doi: org/10.5194/amtd-4-5275-2011.

Kedia S. and Ramachandran S. (2008) Latitudinal and longitudinal variation in aerosol characteristics from sun photometer and MODIS over the Bay of Bengal and Arabian Sea during ICARB; Journal of Earth System Science, 117(S1), 375-387.

Kedia S. and Ramachandran S. (2011) Seasonal variation in aerosol characteristics over an urban location and a remote site in western India; Atmospheric Environment, 45, doi.org/10.1016/j.atmosenv.2011.01.040.

Krishna Moorthy, K., S.K. Satheesh and B.V. Krishna Murthy. Investigations of Marine Aerosols Over the Tropical Indian Ocean. J. Geophys. Res., 102(15), 18827-18842, 1997.

Krishnamurti, T. N. ; Jha, B. ; Prospero, J. ; Jayaraman, A. ; Ramanathan, V. (1998) Aerosol and pollutant transport and their impact on radiative forcing over the tropical Indian ocean during the January - February 1996 pre-INDOEX cruise Tellus B, 50 (5). pp. 521-542.

Krishnamurti, T.N., B. Jha, P.J. Rasch and V. Ramanathan. A High Resolution Global Reanalysis Highlighting the Winter Monsoon, Meteorology and Atmospheric Physics, 64:123-150, 1997. C4 publication #181.

Kumar, K. R., K. Narasimhulu, G. Balakrishnaiah, B. S. K. Reddy, K. R.Gopal,R.R. Reddy, L.S.S. Reddy, K. K. Moorthy, S. Suresh Babu and C.B.S. Dutt, Spatial heterogeneities in aerosol properties over Bay of Bengal inferred from ship-borne and MODIS observations during ICARB-W cruise campaign: Implications to radiative forcing, 2011, Atmospheric Environment, 45, 404-412.

Livingston, J. M., Kapustin, V., B.Schmid, Russell, P. B., Quinn, P. K., Bates, T. S., Durkee, P. A., Smith, P. J., Freudenthaler, V., Wiegner, M., Covert, D. S., Gasso, S., Hegg, D., Collins, D. R., Flagan, R. C., Seinfeld, J. H., Vitale, V., and Tomasi, C. 2000. Shipboard sunphotometer measurements of aerosol optical depth spectra and columnar water vapor during ACE 2 and comparison with selected land, ship, aircraft, and satellite measurements. Tellus 52B, 594-619.

Lohmann, U. & Feichter, J. (2005), Global indirect aerosol effects: a review. Atmos. Chem. Phys. 5, 715–737

Menon H.B., Sangekar, N., Lotliker, A., Krishnamoorthy, K., Vethamony, P., 2011. Aerosol optical thickness and spatial variability along coastal and offshore waters of the eastern Arabian sea. ICES journal of Marine Science 68 (4), 745-750. doi.10.1093/icesjms/fsq19

Menon, H.B., Shirodkar, S., Kedia, S., Ramachandran, S., Babu, S.S., Moorthy, K.K., 2014. Temporal variation of aerosol optical depth and associated shortwave radiative forcing over a coastal site along the west coast of India. Science of the Total Environment 468-469, http://dx.doi.org/10.1016/j.scitotenv.2013.08.013.

Moorthy K,K., Babu, S.S., Manoj M, R., and Saheesh, S.K., 2013a. Build-up of aerosols over the Indian Region, Geophysical Research Letters., 40, doi: 10.1002/grl.50165.

Moorthy K. K., Nair P.R. and Murthy B.V.K. (1991) Size distribution of coastal aerosols: effects of local sources and sinks; Journal of Applied Meteorology, 30, 844-852.

Moorthy,K,K., Beegum S.N, Srivastav, N., Satheesh, S.K., Mian Chin., Nadege Blond, Babu, S.S., Singh, S., 2013b. Performance evaluation of chemistry transport models over India, Atms. Environment, 71, 210 – 225.

Narasimhan, D and Satheesh, S.K., 2013, Estimates of aerosol absorption over India using multi-satellite retrieval, Ann. Geophys, 31, doi: 10.5194/angeo-31, 1773 – 2013.

Neusüß, C., Weise, D., Birmili, W., Wex, H., Wiedensohler, A., and Covert, D. 2000. Size-segregated chemical, gravimetric and number distribution-derived mass closure of the aerosol in Sagres, Portugal during ACE-2. Tellus 52B, 169-184.

Nick D'Adamo, Planning and implementation for the Second International Indian Ocean Expedition (IIOE-2), 2015, IIOE-2 Symposium, Port Louis, Mauritius.

Petroff, A., Mailliat, A., Amielh, M., and Anselmet, F.: Aerosol dry deposition on vegetative canopies. Part I: Review of present knowledge, Atmos. Environ., 42, 3625–3653, 2008

Prospero, J. M., and D. L. Savoie, (1989b): Nitrate concentrations over the Pacific: Oceanic background and continental impacts. Nature, 339, 687–689.

Prospero, J. M., Uematsu, M. and Savoie, D. L., (1989a) Mineral transport to the Pacific Ocean Chem. Oceanogr., , 10, 187–218.

Prospero, J.M., R.J. Charlson, V. Mohnen, R. Jaenicke, A.C. Delany, J. Meyers, W. Zoller, and K. Rahn, The atmospheric aerosol system: An overview, (1983) Rev. Geephys. and Space Phys., 21, 1607-1629,.

Whitby, K. T. (1978). The physical characteristics of sulfur aerosols. Atmos. Environ. 12, 135-159.

Putaud, J. P., van Dingenen, R., M., M., Virkkula, A., Raes, F., Maring, H., Prospero, J. M., Swietlicki, E., Berg, O. H., Hillamo, R., and Mäkelä, T. 2000. Chemical mass closure and assessment of the origin of the submicron aerosol in the marine boundary layer and the free troposphere at Tenerife during ACE-2. Tellus 52B, 141-168.

Quinn, P. K., and Coffman, D. J. 1998. Local closure during the First Aerosol Characterization Experiment (ACE 1): Aerosol mass concentration and scattering and backscattering coefficients. J. Geophys. Res. 103, 16575-16596.

Ramanathan, V., P.J. Crutzen, J. Coakley, R. Dickerson, A. Heymsfield, J. Kiehl, D. Kley, T.N. Krishnamurti, J. Kuettner, J. Lelieveld, A.P. Mitra, J. Prospero, R. Sadourny, F.P.J.

Valero and E.L. Woodbridge. Indian Ocean Experiment (INDOEX) White Paper. July 1995. C4 publication #143.

Ramanathan, V., P.J. Crutzen, J.A. Coakley, A. Clarke, W.D. Collins, R. Dickerson, D. Fahey, B. Gandrud, A. Heymsfield, J.T. Kiehl, J. Kuettner, T. Krishnamurti, D. Lubin, H. Maring, J. Ogren, J. Prospero, P.J. Rasch, D. Savoie, G. Shaw, A. Tuck, F.P.J. Valero, E.L. Woodbridge and G. Zhang. Indian Ocean Experiment (INDOEX), A Multi-Agency Proposal for a Field Experiment in the Indian Ocean. June 1996. C4 publication #162.

Rhoads, K.P., P. Kelley, R. Dickerson, T. Carsey, M. Farmer, D. Savoie and J. Prospero. The Composition of the Troposphere over the Indian Ocean during the Monsoonal Transition. J. Geophys. Res., 102(15): 18981-18995, 1997. C4 publication #179.

Russell, P. B., and Heintzenberg, J. 2000. An Overview of the ACE 2 Clear Sky Column Closure Experiment (CLEARCOLUMN). Tellus 52B, 463-483.

Russell, P. B., Hobbs, P. V., and Stowe, L. L. 1999. Aerosol properties and radiative effects in the Unites States East Coast haze plume: An overview of the tropospheric aerosol radiative forcing observational experiment (TARFOX). J. Geophys. Res. 104, 2213-2222

Satheesh, S.K. and K. K. Moorthy. Aerosol Characteristics Over Coastal Regions of the Arabian Sea. Tellus, 49B, 417-428, 1997.

Schmid, B., Livingston, J. M., Russell, P. B., Durkee, P. A., Jonsson, H. H., Collins, D. R., Flagan, R. C., Seinfeld, J. H., Gassó, S., Hegg, D. A., Öström, E., Noone, K. J., Welton, E. J., Voss, K. J., Gordon, H. R., Formenti, P., and M. O. Andreae 2000. Clear sky closure studies of lower tropospheric aerosol and water vapour during ACE 2 using airborne sunphotometer, airborne in-situ, space-borne, and ground-based measurements. Tellus 52B, 568-593.

Schuster, G. L., Dubovik, O. and Holben, B. N. 2006. Angstrom Exponent and Bimodal Aerosol Size Distributions. J. Geophys. Res., 111: D07207

Seinfeld J.H., Pandis S.N. (1998) Atmospheric chemistry and Physics: From air pollution to climate change, Wiley-Inter Science.

Sinha P. R., R. K. Manchanda, J. V. Subbarao, U. C. Dumka, S. Sreenivasan, S. Suresh Babu and K. Krishna Moorthy, Spatial distribution and Vertical Structure of the MABL Aerosols over Bay of Bengal during winter: Results from W-ICARB Experiment, 2011, Journal of Atmospheric Solar Terrestrial Physics, 73 (4), pp. 430-438.

Soni K., Singh S., Bano T., Tanwar R. S. and Nath S. (2011) Wavelength dependence of the aerosol angstrom exponent and its implications over Delhi, India; Aerosol science and technology, 45, 1488-1498, doi: 10.1080/02786826.2011.601774.

Sportisse, B. (2007), A review of parameterizations for modelling dry deposition and scavenging of radionuclides, Atmos Environ, 41(13), 2683-2698.

Stein, A.F., Draxler, R.R, Rolph, G.D., Stunder, B.J.B., Cohen, M.D., and Ngan, F., (2015). NOAA's HYSPLIT atmospheric transport and dispersion modeling system, Bull. Amer. Meteor. Soc., 96, 2059-2077, http://dx.doi.org/10.1175/BAMS-D-14-00110.1

Stull, R.B., An introduction to boundary layer meteorology (Kluwer Academic Publishers, Dordrecht, 1988

V. Sreekanth, K. K.Moorthy, S. K. Satheesh, S. S. Babu, V. S. Nair, K. Niranjan, Airborne measurements of aerosol scattering properties above the MABL over Bay of Bengal during W-ICARB – characteristics and spatial gradients, 2011, Annales Geophysicae, 29, 895–908, www.ann-geophys.net/29/895/2011/ doi:10.5194/angeo-29-895-2011.

William G. Sunda (1989) Trace Metal Interactions with Marine Phytoplankton, Biological Oceanography, 6:5-6, 411-442

McFarquhar, G., J.P. Chen, C. Volpe and A. Thakur. INDian Ocean EXperiment: A preliminary survey of available observations of atmospheric chemistry over the Indian Ocean region. October 1994. C4 publication #125.

Wizelius, Tore (2007). Developing Wind Power Projects. London: Earthscan Publications Ltd. p. 40. ISBN 1-84407-262-2. The relation between wind speed and height is called the wind profile or wind gradient.

Deep-Sea Research II 118 (2015) 142–151

Contents lists available at ScienceDirect

Deep-Sea Research II

journal homepage: www.elsevier.com/locate/dsr2

Spatial heterogeneity in spectral variability of aerosol optical depth and its implications to aerosol radiative forcing in the Tropical Indian Ocean and in the Indian Ocean Sector of Southern Ocean

Harilal B. Menon [a,*], Shrivardhan Hulswar [a], N. Anilkumar [b], Achuthankutty Chittur Thelakkat [b], K.Krishna Moorthy [c], Suresh Babu [d]

[a] Department of Marine Sciences, Goa University, University P.O, Goa 403206, India
[b] ESSO-National Centre for Antarctic and Ocean Research, Ministry of Earth Sciences, Vasco-da-Gama, Goa 40384, India
[c] Indian Space Research Organisation, Antariksh Bhavan, Bangalore 560231, India
[d] Space Physics Laboratory, Vikram Sarabhai Space Centre, Indian Space Research Organisation, Thiruvananthapuram, Kerala 695022, India

ARTICLE INFO

Available online 27 March 2015

Keywords:
Aerosol optical depth (AOD)
Polynomial fit
Microtops II sunphotometer
Aerosols
ITCZ
Tropical Indian Ocean
Indian Ocean Sector of Southern Ocean

ABSTRACT

The aerosol optical depths (AODs) in the wavelength range 380–875 nm and black carbon (BC) mass concentrations were estimated over the tropical Indian Ocean and in the Indian Ocean sector of Southern Ocean, between 14°N and 53°S, during December 2011–February 2012, onboard the Ocean Research Vessel (ORV) Sagar Nidhi. The data were analysed to understand the spectral variability, micro-physical characteristics of aerosols and the associated radiative forcing. Concurrent MODIS-derived chlorophyll a (Chl-*a*) and sea-surface temperature (SST) provided ancillary data used to understand the variability of biomass in association with fronts and the possible role of phytoplankton as a source of aerosols. AODs and their spectral dependencies were distinctly different north and south of the Inter-Tropical Convergence Zone (ITCZ). North of 11°S (the northern limit of ITCZ), the spectral distribution of AOD followed Ängstrom turbidity formule (Junge power law function), while it deviated from such a distribution south of 16°S (southern boundary of ITCZ). At the southern limit of the ITCZ and beyond, the spectral variation of AOD showed a peak around 440 nm, the amplitude of which was highest at ~43°S, the axis of the subtropical front (STF) with the highest Chl-*a* concentration (0.35 μg l^{-1}) in the region. To understand the role of Chl-a in increasing AOD at 440 nm, AOD at this wavelength was estimated using Optical properties of Aerosols and Clouds (OPAC) model. The anomalies between the measured and model-estimated (difference between the measured and estimated AOD values at 440 nm) AOD_{440} were correlated with Chl-*a* concentrations. A very high and significant association with coefficient of determination (R^2=0.80) indicates the contribution of Chl-*a* as a source of aerosols in this part of the ocean. On the basis of the measured aerosol properties, the study area was divided into three zones; Zone 1 comprising of the area between 10°N and 11°S; Zone 2 from 16°S to 53°S; and Zone 3 from 52°S to 24°S during the return leg. BC mass concentration was in the range 520 ng m^{-3} to 2535 ng m^{-3} in Zone 1, while it was extremely low in the other zones (ranging from 49.3 to 264.4 ng m^{-3} in Zone 2 and from 61.6 ng m^{-3} to 303.3 ng m^{-3} in Zone 3). The atmospheric direct-short wave radiative forcing (DRSF), estimated using a radiative transfer model (Santa Barbara DISORT Atmospheric Radiative Transfer – SBDART), was in the range 4.72–27.62 wm^{-2} north of 16°S, and 4.80–6.25 wm^{-2} south of 16°S.

1. Introduction

The longevity of aerosols in the troposphere is a topic of research ever since their significant role in moulding the climate have been realised (Kaufman and Holben, 1996). The heterogeneity of the aerosols concentration in the spatial domain and their strong correlation with activities such as biomass burning, combustion of fossil fuel, sea salt spray and dust from the deserts clearly underline the need for a proper and systematic analysis of their interaction with incoming solar radiation for climate related studies (IPCC, 2013). In this regards many region-specific experiments pertaining to columnar aerosols have been performed. Some examples are the Aerosol Characterisation Experiment (ACE I and II), the Smoke, Clouds, Aerosols, Radiation-Brazil (SCAR-B) (Kaufman and Holben, 1996), the Tropospheric Aerosol

* Corresponding author.
E-mail address: harilalm@gmail.com (H.B. Menon).

http://dx.doi.org/10.1016/j.dsr2.2015.03.012
0967-0645/

Radiative Forcing Observational Experiment (TARFOX) (Russell et al., 1999), the Indian Ocean experiment (INDOEX) (Ramanathan et al., 2001) and the Integrated Campaign for Aerosols, Gases and Radiation Budget (ICARB) (Krishnamoorthy et al., 2008). The possibility of anthropogenically-derived continental aerosols getting advected to neighbouring ocean basins due to seasonally-reversing winds cannot be ruled out. This was the objective while carrying out a coordinated campaign for concurrent observations of aerosols over land and ocean (ICARB, March–May 2006). The results of the study gave insight into the spatial and temporal variability of composite aerosols over the Indian subcontinent and the adjoining Arabian Sea and the Bay of Bengal (Kalapureddy et al., 2009; Kaskaoutis et al., 2009; Badarinath et al., 2010; Kaskaoutis et al., 2010, 2011). For the first time, the study revealed high BC mass concentration in the middle troposphere (Krishnamoorthy et al., 2008). This led to the installation of multi-wavelength radiometers for measurements of the aerosol optical depth (AOD), at carefully chosen locations across India under the aegis of the Aerosol Radiative Forcing over India (ARFI), project funded by the Geosphere Biosphere Programme of the Indian Space Research Organisation (ISRO). Many documents have already been published, highlighting the results of ARFI initiatives (Menon et al., 2011; Moorthy et al., 2013a,2013b; Narasimhan and Satheesh, 2013; Gogoi et al., 2014; Menon et al., 2014). While ICARB and ARFI acted as stimulus for aerosol studies, the knowledge on the spatial variation of aerosol properties from north to south is more important and has been less attempted, especially over the Indian Ocean sector of the Southern Ocean. Some of the limited studies carried out in this area (Babu et al., 2010; Chaubey et al., 2013) mainly focussed on the continental impact and sea spray aerosols on climate. However, the role of marine phytoplankton has virtually been unexplored in any of these studies. This encouraged researchers to extend the observations to different sectors of the Indian Ocean. One such study has been carried out between 14°N and 53°S from December 2011 to February 2012 as part of the Southern Ocean Expedition (SOE) program, organised by the National Centre for Antarctic and Ocean Research (NCAOR), Ministry of Earth Sciences (MOEs) of the Government of India. The results of the study are presented and discussed here. The study was carried out with the following objectives.

1. To understand the spatial heterogeneity of spectral characteristics of aerosols between 14°N and 53°S, area covering the southern Arabian Sea and the Indian Ocean sector of the Southern Ocean.
2. To generate a spectrally resolved Angstrom wavelength exponent (α) to delineate the source of aerosols in the area of study.
3. To examine the role of phytoplankton in modifying the aerosol properties in the area of study.
4. To quantify the spatial gradients of AOD/BC mass concentration and the north-south distinctiveness in aerosol types of the study area.
5. To examine the spatial variability of short wave direct aerosol radiative forcing (SDRF) in the study area.

2. Material and methods

The measurements have been carried out in a campaign mode, during the period 26 December 2011 to 4 February 2012, aboard the ORV Sagar Nidhi (Fig. 1). The measurements started from Goa, progressed along the track (Fig. 1) and culminated at Mauritius on February 4. During the campaign period, the ITCZ was located between 11°S and 16°S, and as such, the cruise provided an opportunity to examine the outflow of aerosols from Asian continent in association with the north-east monsoon winds beyond its northern limit, in contrast with the more pristine Southern Ocean.

A Microtops II Sunphotometer (Solar light Co) and an Aethalometer (Magee Scientific, AE 42) were used to estimate columnar spectral AOD and near-surface BC mass concentration on board ORV Sagar Nidhi during its cruise. A hand-held automatic weather station (AWS-Nielsen Kellerman) was used to derive wind parameters. The onward leg of the cruise terminated at 53°S on 23 January 2012, while the return leg ended at 24°S near Mauritius. Since the aerosol characteristics are known to be distinct on either side of the ITCZ (for example Moorthy et al., 1999), the first leg between 14°N and 53°S has been divided into two zones, namely; Zone 1 comprising of the area between 10°N and 11°S and Zone 2 from 16°S to 53°S. The return leg has been considered as separate zone (Zone 3) as it has more continental proximity than Zone 2. The numbers shown in Fig. 1 are AODs at 500 nm (AOD_{500}) corresponding to the locations of measurements. Since measurements were taken on clear sky conditions (only in the absence of visible clouds) while the ship was sailing, the AODs corresponding to those locations are shown in the figure. Moreover, long range transport of aerosols to the study area computed by the Hybrid Single Particle Lagrangian Interpolated Trajectory (HYSPLIT) model (http://ready.arl.noaa.gov/) (Draxler and Hess, 1998) for each measurement location, and arrival altitudes of 0.5 km, 1 km and 1.5 km above mean sea level are shown by plotting the back trajectory to various points on the track. Prior to the cruise, all the instruments were calibrated by the manufacturers. Details of estimation of AOD and BC are given below.

2.1. Aerosol optical depth (AOD)

AODs were estimated from the multichannel Microtops II sunphotometer measurements at five bands centered at 380, 440, 500, 675 and 870 nm, following a standard protocols (Frouin et al., 2003). A Sunphotometer works on the principle of the Beer-Lambert law. The field of view of the Microtops II is 2.5° at full-width half maximum. From the spectral measurements of direct solar flux, the instrument computes AOD using internal calibration coefficients (which represent the corresponding top of the atmosphere fluxes) and the coordinates of the observation points provided by a Global Position System attached to it. All the observations were made from 0900 h to 1730 h during clear-sky periods at an interval of 30 min. Typical accuracies in the estimated AOD over maritime environment using Microtops II instrument are $\sim \pm 0.015$ (Knobelspiesse et al., 2004).

2.2. Black carbon (BC)

A seven-band Aethalometer (model AE-42) operating at 370, 470, 520, 590, 660, 880 and 950 nm was used to estimate BC mass concentration. Filtration and optical transmission techniques were used to estimate BC mass concentration from the absorbance at 880 nm (Hansen et al., 1984). The instrument aspirated ambient air through a size-segregating inlet that pre-segregates all the particles larger than 1 μm. The instrument was operated at a rate of 3 l/minute (LPM) every 2 min till 11°S and at a rate of 5 LPM during the surveys south of 16°S (in view of the reduced BC concentrations in these regions). The particles in the airflow get deposited on the quartz fibre filter tape of the Aethalometer. The difference between the sample spot (deposit of particles on the quartz fibre filter tape of the Aethalmeter) and reference spot (particle free) gives the attenuation. Using the factory-set wavelength dependent calibration factors, the equivalent BC mass was computed. During the field measurement, the Aethalometer was placed in the ship's cabin and the inlet pipe was placed at a height of about 12 m at the bow of the ship (sampling into the wind) to avoid any contamination due to ship fumes. To protect the instrument from varying humidity, a heated sample line was

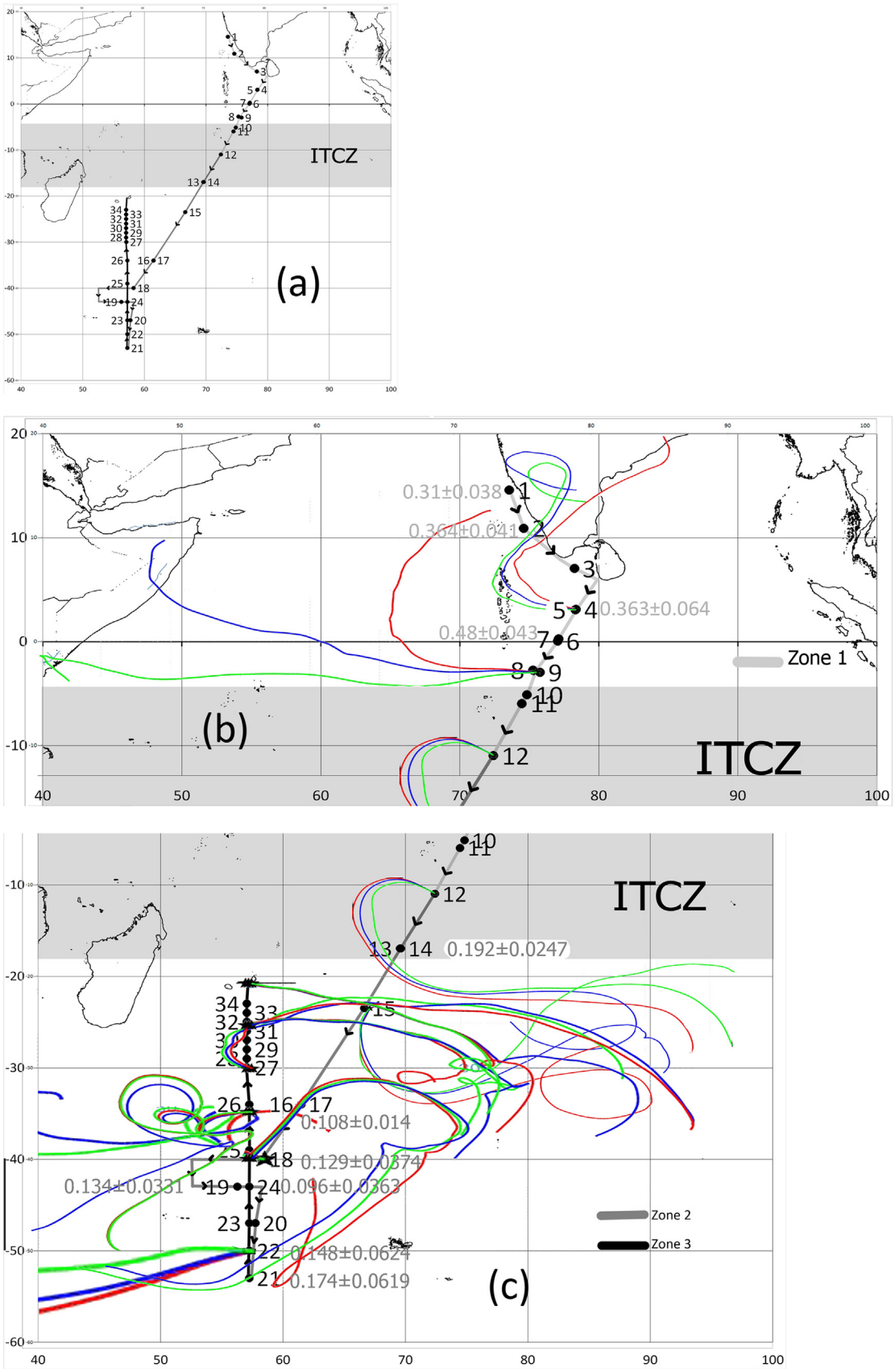

Fig. 1. (a) Study area showing the ORV, Sagar Nidhi's cruise track. (b) Zone 1 with back trajectory and AOD $_{500}$ along with standard deviation (in numbers) at all the locations north of 16°S (c) Zones 2 and 3 with back trajectories and AOD $_{500}$ with standard deviation at all locations south of 16°S. Zone 3 comprises of all stations between 52°S and 23°S (return leg).

connected to the inlet and the humidity was always maintained at less than 60%.

To locate thermal fronts and areas of high Chl-*a* concentration in waters south of equator, SST and Chl-*a* level III data derived from the Aqua – MODIS sensor (equatorial crossing time of 1330 h in an ascending mode) were used (http://nsidc.org/data/modis/terra aqua differences).

2.3. Meteorological parameters

Wind speed, direction and relative humidity were measured every 10 min using a pre-calibrated Kestrel 4500 weather tracker. The head wind and cross wind components due to the movement of the ship were calculated and necessary corrections were made to the measured wind speed and direction. Details of the data are shown in Table 1. As the AOD represents columnar aerosol, to get an understanding of the source region of the aerosol before it reaches the observation point, it is necessary to analyse the back trajectories with longitude, latitude and height (three dimensional descriptions of the pathways of aerosol parcel) as a function of time using HYSPLIT model for each measurement location, and arrival altitudes of 0.5 km, 1 km and 1.5 km above mean sea level. On an average, as the residence time of different modes of aerosols in the lower troposphere is seven days, all the back trajectories were calculated for seven days to the mean latitude and longitude positions of the ship on different days (Fig. 1). The heights were chosen to understand the flux of aerosols at the surface within the planetary boundary layer and from the free troposphere.

2.4. Radiative forcing

To compute the direct short wave aerosol radiative forcing (DSRF), three important optical properties are required: the single scattering albedo (SSA), the spectral AOD and the asymmetric parameter. These three parameters were computed using the OPAC model (Hess et al., 1998). The input to the model for the sector north of 11°S are species such as insoluble component, water soluble component, soot component, sea-salt accumulation mode component, sulphate and mineral dust transported component in terms of number of density. However, for the sector south of 16°S marine model was run with variable mixture modes for different sectors of the cruise track so that computed AODs corroborated well with the measured AODs and the sigma error between them was well within the limit (RMS error ≤ 0.03).

In the present study, the mixed-layer height was approximately 1 km (in the southern tropical Indian Ocean), while towards higher latitudes, the height was reduced to 0.8 km. Wavelengths from 0.25 μm to 4.0 μm have been chosen for computing the short wave optical parameters.

The direct aerosol short wave radiative forcing was computed using the SBDART model (Ricchiazzi et al., 1998). The output of OPAC was used as input for this model. An important factor influencing radiative forcing is the surface reflectance (Haywood and Shine, 1995). The MODIS –derived surface reflectance values have been used in this study.

The radiative forcing at any layer of the atmosphere is the net flux of downwelling and upwelling irradiances with and without aerosol at that layer (Charlson et al., 1992; Russell et al., 1999; Yu et al., 2001). An estimation of the difference in the flux at the top of the atmosphere (TOA) and at the surface (SFC) with and without aerosols provides the respective forcing; the difference between the two is an estimation of the forcing in the atmosphere. Therefore the aerosol radiative forcing is,

$$\mathrm{ARF} = \mathrm{Flux(net)}_{\mathrm{TOA/Surface\ with\ aerosols}} - \mathrm{Flux(net)}_{\mathrm{TOA/Surface\ without\ aerosols.}} \quad (1)$$

Hence the atmospheric forcing is,

$$\mathrm{ARF}_{\mathrm{ATM}} = \mathrm{ARF}_{\mathrm{TOA}} - \mathrm{ARF}_{\mathrm{SURFACE}} \quad (2)$$

3. Results and discussion

3.1. Variability of AOD and α

Referring to Fig. 1 and Table 2, it clearly emerges that AOD_{500} for Zone 1 (0.35 ± 0.067) was 3 times the mean magnitude (0.157 ± 0.048) for Zone 2 and (0.153 ± 0.034) Zone 3. This reveals an expected trend with values decreasing from coastal waters to

Table 1
Meteorological parameters prevailing at different locations during the cruise.

Station no.	Latitude (deg)	Atm TEMP (°C)	RH (%)	Pressure (mb)	Wind Direction (deg)	Wind Speed (m s^{-1})
7	0.25	28.26 ± 0.58	78.97 ± 4.42	1008.32 ± 2.25	300.17 ± 38.12	6.81 ± 1.66
8	2.8	28.47 ± 0.35	79.57 ± 2.30	1008.44 ± 1.36	231.16 ± 101.46	4.67 ± 2.96
10	5.15	31.39 ± 1.89	71.67 ± 6.38	1007.56 ± 1.22	302.65 ± 68.74	6.67 ± 1.08
12	11	28.30 ± 0.94	83.51 ± 4.44	1005.42 ± 3.10	303.22 ± 78.05	7.68 ± 2.39
13	16.694	26.61 ± 0.50	77.11 ± 0.46	1007.61 ± 1.05	215.04 ± 17.23	3.82 ± 1.20
14	19.5	25.90 ± 0.36	72.79 ± 3.32	1008.38 ± 0.57	247.44 ± 24.27	4.83 ± 1.30
15	22.21	24.65 ± 0.32	80.42 ± 3.62	1009.63 ± 0.91	242.26 ± 43.68	5.29 ± 1.55
	28.43	23.82 ± 0.56	79.80 ± 3.15	1010.90 ± 0.76	218.19 ± 16.16	4.22 ± 0.96
16	34.97	21.08 ± 0.75	81.31 ± 4.87	1019.68 ± 4.23	148.78 ± 81.04	2.55 ± 1.13
19	42.9	12.65 ± 1.69	89.45 ± 7.38	1017.52 ± 1.45	265.33 ± 96.96	5.95 ± 3.27
20		6.13 ± 1.46	85.68 ± 4.72	1003.77 ± 7.65	232.33 ± 107.28	5.48 ± 2.60
21	50.216	3.25 ± 0.42	80.16 ± 5.46	1005.82 ± 2.62	296.19 ± 71.12	8.46 ± 3.31
22		6.31 ± 1.31	92.24 ± 3.92	1019.87 ± 3.40	283.57 ± 20.24	7.81 ± 1.60
24	42.46	8.01 ± 1.42	82.66 ± 4.04	1018.94 ± 2.49	224.04 ± 150.77	11.74 ± 1.47

Table 2
Mean and standard deviation of AOD_{500} in the three zones of the study area.

	0.380 (μm)	**0.440 (μm)**	**0.500 (μm)**	**0.675 (μm)**	**0.870 (μm)**
Zone 1	0.527 ± 0.068	0.484 ± 0.064	0.355 ± 0.067	0.285 ± 0.065	0.254 ± 0.07
Zone 2	0.292 ± 0.055	0.336 ± 0.057	0.157 ± 0.048	0.155 ± 0.046	0.180 ± 0.046
Zone 3	0.316 ± 0.04	0.361 ± 0.051	0.153 ± 0.034	0.154 ± 0.031	0.179 ± 0.028

farther offshore locations. However, an exception was at a location near the equator, where the AOD_{500} was slightly higher than north of it (Fig. 1). The MODIS derived AOD_{500} also exhibited such an isolated pocket (http://neo.sci.gsfc.nasa.gov). The seven day back trajectory analysis unveiled that air mass with high AOD at a height of 1.5 km at the above mentioned location near the equator was advected from a height of 6.0 km above the African continent, indicating that an increase in AOD at this location could be associated with the advection of dust aerosols from the African continent.

In Zone 1, the AOD decreased with increasing wavelength between 380 and 870 nm. However, the spectra in Zones 2 and 3 were distinctly different. In these two Zones, the AOD spectra depicted a primary peak at 440 nm and a not-so-prominent increase at 870 nm (Fig. 2a–c). Moreover, the standard deviation of AOD at each wavelength in Zone 1, shown as vertical bar, was more or less uniform at all wavelengths, while it was higher at the shorter wavelengths (380 nm–440 nm) than at the longer ones in the other two Zones. Locations in Zone 2 were covered between 5 January and 23 January. Those covered between 5 and 11 January (at 34°S) were subjected to marine aerosol characteristics, both from local meteorology and long range transport, while those south of 34°S were from both marine and continental sources (as observed from back trajectory analysis), advected from the Antarctica. However, the spectra resembled those of Zone 2, as the aerosols from the pristine atmosphere of the Antarctic continent have different characteristics compared to the aerosols from the African or Indian continents.

The winds at each location in Zone 1 were of north-north-westerly with speeds varying in the range 2–10 m s^{-1} (Table 1). As mentioned earlier, two distinct features of AOD spectra seen in Zones 2 and 3 were of a primary peak at 440 nm and a non-so-significant increase at 870 nm. An increase in AOD at 870 nm due to influx of coarse mode marine aerosol (Moorthy et al., 1991), was prominent in Zones 2 and 3, while absent in Zone 1. A poor regression $R^2 \sim 0.02$ between wind speed and AOD_{870} indicates a small influence of wind on AOD_{870}. This has been probed by examining the surface salinity along the entire track, as salinity is a decisive factor while analysing wind transported marine aerosols. The period of study (December) witnessed the advection of low saline (~33) Bay of Bengal water along the eastern Arabian Sea (Zone 1). Low saline waters are always present in the equatorial region as the area is under the influence of water column divergence. The salinity during the period of observation was ~33.9 (neo.sci.gsfc.nasa.gov). It was also observed that south of ITCZ, the surface salinity increased gradually from 34.8 to 35.5 and the same was maintained till the northern boundary (43°S) of Subtropical front (STF). Across the STF, the salinity decreased to 34.8 and maintained at 34.09 south of it (neo.sci.gsfc.nasa.gov). Wind generates coarse-mode sea-salt particles, due to bursting of bubbles at wave crests (Monahan et al., 1986; Fitzgerald, 1992) over saline waters with salinity 35 or above. However, when low salinity waters prevailed (as in the case of Zone 1 where the surface salinity was in the range 33–33.9), the sea-salt particles would be finer, resulting in the decrease of AOD_{870}.

In their studies, O'Dowd et al., (1999) and Martensson et al., (2003) observed the role of salinity and wind in the aerosol droplet formation. This means wind acts as an external mechanism for the marine aerosol flux and surface salinity is the decisive factor for the aerosol size distribution. As the salinity increases towards STF, the viscosity increases. However, the relation between viscosity and salinity is not as simple as explained above. More than salinity, SST plays a dominant role in determining the viscosity. A decrease in SST towards STF and further south increases the viscosity. Since the viscosity increases towards high latitude (due to increase in salinity and decrease in SST), the wind prevailing over there produces coarse mode aerosols, which is clearly depicted by an increase of AOD_{870}. Typical examples are the locations at 11°S and 42.46°S, where though the wind velocities went up to 10 m s^{-1} and 13 m s^{-1} respectively (Table 1), a one to one correspondence between AOD_{870} and wind speed was not discernible. Hence, an increase in AOD_{870} in both zones south of 16°S was due to the abundant sea salt coarse-model aerosols in the marine boundary layer mediated by high saline surface water,

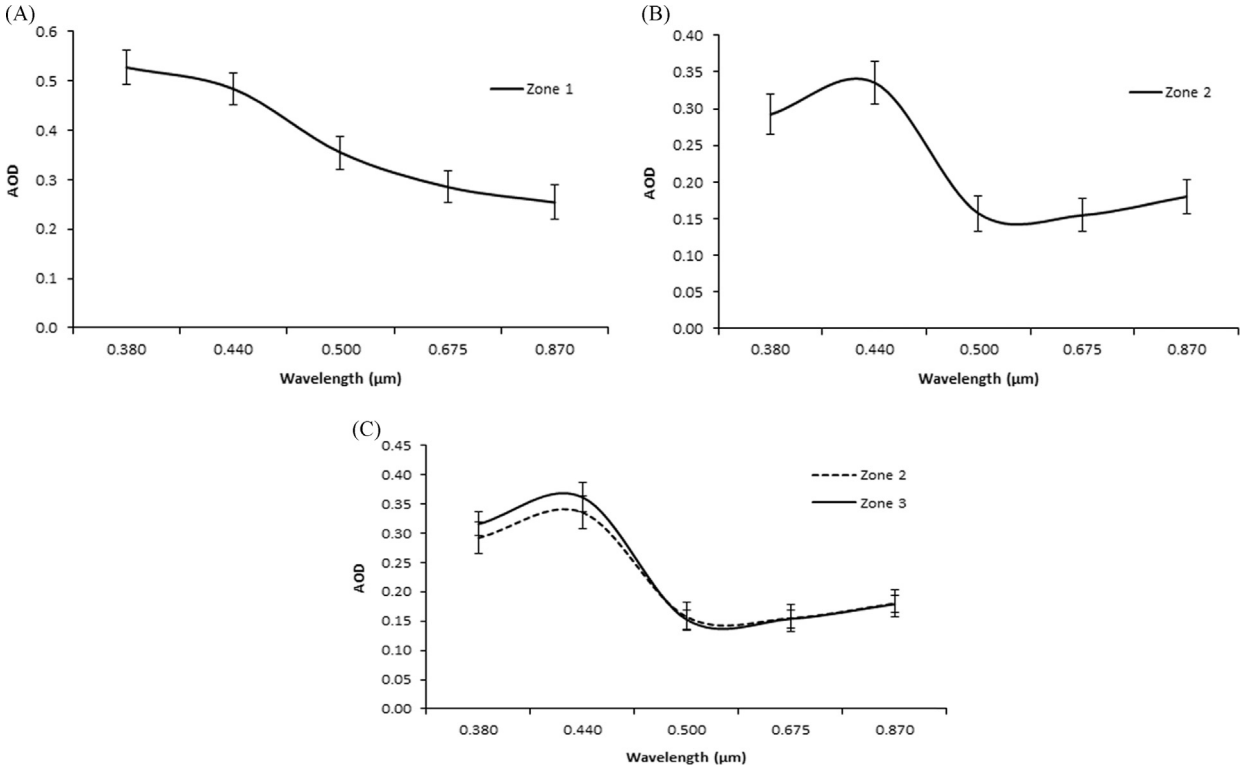

Fig. 2. Mean AOD spectra and standard deviation in (a) Zone 1 (b) Zone 2 and (c) Zone 3.

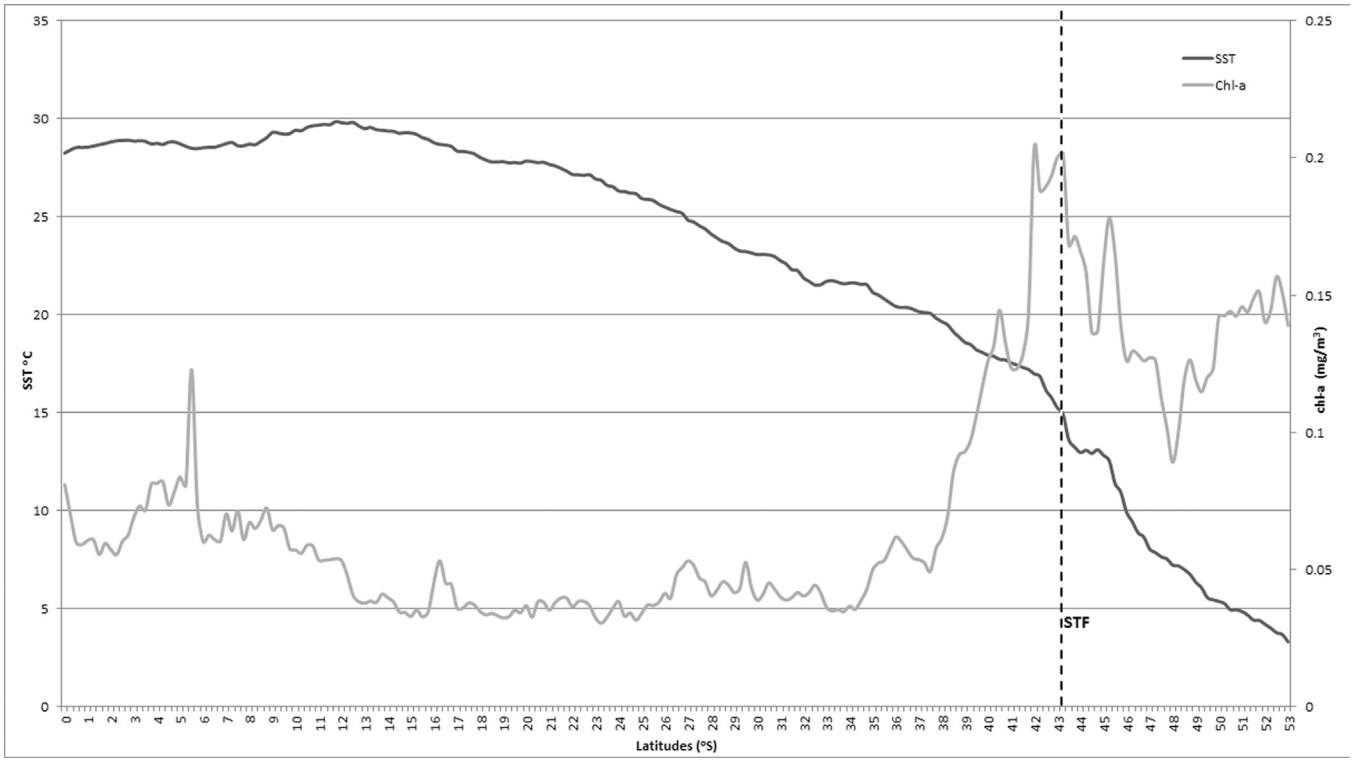

Fig. 3. Latitudinal variability of SST and Chl-a, demarcating subtropical front and associate increase in Chl-a values.

while absence of such an increase in the Zone north of 16°S could be attributed to low saline surface water.

An increase in AOD_{440} observed in Zones 2 and 3 could be due to the following. The marine aerosol is primarily comprised of sea salt particles formed from ocean spray, bubble bursting or wind triggered wave breaking (O'Dowd et al., 1977). The secondary aerosol type is composed mostly of non-sea-salt sulphate such as dimethyl sulhphide (DMS) and organic materials formed through gas to particle conversions (O'Dowd et al., 1977). The Chl-*a* pigment of single cell plants, phytoplanktons, emit DMS into the atmosphere (Garbic et al., 2001). In the atmosphere, DMS undergoes oxidation forming metanesulfonic acid (MSA) aerosols and sulphate particles (Garbic et al., 2005). The Chl-*a* pigment in the water column, which is the base of ocean food chain, has a primary absorption band at 440 nm (Menon et al., 2005). An increase in surface Chl-*a* concentration was observed at STF and further south of it (Fig. 3). On clear sky days, optimum light is available to phytoplankton for photosynthesis. When the visible spectrum interacts with such molecules of DMS in the atmosphere, AOD_{440} is bound to have a value higher than that at 380 nm. However, a word of caution is that such a spectral characteristic is site/environment specific. For example, high concentrations of Chl-*a* encountered in the coastal waters of Zone 1 were not reflected in the values of AOD_{440}. This could be attributed to the presence of fine-mode aerosols of continental origin as dominant species in this Zone. To substantiate this argument further, the $AODs_{440}$ have been estimated using the OPAC model without incorporating the effect of sulphate aerosols. A coefficient of determination (R^2) of 0.80 between the anomaly of AOD (difference between measured AOD and estimated AOD) and Chl-*a* concentration highlights the fact that DMS is responsible for an increase in AOD at this wavelength (Fig. 4).

An interesting feature noticed was the higher AOD values in the short wavelength range in Zone 3 (return leg) than in Zone 2 (Zones 2 and 3 are basically same, except that Zone 3 is spatially closer to the continent and measurements were taken after few days). From the SST analysis, it is observed that the STF in both Zones are around

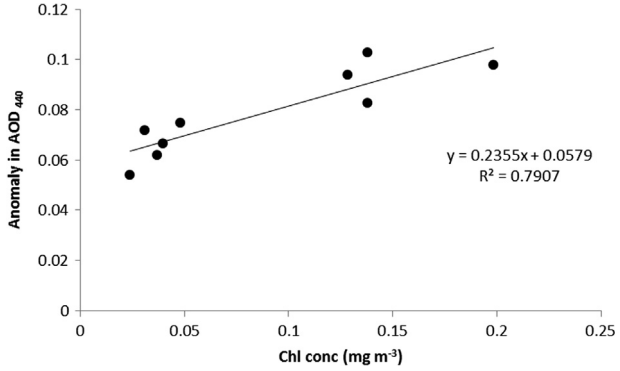

Fig. 4. Correlation of chlorophyll–*a* concentration and differences between measured AOD and modelled AOD at 440 nm.

43°S (Fig. 3). Since STF in Zone 3 was stronger due to the confluence of the Agulhas retroflection (Anilkumar et al., 2006), an increased Chl -*a* concentration might have been responsible for higher DMS and high non-sea-salt sulphate generation in Zone 3. Since the observations carried out during the return leg were from low Chl-*a* waters to high Chl-a waters (as the ship was approaching STF), predominance of fine mode particles of marine origin formed as a result of gas-to-particle conversion responsible for increasing AOD at short wavelength. This is also evident from the fact that the winds were southwesterlies embedded with wind gust (fluctuations in the wind velocitiy). Southwesterly to southeasterly winds with velocities from 3 to 12 m s^{-1} also mediated influx of continental aerosols of fine mode fraction, which in turn increased AOD_{380}.

To further establish the above argument quantitatively, the Angstrom exponent (α) has been generated using a polynomial fit. The coefficient, which parameterises the aerosol size distribution, α, was derived from Ångstrom (1961). This is on the basis of the assumption that spectral AOD follows the Junge power-law

exponential function. Thus aerosol extinction and the wavelengths are related in the following manner:

$$\mathcal{T} = \beta(\lambda)^{-\alpha} \quad (3)$$

where $\mathcal{T}(\lambda)$ is AOD (λ) and β is the atmospheric turbidity parameter. From the linear regression analysis, α is derived as the slope of the regression line connecting ln $\mathcal{T}(\lambda)$ and ln (λ). However, such a relation breaks in areas similar to Zones 2 and 3. In such cases, the spectral AOD follows better a second degree polynomial. In those situations, α could be estimated using a pair of wavelengths λ_1 and λ_2 following the Volz method, (Naseema Beegum et al., 2009)

$$\alpha = \frac{d \ln \tau}{d \ln \lambda} = -\frac{ln\frac{\tau_1}{\tau_2}}{ln\frac{\lambda_1}{\lambda_2}} \quad (4)$$

where $\mathcal{T}_1$ and $\mathcal{T}_2$ are the extinction coefficients at the two wavelengths, $\lambda 1$ and λ_2, respectively. Several studies revealed negative values of α in wavelength ranges, where AOD is higher at longer wavelengths than at shorter ones (Adeyewa and Balogun, 2003). Under such situations, a second degree polynomial was fitted between ln(AOD) and ln (λ) to generate α (Eck et al., 1999),

$$\ln \tau = \alpha_2 (\ln \lambda)^2 + \alpha_1 \ln \lambda + \alpha_0 \quad (5)$$

and the second derivative α' was derived as follows (Eck et al., 1999),

$$\alpha' = \left(\frac{-2}{\ln \lambda_{i+1} - \ln \lambda_{i-1}}\right)\left(\frac{\ln \tau_{i+1} - \ln \tau_i}{\ln \lambda_{i+1} - \ln \lambda_i} - \frac{\ln \tau_{i-1} - \ln \tau_i}{\ln \lambda_{i-1} - \ln \lambda_i}\right) \quad (6)$$

where α_0, α_1, and α_2 are the constants and α_2 represents the curvature observed in the AOD spectra. From the above equations,

$$\alpha' = d\alpha / d\ln\lambda = -2\alpha_2 \quad (7)$$

α_2 and α' were estimated for each spectral AOD data set and analysed for the curvature effect.

Since the spectral shape of AOD in Zones 2 and 3 were similar, α' values in these two Zones were put together. All the values north and south of 16°S (southern boundary of ITCZ) have been grouped separately to understand the dominant components of aerosols in these sectors. There were 173 values ($n=173$) north of 16°S and 354 values ($n=354$) south of it (Fig. 5). In the area north of 16°S, most of the α' values were near zero and the minimum values near −3. Among them only two values were positive. Near zero values indicate compliance with Angstrom relation, while higher α' values suggest non-complaince to the simple Angstrom relation. Positive α' values indicate the dominance of fine-mode aerosols, while near zero to negative α' values suggest the dominance of coarse mode aerosols in the bimodal aerosol distribution and presence of fine mode aerosols, due to the advection of continntal aerosols. Since the area was surveyed when the northeasterly winds prevailed due north of the northern limit of the ITCZ, with the continental advection (as evidenced from the back trajectory analysis, Fig. 1), it is possible that the advected submicron continental aerosols would have greatly contributed to the aerosol loading, leading to a steeper AOD spectrum. However, in the area south of 16°S, most of the α' was in the range −2 to −6. This suggests a bimodal aerosol size distribution with dominant coarse mode particles, which are of maritime origin. The lower values of α' indicate relatively significant magnitude of coarse-mode and fine-mode particles, which is clearly seen from the AOD spectra having peak at 440 nm and an increase at 870 nm in this area.

3.2. BC mass concentration

Daily mean values of BC mass concentration along with standard deviation in different zones are shown in Fig. 6. Among the three zones, the highest BC was encountered in Zone 1 with a value of 2535 ng m^{-3} at around 10°N, on 27 December 2011. Further southwards, the concentration gradually decreased and a minimum value of 470 ng m^{-3} was encountered at 6°S on 3 January 2012. In Zone 2, BC was in the range 49.3–264.4 ng m^{-3}. An irregular pattern of distribution with high and low BC mass having values of 465.8 ngm^{-3}, 264.4 ng m^{-3} and 167.9 ng m^{-3} were encountered on 6, 14 and 24 January 2012, respectively. Two possibilities could be ascribed to such a distribution of BC. One among them is due to *in situ* source while the second one is remote forcing. The *in-situ* source is emissions from the ship. The remote forcing is due to the advection of continental BC. As Zone 2 is an area in the deep sea, the possibility of *in-situ* source is not so prominent compared to Zone 3. Therefore, the reason for such a BC distribution can be assigned only to continental outflow. Zone 3 encountered the lowest BC among all the three zones. In this zone, the BC ranged from 61.6 (50°S and 25 January 2012) to 303.6 ng m^{-3} (45°S and 27 January, 2012).

3.3. Radiative forcing

The Short wave direct radiative forcing (SDRF) estimated at TOA, SFC and the resultant forcing in the atmosphere (ATM) are shown in Fig. 7. A location at 43°S was imminent to understand the role of confluence of retroflection of the Agulhas current with STF and subsequent effect on atmospheric forcing. To achieve this goal, measurements were taken along 43°S at different longitudes between 53.5°E and 58°E, during the onward leg of the survey, while it was repeated at one location around 43°S and 57.5°E during the return leg. The entire duration of the cruise witnessed negative SFC and TOA forcings. Since locations 1 (14.5°N) and 2 (10.8°N) were directly under the influence of northeasterly monsoon winds, the turbulent nature of the sea surface resulted in high surface forcing (Fig. 1). The high surface forcing and low TOA forcing led to high atmospheric forcing at these two locations. The enhanced BC associated with continental outflow and reduced precipitation during this period is responsible for the high atmospheric forcing. Since the atmospheric forcing is governed by chemical composition and size distribution of aerosols, the high atmospheric forcing at these locations are as expected. Barring these two locations, the pattern of latitudinal variability of SFC and TOA forcings were almost similar. It followed a bimodal distribution with a primary peak at location 7 (0.2°S, in the equatorial zone), which is under the influence of southeasterly trade winds and a secondary peak at location 24 (43°S), where the Agulhas retroflection confluences with STF (Zone 3). A comparatively high AOD_{500} (0.48 ± 0.0437) and a moderate-to-high sea-surface albedo might have been responsible for such a forcing at location 7. At location 24, the confluence of the Agulhas retroflection with STF was responsible for more albedo and surface forcing. Both the SFC and TOA forcings were minimum at location 16 (34°S). The SDRF in Zone 1 at TOA was in the range −9.76 to −18.16 W m^{-2} and the corresponding forcing at SFC was −20.97 to −38.37 W m^{-2}. The resultant atmospheric forcing varied between 5.56 and 27.64 W m^{-2}. In the oceanic sector south of 16°S, the TOA forcing was between −5.01 and −15.0 W m^{-2}. The SFC and ATM were in the range −9.93 to −20.47 W m^{-2} and 4.80 to 5.46 W m^{-2}, respectively. In general, the atmospheric forcing was more or less the same except at two locations in the coastal waters of the tropical Indian ocean (locations 1, 2), which revealed that the atmospheric forcing is governed by aerosols of absorbing nature at those two coastal locations. The proportionate variability of SFC and TOA forcings at each location away from the coastal waters implied a restricted effect of anthropogenically-derived aerosol while moving towards the Southern Ocean.

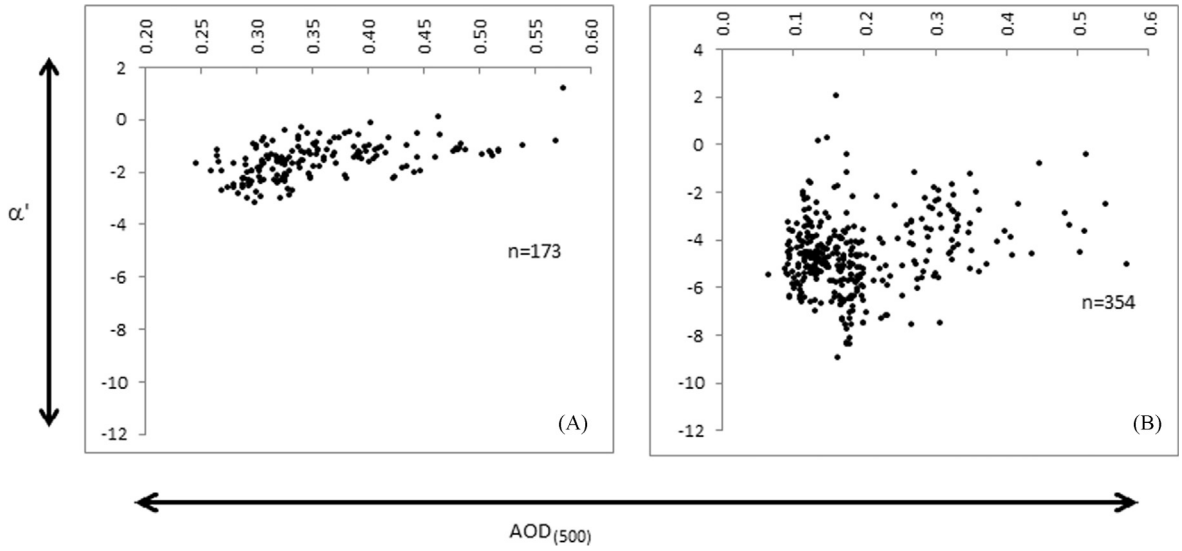

Fig. 5. Scatter diagram between α′ and AOD $_{500}$ (a) north of 16°S and (b) south of 16°S.

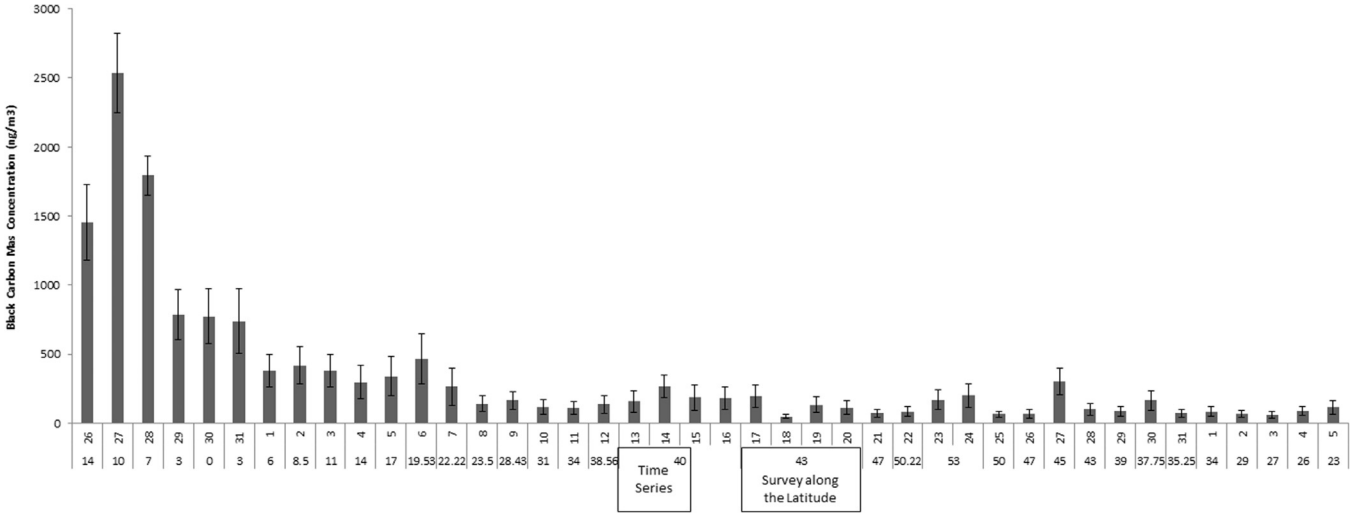

Fig. 6. Latitudinal variability of BC mass concentration. The first row on the *x*-axis represents the date of observation and the second row the latitude. The vertical bars indicate standard deviation.

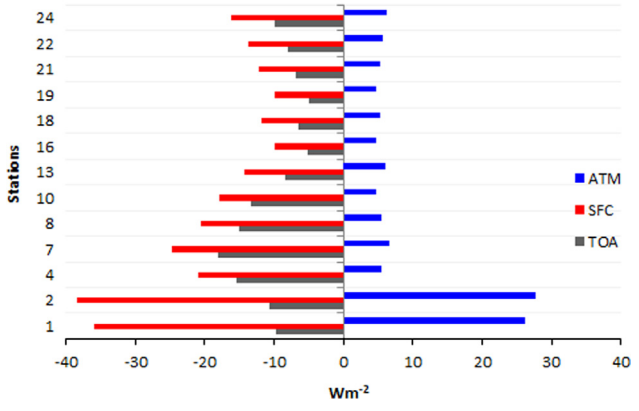

Fig. 7. SDRF, at SFC, TOA and ATM along the entire cruise track.

4. Conclusions

The latitudinal variation of the aerosol optical properties and the associated radiative forcings were studied in the southern tropical Indian Ocean and the Indian Ocean Sector of the Southern Ocean (between 14 N and 53°S), during December 2011–February 2012. To achieve the goal, concurrent measurements were made to estimate columnar AOD and BC mass concentration. The main findings of the study are:

1. Continental aerosols dominate the ocean sector north of 16°S; however, maritime aerosols with sea salt and non-sea-salt components dominate south of 16°S.
2. North of 11°S (the northern limit of the ITCZ), the spectral distribution of AOD follows the Angstrom turbidity formula (Junge power law function), while it deviates from such a distribution south of 16°S (southern boundary of ITCZ). The spectral variability south of 16°S is bimodal with a primary peak at 440 nm and a secondary, not-so significant increase at 870 nm.
3. An increase in AOD_{440} is due to the aerosols of non-sea salt component contributed by phytoplankton. Following a modelling approach, it has been shown that the peak in AOD_{440} has been associated with increased non-sea-salt aerosols, produced by marine phytoplankton prevailing over the region. The analysis revealed a high and significant correlation of $R^2=0.8$ between Chl-a concentration and AOD anomaly (*i.e.*, the

difference in AOD with sea salt included and excluded); such observation is reported for the first time over the Indian Ocean sector of the Southern Ocean.
4. The STF acts as a biogeographic boundary to ventilate marine boundary layer with non-sea-salt components. This was more visible when the Agulhas retroflection confluences with STF.
5. The aerosol SDRF at the surface ranged from -9.82 to -38.37 W m^{-2}, whereas at the TOA it ranged from -5.01 to -18.16 W m^{-2}; thus, the atmospheric forcing ranged from 4.72 to 27.64 W m^{-2}.
6. A positive atmospheric forcing revealed a BC-controlled albedo in the atmosphere. A negative TOA and SFC forcing indicate that the albedo is controlled by aerosols of scattering nature. Barring coastal stations, since TOA and SFC forcings varied proportionately across the latitude, the atmospheric forcing remained more or less uniform.

Acknowledgments

The first and second authors wish to thank the Space Physics Laboratory (SPL), Vikram Sarabhai Space Centre (VSSC) of the Indian Space Research Organisation (ISRO) for the R&D project sanctioned under the programme Aerosol Radiative Forcing (ARFI) of ISRO Geosphere Biosphere Programme. This is the third scientific manuscript from the funding. They also wish to thank the Director, National Centre for Antarctic and Ocean Research and the Vice Chancellor of Goa University for permitting to participate in the Southern Ocean expedition of December 2011–February 2012 and for providing all the facilities. The authors thank the officers and crew of ORV Sagar Nidhi for all the help rendered for collection of samples and data.

References

Adeyewa, Z.D., Balogun, E.E., 2003. Wavelength dependence of aerosol optical depth and the fit of the Ångstrom law. Theor. Appl. Climatol. 74, 105–122.
Ångstrom, A., 1961. Techniques of determining the turbidity of the atmosphere. Tellus 13, 214–223.
Anilkumar, N., Alvarinho, J.L., Somayajulu, Y.K., Ramesh Babu, V., Dash, M.K., Pednekar, S.M., Babu, K.N., Sudhakar, M., Pandey, P.C., 2006. Fronts, water masses and heat content variability in the Western Indian sector of the Southern Ocean during austral summer 2004. J. Mar. Syst. 63, 20–34.
Badarinath, K.V.S., Kharol, Shailesh Kumar, Kaskaoutis, D.G., Sharma, Anu Rani, Ramaswamy, V., Kambezidis, H.D., 2010. Long range transport of dust aerosols over Arabian Sea and Indian region–A case study using satellite data and ground-based measurements. Glob. Planet. Change 72, 164–181.
Babu, S.S., Moorthy, K.K., Satheesh, S.K., 2010. Latitudinal gradient in aerosol properties over the Indian and Southern Oceans during the austral summer. Curr. Sci. 99 (10), 1384–1389.
Charlson, R.J., Schwartz, S.E., Hales, J.M., Cess, R.D., Coakley Jr., J.A., Hansen, J.E., Hofmann, D.J., 1992. Climate forcing by anthropogenic aerosols. Science 255, 423–430. http://dx.doi.org/10.1126/science.255.5043.423.
Draxler, R., Hess, G.D., 1998. An overview of the HYSPLIT-4 modeling system for trajectories, dispersion and deposition. Aust. Meteorol. Mag. 47, 295–3008.
Eck, T.F., Holben, B.N., Reid, J.S., Dubovik, O., Smirnov, N.T., O'Niel, Slutsker, I., Kinne, S., 1999. Wavelength dependence of the optical depth of biomass burning, urban and desert dust aerosols. J. Geophy. Res. 104 (D24), 349 31,333–31.
Frouin, R., Holben, B., Miller, M., Pietras, C., Kirk, K.D., Fargion, G.S., Porter, J., Voss, K., 2003. Sun and sky radiance measurements and data analysis protocols. In: Mueller, J.L., Fargion, G.S., MacClain, C.R. (Eds.), Ocean Optical protocols for Satellite Ocean Color Sensor Validation, Revision 4, radiometric measurements and data analysis protocols, NASA/TM-2003-211621/Rev4-Vol-III, Vol-III. NASA, Goddard Space Flight Center, Greenbelt, MA, pp. 60–69.
Fitzgerald, J.M., 1992. Numerical simulation of the evalution of the aerosol size distribution in a remote marine boundary layer. In: Fukuta, N., Wagner, P.E., Deepak, A., Hampton, V.A. (Eds.). Nucleation and Atmospheric Aerosols. pp. 157–160.
Garbic, A.J., Gregg, W., Najjar, R., Erickson, D., Matrai, P., 2001. Modelling the biogeochemical cycle of dimethylsulphide in the upper ocean: a review. Chemosphere- Global Change. Science 3, 377–392.
Garbic, A.J., Shepard, J.M., Knight, J.M., Jones, G., Trevena, A.J., 2005. Correlation between the satellite-derived seasonal cylces of phytoplankton biomass and aerosol optical depth in the Southern Ocean: evidence for the influence of sea ice. Glob. Biogeochem. Cycles 19, GB4018.
Hansen, A.D.A., Rosen, H., Novakov, T., 1984. The Aethalometer: an instrument for the real time measurements of optical absorption by aerosol particles. Sci. Total Environ. 36, 191–196.
Haywood, J.M., Shine, K.P., 1995. The effect of anthropogenic sulphate and soot on the clear-sky planetary radiation budget. Geophys. Res. Lett. 22, 603.
Hess, M., Koepke, P., Schultz, I., 1998. Optical properties of aerosols and clouds: the software package OPAC. Bull. Am. Meteorol. Soc. 79, 831–844.
IPCC, 2013. In: Stocker, T.F., Qin, D., Plattner, G.K., Tignor, M., Allen, S.K., Boschung, J., Nauels, A., Xia, Y., Bex, V, Midgley, P.M (Eds.), Climate Change 2013: The Physical Science Basis. Contribution of Working Group I to the Fifth Assessment Report of the Intergovernmental Panel on Climate Change. Cambridge University Press, Cambridge, United Kingdom and New York, NY, USA, p. 1535.
Chaubey, J.P., Krishnamoorthy, K., Suresh Babu, S., Gogoi, Mukund M., 2013. Spatio-temporal variations in aerosol properties over the Oceanic regions between coastal India and Antarctica. J. Atmos. Solar-terr. Phys. 104, 18–28.
Kalapureddy, M.C.R., Kaskaoutis, D.G., Ernest Raj, P., Devara, P.C.S., Kambezidis, H.D., Kosmopoulos, P.G., Nastos, P.T., 2009. Identification of aerosol type over the Arabian Sea in the pre- monsoon season during the ICARB campaign. J. Geophys. Res 114, D17203.
Kaufman, Y.J., Holben, B.N., 1996. Hemispherical backscattering by biomass burning and sulfate particles derived from sky measurements. J. Geophys. Res. **101**, 19433–19445.
Moorthy, K. Krishna, Saha, Auromeet, Niranjan, K., Pillai, Preetha S., 1999. Optical properties of atmospheric aerosols over the Arabian Sea and Indian Ocean: North-South contrast across the ITCZ. Curr. Sci. 76 (7), 956–960.
Krishnamoorthy, K., Satheesh, S.K., Babu, S.S., Dutt, C.B.S., 2008. Integrated campaign for aerosols, gases and radiation budget (ICARB): an overview. J. Earth Syst. Sci. 117, 243–262.
Knobelspiesse, K.D., Pietras, Fargion, G.S., Wang, M., Frouin, R., Miller, M.A., Subramaniam, A., Blch, W.M., 2004. Maritime aerosol optical thickness measured by hand held sun photometers. Remote Sens. Environ. 93, 87–106.
Kaskaoutis, D.G., Kalapureddy, M.C.R., Devara, P.C.S., Kosmopoulos, P.G., Nastos, P.T., Krishna Moorthy, K., Kambezidis, H.D., 2009. Spatio-temporal aerosol optical charactiristcs over the Arbain Sea during the pre-monsoon season. Atmos. Chem. Phys. Disc 9, 22223–22269.
Kaskaoutis, D.G., Kalapureddy, M.C.R., Krishna Moorthy, K., Devara, P.C.S., Nastos, P.T., Kosmopoulos, P.G., Kambezidis, H.D., 2010. Heterogeneity in pre-monsoon aerosol types over the Arabian Sea deduced from ship-borne measurements of spectral AODs. Atmos. Chem. Phys. 10, 4893–4908.
Kaskaoutis, D.G., Kumar Kharol, S., Sinha, P.R., Singh, R.P., Kambezidis, H.D., Rani Sharma, A., Badarinath, K.V.S., 2011. Extremely large anthropogenic-aerosol contribution to total aerosol load over the Bay of Bengal during winter season. Atmos. Chem. Phys. 11, 7097–7117.
Martensson, E.M., Nilson, E.D., De leeuw, G., Cohen, L.H., Hansson, H.C., 2003. Laboratory simulations and parameterisation of the primary marine aerosol production. J. Geophys. Res. 108, 4297.
Menon, H.B., Lotliker, A., Nayak, S.R., 2005. Pre-monsoon bio-optical properties in estuarine, coastal and Lakshadweep waters. Estuar. Coast. Shelf Sci. 63 (1), 211–223.
Menon, H.B., Sangekar, N., Lotliker, A., Krishnamoorthy, K., Vethamony, P., 2011. Aerosol optical thickness and spatial variability along coastal and offshore waters of the eastern Arabian sea. ICES J. Mar. Sci. 68 (4), 745–750. http://dx.doi.org/10.1093/icesjms/fsq191.
Menon, H.B., Shirodkar, S., Kedia, S., Ramachandran, S., Babu, S.S., Moorthy, K.K., 2014. Temporal variation of aerosol optical depth and associated shortwave radiative forcing over a coastal site along the west coast of India. Sci. Total Environ., 468–469. http://dx.doi.org/10.1016/j.scitotenv.2013.08.013.
Monahan, E.C., Spiel, D.E, Davidson, K.L., 1986. A model of marine aerosol generation via whitecaps and wave disruption, in Oceanis white-caps. In: Monahan, E., Niocail, G.M (Eds.), D. Reidel, Norwell, Mass, pp. 167–174.
Moorthy, K.K., Nair, P.R., Murthy, B.V.K., 1991. Size distribution of Coastal Aerosols: effects of local sources andsinks. J. Appl. Meteor 30, 844–852.
Moorthy, K.K., Saha, A., Niranjan, K., Pillai, P.S., 1999. Optical properties of atmospheric aerosols over the Arabian Sea and Indian Ocean: North-south contrast across the ITCZ. Curr. Sci. 76, 956–960.
Moorthy, K.K., Babu, S.S., Manoj, M.R., Saheesh, S.K., 2013a. Build-up of aerosols over the Indian Region. Geophys. Res. Lett., 40. http://dx.doi.org/10.1002/grl.50165.
Moorthy, K.K., Beegum, S.N., Srivastav, N., Satheesh, S.K., Chin, Mian, Blond, Nadege, Babu, S.S., Singh, S., 2013b. Performance evaluation of chemistry transport models over India. Atmos. Environ. 71, 210–225.
Gogoi, Mukunda. M., Moorthy, K.K., Kompalli, S.K., Chaubey, J.P., Babu, S.S., Manoj, M.R., Nair, V.S., Prabhu, P.T., 2014. Physical and optical properties of aerosols in free troposphere environment: results from long term observations over western trans-Himalayas. Atmos. Environ. 84, 262–274.
Narasimhan, D., Satheesh, S.K., 2013. Estimates of aerosol absorption over India using multi-satellite retrieval. Ann. Geophys. 31, 1773–2013. http://dx.doi.org/10.5194/angeo-31.
Naseema Beegum, S., Krishna Moorthy, K., Suresh Babu, S., 2009. Aerosol microphysics over a tropical coastal station inferred from the spectral dependence of Angstrom wavelength exponent and inversion of spectral aerosol optical depths. J. Atmos. Solar-Terr. Phys. 71, 1846–1857 29.

O'Dowd, C.D., Smith, M.H., Consterdine, I.E., Lowe, J.A., 1977. Marine Aerosol Sea-Salt and the Marine Sulphur cycle: a short review. Atmos. Environ. 31, 73–80.

O'Dowd, C.D., Lowe, J.A., Smith, M.H., Kaye, A.D., 1999. The relative importance of non-sea-salt sulphate and sea-salt aerosol to the marine cloud condensation nuclei population: an improved multi-component aerosol-cloud droplet parameterization. Q. J. R. Meteorol. Soc. 125, 1295–1313.

Ramanathan, V. Crutzen, P.J., Lelieveld, J., Mitra, A.P., Althausen, D., Anderson, J., Andreae, W., Cantrell, M.O., Cass G.R., Chung, C.E., Clarke A.D., Coakley, J.A., Collins, W.D., Conant, W.C., Dulac, F., Heintzenberg, J., Heymsfield, A.J., Holben, B., Howell, S., Hudson, J., Jayaraman, A., Kiehl, J.T., Krishnamurti, T.N., Lubin, D., McFarquhar, G., Novakov, T., Ogren, J.A., Podgorny, I.A., Prather, K., Priestley, K., Prospero, J., Quinn., M. Rajeev, P.K. Rasch, K. Rupert, P. Sadourny, S. Satheesh, R. Shaw, S. K. Sheridan, G.E. Valero., P. F.P.J., Indian Ocean Experiment: an integrated analysis of the climate forcing and effects of the great Indo-Asian haze, J. Geophys. ResJ. Geophys. Res. 106, 2001, 28371–28398.

Ricchiazzi, P., Yang, S., Gautier, C., Sowle, D., 1998. SBDART: a research and teaching tool for plane-parallel radiative transfer in the Earth's atmosphere. Bull. Am. Meteorol. Soc. 79, 2101–2114.

Russell, P.B., Hobbs, P.V., Stowe, L.L., 1999. Aerosol properties and radiative effects in the United States East Coast haze plume: an overview of Tropospheric Aerosol Radiative Forcing Observational Experiment (TARFOX). J. Geophys. Res. 104, 2213–2222.

Yu, S., Zender, C.S., Saxena, V.K., 2001. Direct radiative forcing and atmospheric absorption by boundary layer aerosols in the southeastern US: model estimates on the basis of new observations. Atmos. Environ. 35, 3967–3977.